2mi4

AN AEROMAGNETIC SURVEY IN THE VALLEY

OF TEN THOUSAND SMOKES, ALASKA

A

THESIS

Presented to the Faculty of the

University of Alaska in Partial Fulfillment

of the Requirements

for the Degree of

MASTER OF SCIENCE

By

Kei Anma, B.S., M.S. (Fisheries)

College, Alaska

November, 1971

TABLE OF CONTENTS

1

II

ABSTRACT

An aeromagnetic survey in the Katmai National Monument was carried out by the Geophysical Institute, University of Alaska, in the summers of 1970-1971. Geologic and magnetic studies of the Katmai area have further demonstrated the close relationship between the Katmai Caldera, Novarupta plug, and the pyroclastic flows in the Valley of Ten Thousand Smokes.

The magnetic fields observed appear to be associated with the thickness of the pyroclastic flow and the different rock units within it for lower flight levels, and also the contrast between the valley fill and the rock units at the Valley margins.

Consistent magnetic anomalies are associated with the larger fumarole lines, which were presumably sites of large scale activity, while the smaller fumaroles are not usually seen in the aeromagnetic map. A possible correlation between low positive anomalies and nuee ardente deposits was revealed by the aeromagnetic survey, but was not strong.

Novarupta plug is represented by a large positive anomaly which is thought to represent both the lava dome and concealed intrusive material beneath it. In contrast, the rim around the plug has negative anomalies similar to those associated with Naknek Sediments.

Around Novarupta, radiating lines indicate local fault zones, which in turn have controlled the fumarolic activity. The flank terraces also seem to be associated with local faulting.

Volcanic trends in the Alaska Peninsula are thought to be controlled by the tectonics of the Aleutian island arc system. The magnetic signa-

tures of this tectonic trend are not strong, but some features can be recognized from the distribution of positive anomalies at the 1220 m flight level.

A ground survey was also carried out in several parts of the Valley with a view to detailed delineation of the magnetic signatures of the pyroclastic flow, as an aid to interpreting the aeromagnetic date.

ACKNOWLEDGEMENTS

The author is indebted to his supervisor, Dr. D. B. Stone, for his useful advice and comments. Without his support the work reported here would not have been possible.

The author also appreciates the critical comments of Dr. R. B. Forbes and Dr. J. Kienle, and also Dr. D. Hawkins who read the manuscript.

The author would like to thank Mr. D. R. Packer for his unpublished data. Thanks are due to Miss S. Wiss who gave her time to assist with computer processing and to Mrs. E. Bell who patiently typed the manuscript several times.

iii

List of Figures

mountain camp (4 feet pole). Base line for each day 53700 gammas.

Figure 44.   Total intensity anomaly map over Novarupta, flight height

at 1220 m. BRM: Broken Mt., BKM: Baked Mt.

CHAPTER I

INTRODUCTION

Katmai National Monument, located on the Alaska Peninsula, is part
of the active Circum Pacific Volcanic and Earthquake zone. It is also
part of the island arc system that extends for more than 3000 km from
Kamchatka Peninsula to the Alaska Range. Numerous volcanic and non-volca-
nic peaks are grouped around Mt. Katmai. The higher peaks, up to about
2140 m are volcanic summits superimposed on the Aleutian range, which it-
self reaches 1200 m ∿ 1530 m and is covered by recent glaciers. The vol-
canism of the Aleutian chain is typical of the Pacific Rim "Andesite
line". The volcanics range in age from Tertiary to recent, and consist
mainly of basalts, andesites, and rhyolites.

There are mostly andesites and dacites in the Katmai area, which
have formed typical stratovolcanoes and lava domes, and, in the case of
Mt. Katmai itself, a caldera. The 1912 Mt. Katmai caldera-forming erup-
tion was one of the largest events in historical times, and although many
scientists have investigated the origin and nature of the activity, there
are still many unsolved problems (Fenner 1922, Griggs 1912, Williams 1954,
Keller and Reiser 1959, and Wilcox 1959).

Recently, several petrological, tectonic, and geophysical studies
have been made. Forbes et al. (1968), Ray (1967), Kienle (1967), and
Burk (1965).

Work is currently being undertaken in the Mt. Katmai area by members
of the Geophysical Institute, University of Alaska. The work described in
this dissertation was part of this project, undertaken in the summer of
1970. The main objects of the overall study were to study: 1) Current
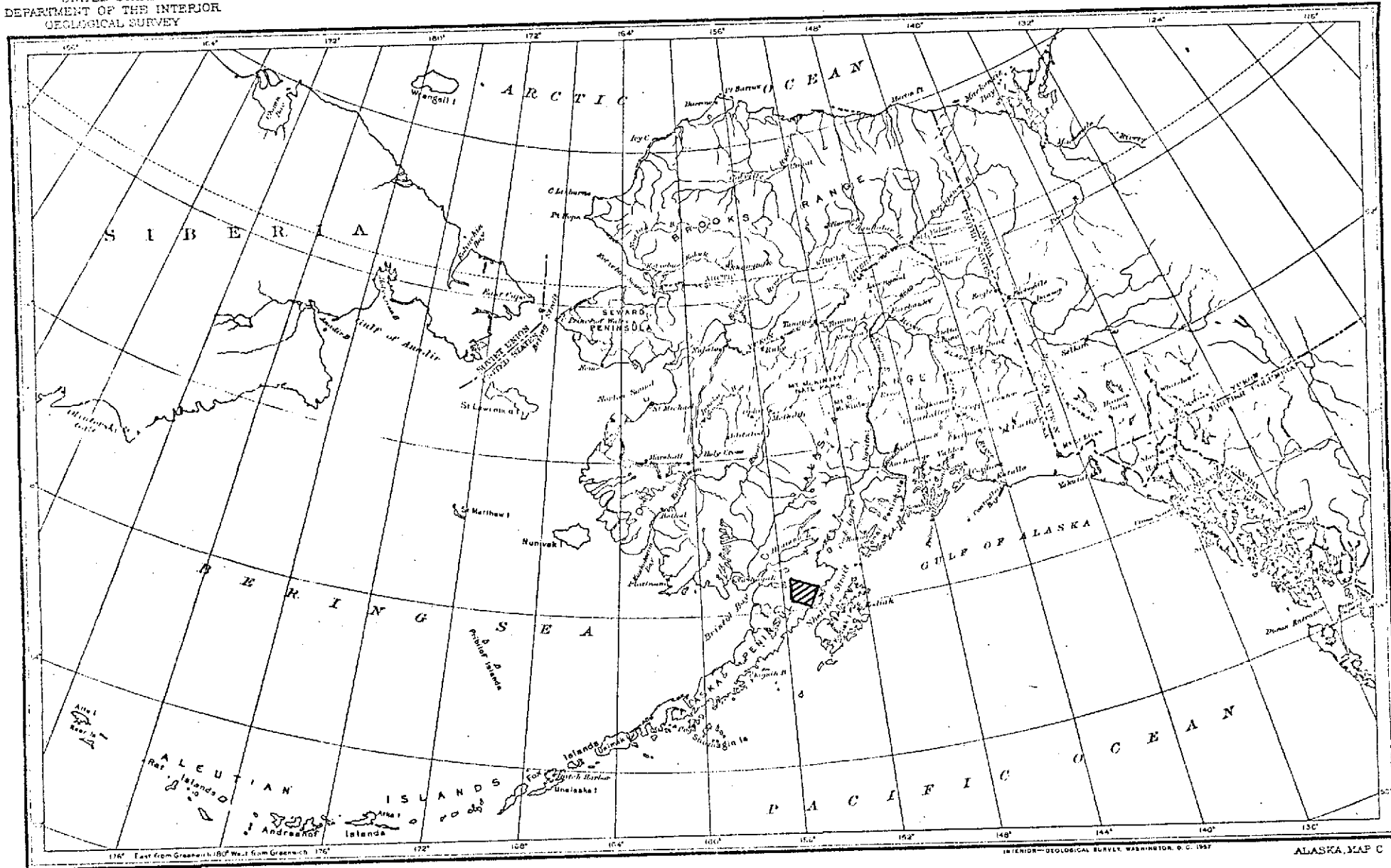
1

Fig. 1 Location map.

volcanic activity; 2) The general geology of the Mt. Katmai area, including reconstruction of the eruptive events of 1912, their origin, and the character of the pyroclastic flow in the Valley of Ten Thousand Smokes; 3) The thickness of the pyroclastic flow in the Valley of Ten Thousand Smokes using seismic, gravity and magnetic techniques; 4) The geomagnetic field anomalies associated with the volcanic activity; 5) The geomorphology and glacial features of the area.

This thesis is concerned principally with the aeromagnetic data. From the magnetic measurements, iso-intensity maps and anomally maps have been compiled.

The base camp was located on the flank of Baked Mountain, which is situated about 7 miles northwest of Mt. Katmai, and about 30 miles from Brooks Camp on Naknek Lake (Fig. 2). It was noted during the course of the investigation that the Alaska Peninsula is a storm lashed area with very unpredictable weather; the wind at times exceeding 50 m/sec. The weather is characteristically foggy, cloudy, and windy, the violence of wind being sufficient to deposit eolian sediments in the lower valley. Although the Alaska Peninsula is narrow, the Katmai National Monument area is a transition zone between the maritime climate of the Aleutian region and semi-continental climate of the terrestrial areas of Alaska.

Geology of Mt. Katmai Area

The Alaska Peninsula consists in part of thick sequences of volcanic and marine geo-synclinal sediments of Permain to Early Jurrassic age, which have been intruded by Early Jurassic granitic plutons. Minor defor-

3
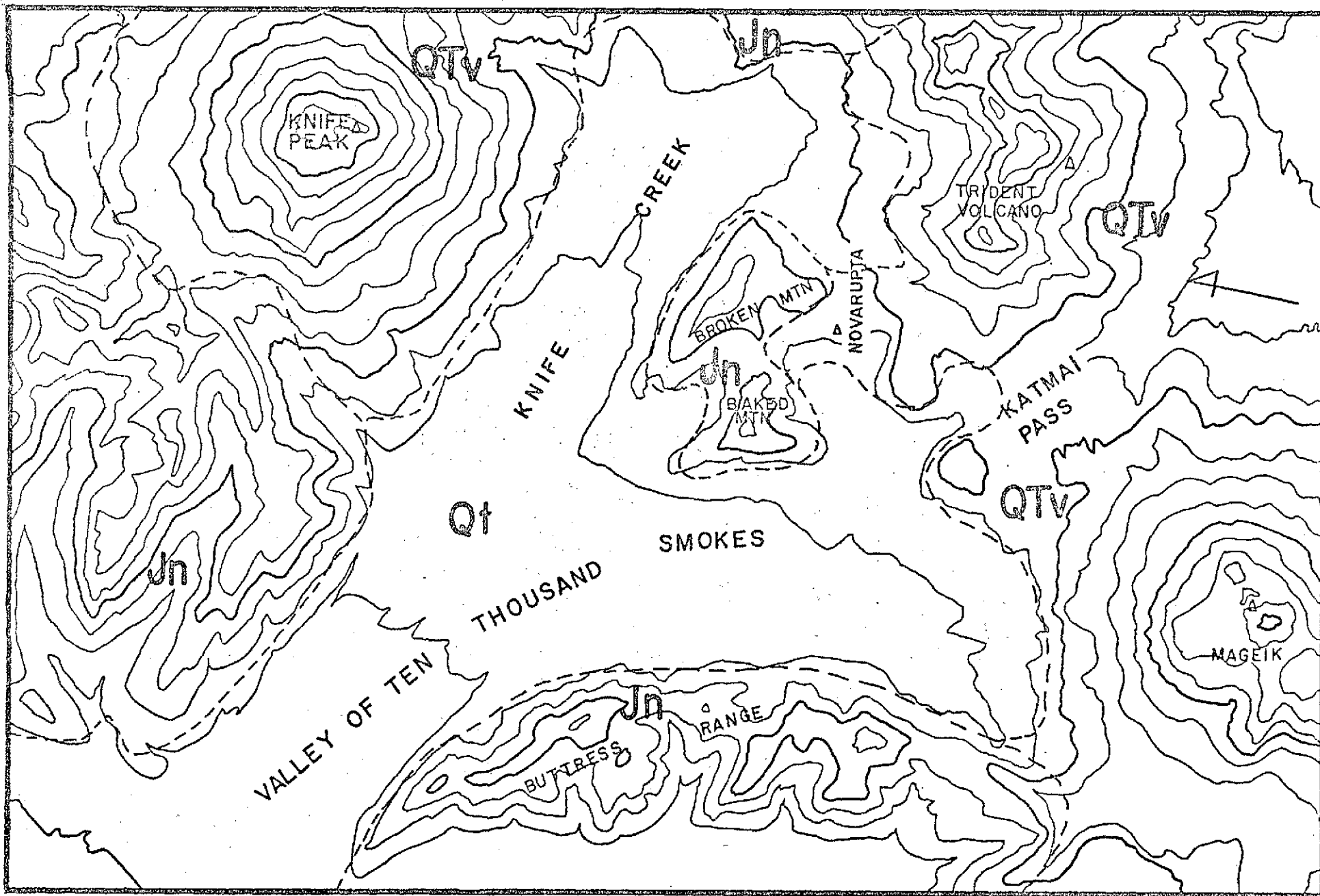
Fig. 2 Geological map of the Katmai area

Jn: Upper Jurassic, Naknek formation
QTv: Quaternary (?) volcanic rocks, chiefly andesite.
Qt: Quaternary tuff, deposited during early phase of 1912 Mount Katmai eruption.

mation and uplift occurred throughout Cretaceous, and Tertiary times, and has continued up to the present. Most of the prominent structural features of the Alaska Peninsula were formed by post Miocene deformation (Burk 1965).

It is said that the island arc volcanism began in the late Tertiary (Kagami et al 1965, Von Huene and Shor 1969) and that the main crustal movement occurred in late Pliocene times.

On January 6, 1912, the peak of Mt. Katmai disappeared accompanied by violent activity in the area, including the eruption of material from vents and/or fissures during a comparatively short time (Griggs 1920). The erupted material consisted of pyroclastics in fragmental condition as ash, lapilli, and bombs, and also Nuee ardentes. Following these events, the National Geographic Society and U.S.G.S. sponsored a comprehensive survey of the area (Fenner 1922, Griggs 1923).

Before the 1912 eruption, the only geological description near Katmai was that reported by J. E. Spurr in 1900. He traversed a deep valley (assumed to be the ancestral Valley of Ten Thousand Smokes) floored with stream and glacial debris, and says that its walls consisted of marine sedimentary rocks containing Jurrassic fossils. These rocks in the Alaska Peninsula are thought to have been lifted and intruded by granitic plutonic rocks before the Cenozoic volcanoes began to erupt.

Generally the volcanic history of the Alaska Peninsula has been characterized by a uniformly developing series, such as strato volcano erosion and/or caldera formation, followed by formation of a new central cone. In the Katmai case, the building of a new central cone has not yet occurred, perhaps because Novarupta and Trident are being formed instead.

The most noteable activity today is associated with Mts. Griggs,
Martin, Mageik, Trident, and Novarupta, and there is no sign of current
activity in the Katmai caldera.

Mt. Griggs, Mt. Mageik, and Mt. Martin are stratovolcanoes and in-
clude andesitic and dacitic lavas of Quaternary age. The lavas are of
different colors and have different mineral compositions, but are very
similar in chemical composition. This probably indicates that they were
derived from the same sources. In considering Novarupta, Williams (1954)
said that "the intimately mingled rhyolitic and andesitic ejecta of which
the avalanche deposit consists were formed, not by assimilation of old
andesitic rocks in fresh rhyolitic magma, but by simultaneous discharge
of rhyolitic and andesitic magmas from the same or closely adjacent fis-
sures. The lithological fragments of andesite and sedimentary rocks in-
cluded among the ejecta, and the banded lava in the dome of Novarupta
only showed a trivial amount of assimilation". On this basis, it would
seem that there are two kinds of magma which were erupted together. Berg
and Kubota (1967) show evidence that supports two magma chambers at dif-
ferent depths in the vicinity of Baked Mountain base camp.

In contrast to this, Fenner (1925) suggested that before and during
the Katmai eruptions, a "lake" of rhyolitic lava dissolved approximately
two cubic miles of the andesitic and sedimentary rocks of the flanks of
Katmai before being erupted as a hybrid pumice. This concept was based on
the idea of volcanic cycles (Bowen 1928) that change from basic to acidic.

At or about the same time as the glowing avalanches were discharged,
presumably from Novarupta and adjacent fissures at the head of the Valley
of Ten Thousand Smokes, the entire top of Mt. Katmai volcano collapsed,

leaving in place of its pointed peak an oval crater almost 5.0 km long
and 3.2 km wide. It seems probable that a connection between Katmai and
Novarupta existed at some depth, perhaps in the form of lava conduits.
During the final phase of the eruption, rhyolitic lava issued sluggishly
to build a dome within the Novarupta Crater. According to Williams, the
main eruption of Novarupta certainly occurred after the collapse of Mt.
Katmai.

Williams classifies volcanic calderas as of Krakatoan type, when
the caldera is associated with voluminous explosive eruptions of siliceous
magmas, and of Katmai type when the collapse results from drainage of the
central conduit of a volcano and perhaps also of some of the underlying
reservoir by discharge of magma through adjacent conduits. He claims that
"the top of Mt. Katmai collapsed in 1912, when its central conduit was
drained by eruption of ash and pumice flows from vents in the adjacent
Valley of Ten Thousand Smokes".

Naknek Formation

The name Naknek Formation is applied to a sequence of rocks of late
Jurrassic age, locally having a basal conglomerate member. This basal
member is identified by Mather (1963) as the Chisik conglomerate, based
on the lithologic similarities of the conglomerate in Mt. Katmai area
to the one described by Martin and Katz (1912) in the Iliamna Lake region.
The upper part of the Naknek formation in the Katmai area consists of
marine sandstone, silts, shales, and occasional lenticular fossil beds.
Rocks of the Naknek formation are wide spread on the Alaska Peninsula as
well as in other areas. The upper parts of Naknek Formation are Kimmerid-
gian to basal Portlandian in age (See Fig. 3).

—Correlation chart of Cenozoic rocks of Alaska Peninsula and adjacent areas. asterisk indicates type locality.

AGE	COLD BAY AREA	PORT MOLLER UNGA IS. AREA	MT. YENLAMINOF AREA	CHIGNIK BAY AREA	KUJULIK AREA	KATMAI AREA	KODIAK AREA	COOK INLET
RECENT AND PLEISTOCENE	Alluvial-Glacial	Alluvial-Glacial	Alluvial-Glacial	Alluvial-Glacial	Alluvial-Glacial	Alluvial-Glacial	Alluvial-Glacial	Alluvial-Glacial
PLIOCENE	Techilni Fm.* / Volcanic Rocks	Marine Clastic Rocks / Volcanic Rocks	Absent ? / Volcanic Rocks	Absent ? / Volcanic Rocks	Absent ?	Absent / Volcanic Rocks	Not Exposed	Absent ?
MIOCENE	? Bear Lake formation	Bear Lake Fm.* / *Unga Cgl. Mbr.	Bear Lake Formation	Bear Lake Fm. / Not Recognized	Present in subsurface	Absent	Marine Clastics	Kenai Fm.* (Non-marine)
OLIGOCENE	Not Exposed / Beaver Bay Group / Belkofski Formation*	Beaver Bay Group / Stepovak Formation*	Beaver Bay Group / Stepovak Formation	Absent ? / Meshik Formation*	Absent ? / Meshik Formation	Largely Nonmarine Clastic Rks	Largely Nonmarine Clastic Rocks	
EOCENE		Tolstoi Formation*	Tolstoi Formation	Tolstoi Formation	Tolstoi Formation	Largely Volcanic Rocks		
PALEOCENE	Not Exposed							
Underlying Rocks		Hoodoo Fm. / Chignik Fm.	Hoodoo Fm. / Chignik Fm.	Hoodoo Fm. / Chignik Fm. / Naknek Fm.	Hoodoo Fm. / Chignik Fm.	Naknek Fm. / Older	Slated Graywacke	Cretaceous Upper Jur.

AGE		CHARACTERISTIC ALASKAN FOSSILS (After Imlay, 1959)	PORT MOLLER	CHIGNIK BAY	MOTHER GOOSE-WIDE BAY AREA	KATMAI AREA	ILIAMNA VOL.
Overlying Rocks			Upper Cretaceous Chignik Formation		Tertiary / Kaguyak Fm.	Tertiary	
L. CRETACEOUS NEOCOMIAN	Barremian	No fossil evidence	HERENDEEN LIMESTONE (0'-500')				
	Hauterivian		(0-2000')				
	Valanginian	Buchia crassicollis		(0'-2000')	(0'-2000')		
	Berriasian	Buchia sublaevis / B. okensis / B. subokensis				Absent ?	Absent
		No fossil evidence					
UPPER JURASSIC	PORTLANDIAN	Buchia piochii	STANIUKOVICH FORMATION* / Arkosic ss. and sltst.	STANIUKOVICH FORMATION / Arkosic ss. and sltst.	STANIUKOVICH FORMATION / Arkosic ss. and sltst.		
	KIMMERIDGIAN	B. mosquensis and B. rugosa	(3,000'+) NAKNEK FM. / Arkosic ss., sltst., cgl., claystone	(5,000'+) NAKNEK FM. / Arkosic ss., sltst., cgl., claystone	(5,000'+) NAKNEK FM. / Dark sltst. and fine ss.	(10,000'+) NAKNEK FM.* / Dark sltst. and fine ss.	(5,600'+) NAKNEK FM. / Arkosic ss., some cgl., tuff.
		Buchia concentrica			Arkosic ss., sltst.	Arkosic ss., sltst., cgl.	
	OXFORDIAN	Amoeboceras (Prionodiceras)	Not Exposed	Not Exposed	"Chisik Cgl."	"Chisik Cgl."* Member	(500'-1300') Siltstone, arkose / (0'-400') Chisik Cgl.* Member
		Cardioceras spp.					
Underlying Rocks					*Shelikof Fm.		*Chinitna Fm.

Fig. 3. Correlation chart of Upper Jurassic-Cretaceous rocks of Alaska Peninsula. Asterisk indicates type locality. GEOLOGY OF THE ALASKA PENINSULA (after Burk 1965)

8

Tertiary Deposits

Tertiary coal bearing rocks are present on the Kenai Peninsula, and east of Mt. Katmai areas. They locally interfinger with volcanic rocks which may be of Eocene age (Keller and Kieser 1959). The formation consists of abundant nonmarine conglomerates, sandstones, silts and coal bearing mudstone. These appear to be lagoonal or swampy sediments and were probably deposited in Eocene times. These coal bearing formations may be comparable with the Kenai Formation which has been disturbed by Miocene to recent movement. However, directly comparable rocks could not be found in the survey area.

Volcanism began at least as early as Eocene time and continued through the Tertiary and Quaternary period to the present. Tectonic activity along parts of the circum Pacific belt has continued at least since Mesozoic times, but the main movement may have occurred between Pliocene and Pleistocene times. There are, however, no signs of a marked change in relative motions similar to those that produced the predominately Miocene volcanism and "green tuff movements" of Japan (Minato, Gorai and Funabashi 1965).

Surficial deposits in the Katmai area are predominately alluvial gravel and glacial moraine, these deposits produced the periglacial and proglacial areas in late glacial ages. Iluk Arm Lake and Brooks Lake show excellent examples of moraine deposits.

Very recent deposits are dominated by the emplacement of the thick tuff deposits of the eruption of Mt. Novarupta. This has been discussed in detail by Griggs (1922), Fenner (1923), and Forbes (1970).

Tectonic and Volcanic Setting

The eastern Aleutian Trench lies parallel to the Alaska Peninsula and seems to disappear beneath the Alaskan Mainland.

The Eastern Aleutians have an arcuate shape of $\sim$ 1380 km radius, centered off Nome; the trench is an asymmetric V-shaped and generally broad depression. It has half graben fault structure on the continental slope side, and is filled with flat-lying undeformed sediment (VonHuene and Shor 1969). The Alaska Peninsula has three main echelon fault blocks which are bounded on one side by a steep reverse fault; these have formed the complex faulted anticlines of Pliocene age (Burk 1965) (Fig. 4).

Burk (1965) in his description of the geology of Alaska Peninsula and the adjacent continental shelf, noted that the present eastern Aleutian Trench could not be older than early Tertiary and possibly much younger.

Hamilton (1966) has estimated the age of the trench as Cretaceous to Miocene, favoring Eocene. However, the eastern Aleutian trench is not very deep, so that it appears more as a trough than a trench as opposed to the western Aleutian island arc which has a well-developed deep trench.

The Alaska Peninsula volcanism and associated trench have only shallow earthquakes indicating a low angle Benioff Zone and also thin undeformed sediments in the trench. This may indicate a young age.

The distance between the trench and volcanic front is about 150 $\sim$ 200 km, the depth of the earthquake zone beneath the volcano line is 80 km so that the angle of the earthquake zone can be calculated to be about 20 degrees.

Kanomori (1970) maintains that because of the relatively shallow

10
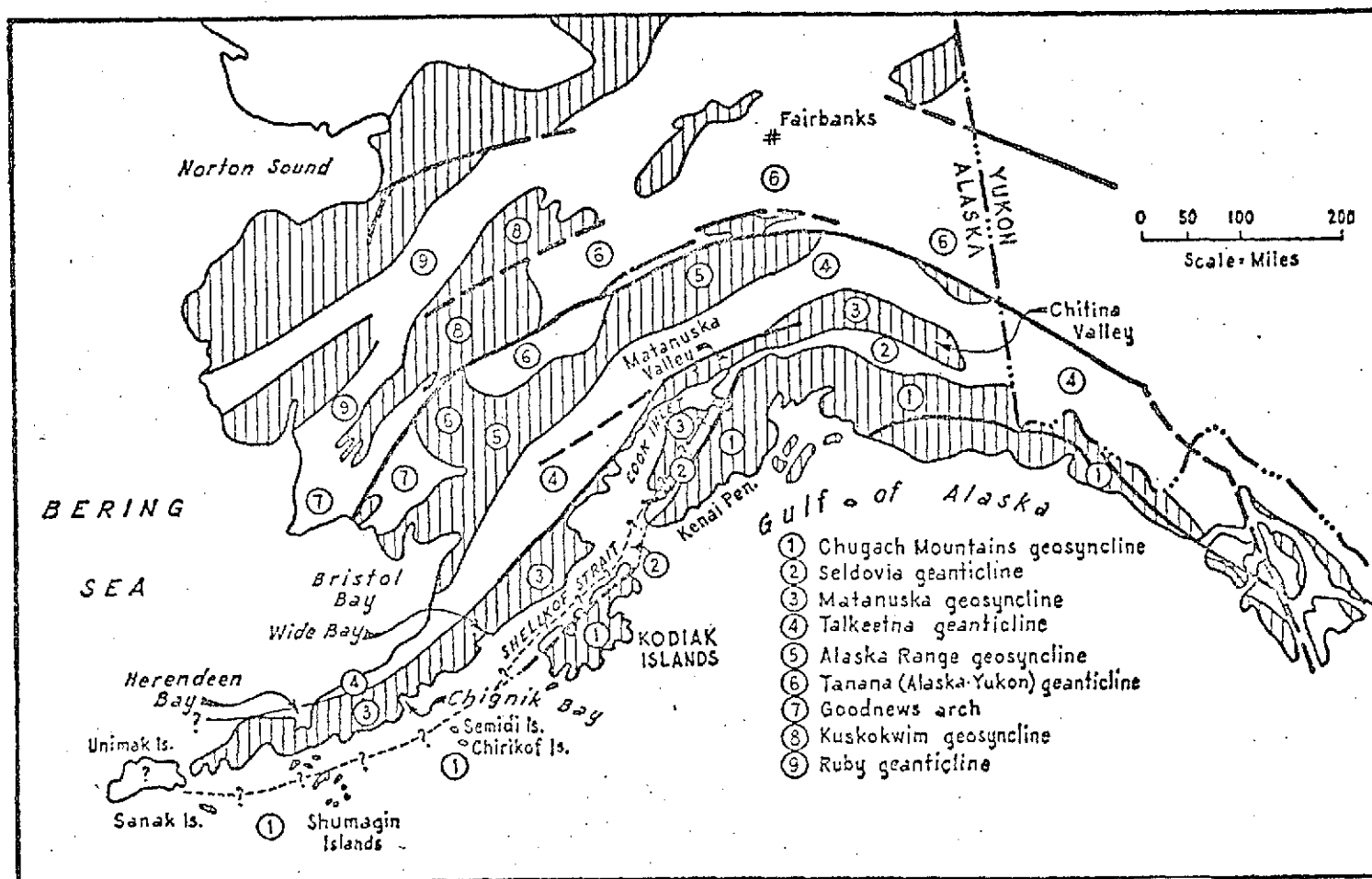
Fig. 4. Late Mesozoic tectonic elements of southern Alaska, modified from Gate and Cryc (1963), Miller and others (1959), and Payne (1955). Areas of deposition are hachured, and areas apparently eroded are blank. Major faults are shown by heavy lines (after Burk 1965).

depth, the temperature and pressure are not enough for large scale melting of magma, hence large stresses can be built up resulting in larger earthquakes in the area.

The origin of andesites from calc-alkali rock series and their bearing on island arc structures was discussed by Kuno (1963). He discusses the possibility of producing the successive magmas by fractionation of a basaltic parent magma. For example, northeast Japan may be divided into zones of tholeiite, high alumina basalt and alkali olivine basalt arranged in order from the Pacific side of the islands toward the continental side. In general, it is found that the pigeonitic rock series, the high alumina basalt series and alkali rock series occur in their respective zones.

Using Kuno's classification of magma, the Aleutian volcanic rocks were generated from a tholeiitic magma. However, the rocks belong to high alumina basalt (Ray 1967), (Sugimura 1967), so parent magma would have to have high alumina and alkali basalt affinities (Ray 1967). Such melts could be derived from the partial fusion of a basaltic layer at the base of the crust. Kuno pointed out that the type of volcanic rock correlates with the depth of the seismic zone. If magma is generated at the seismic zone, tholeiitic basaltic magma would be generated at 130 ∿ 160 km, high alumina basalt at 160 ∿ 250 km, and alkali basalt magma at more than 250 km.

On the other hand, Sugimura (1963) proposed a classification of island arc rock series using an index which is computed according to the formula:

$$\theta = SiO_2 - 47 \ (Na_2O + K_2O) \ / \ Al_2O_3$$

where SiO_2 is in weight per cent and the other oxides in molecular proportion. The value 47 used comes from determination of the values "a" and "b"

W ←   θ̄ = 41.3   → E

Front of the East Japan
Volcanic Belt

θ̄ = 37.5

3,000 km³

θ̄ = 35

θ̄ = 33

580 km³

65 km³ 140 km³

Earth's Surface

Tholeiite Magma

High-alumina
Basalt Magma

Alkali Olivine
Basalt Magma

100

Deep Earthquake Foci

200

300

km   200   100   0 km
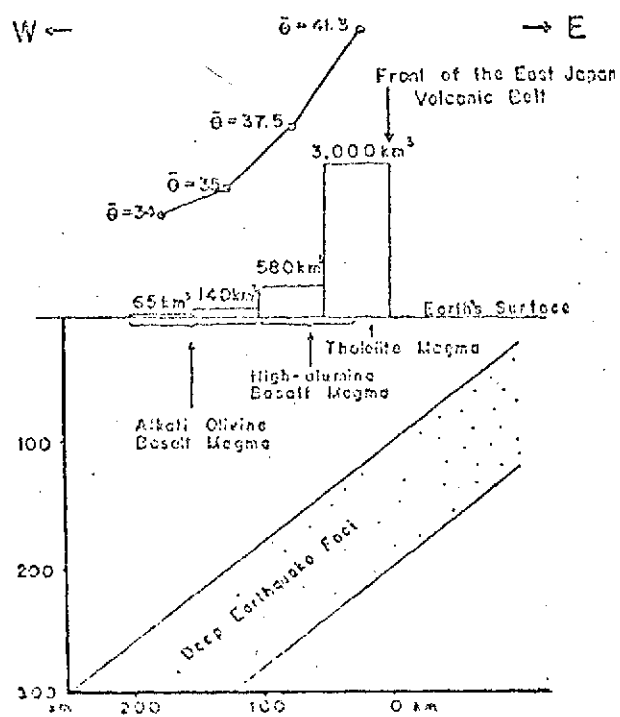
Fig. 5.   Graph showing the spatial variation of
the θ-value and the volume of the Quaternary
volcanic materials across the East Japan
volcanic be t (after Sugimura 1967).

for the relation $SiO_2 = a + b (Na_2O + K_2O) / Al_2O_3$. Studies in Japanese

Islands show that the isobaths of the seismic plane (mantle earthquakes)

are parallel to the volcanic front and also to the boundary lines of

petrologic provinces. This relation is also found in the Aleutian arc,

though the petrologic boundary is not as clear (Barazangi and Dorman 1969).

The volume of the volcanic material decreases with the increase in

distance from the front (Sugimara and Uyeda 1968). It is found that the

Θ - index at the volcanic front is the highest for any part of a given

island arc (Fig. 5). For the Aleutian arc it seems to be generally con-

stant as follows:

TABLE I

N. E. Umnak	36.9
S. W. Umnak	39.0
Adak	35.3
Makushin	37.5
Eider Point	36.1
Kiska	39.1
Little Sitkin	38.3
Trident*	36.88

(after Sugimura),* calculated from (Forbes et al 1967)

The volcanic front of an island arc may be used as one of the char-

acteristics of the primary magma for the island arc.

Gravity Data

A local negative gravity anomaly has been mapped in the Katmai area

by Kienle (1968); -20 ∿ -35 mgal anomaly is centered on the flank of Mt.

Trident (Fig. 43). Kienle (1969) interpreted this anomaly as due to a

very shallow mass deficiency near Mt. Trident, the maximum depth to its

center being about 3 km. The density contrast between andesitic magmas

and the host rock at Mt. Trident are such that the mass deficiency cannot

be due to an andesitic magma chamber. It is interpreted as a volume of

host rock heavily impregnated with low density vesicular andesites and therefore the gravimetrically detected mass deficiency under Mt. Trident may be related to the chambers discovered seismically that underlie the area at about 10 km depth (Kubota and Berg 1967). Kubota and Berg (1967) also claim a direct relationship between Mt. Katmai and Mt. Novarupta, however, the proposed chambers have diameters of no more than 5 km and a 10 km depth.
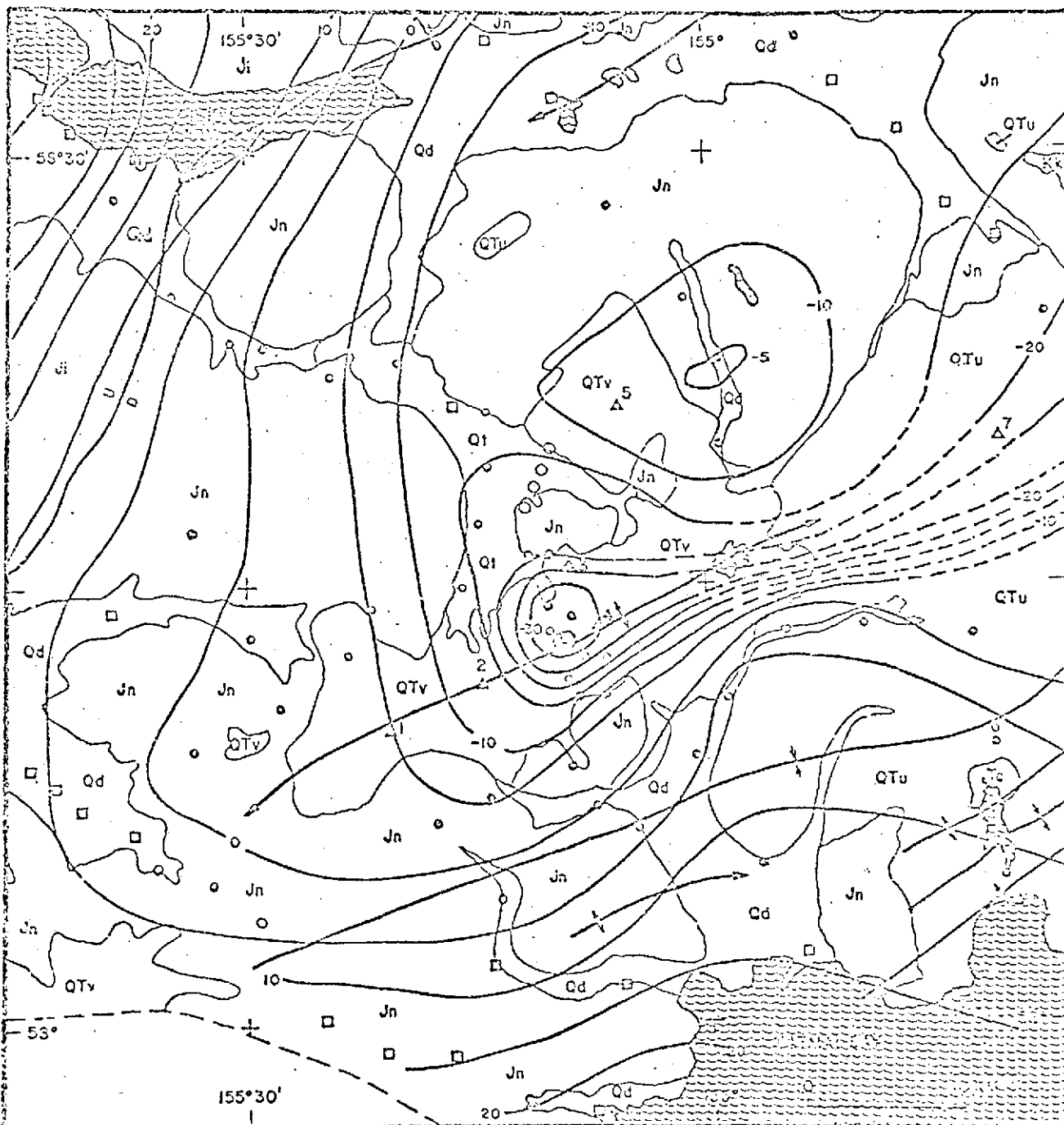
Fig. 6.   Complete Bouguer (2.67) gravity map of the Mt. Trident-Knife
          Peak area.

KM 0 5 10 15 KM

KM
0

-10

-20

-30

SALIC
MAGMA

MAFIC MAGMA

?

MOHO
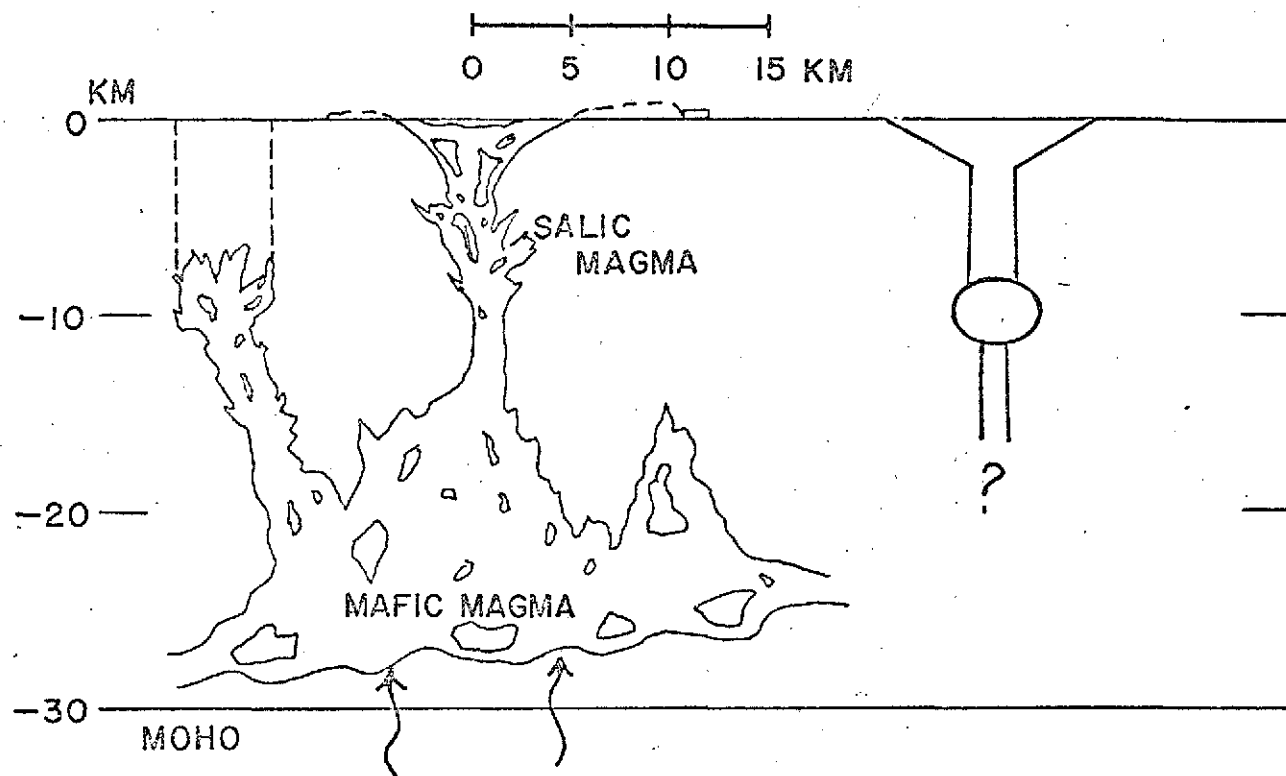
Fig. 7.   Imaginary cross section of Crater Lake type Caldera.

CHAPTER II

METHODS AND TECHNIQUES

Equipment

The proton precession magnetometer measures only the total magnetic intensity. It was first used to measure the Earth's field by Packard and Varian (1954). The method depends on the fact that in the presence of a magnetic field the spin axes of a small proportion of the protons in liquids such as water, become aligned in the direction of field; if the direction of the field changes, the protons will precess about the new field direction with a frequency given by $2\Pi f = r_p F$ where r_p is the gyromagnetic ratio of the proton, and F is the field strength in gauss. The value of r_p adopted by the IUGG is $r_p = (2.67513 \pm 0.00002) \times 10^4/\text{Oe. sec.}$

The working relation for F is the $F = 23,487.4f$ gammas, $(F = 234,874 \times 10^{-6} f \text{ gauss})$. For the Earth's field f lies between 1.5 and 3.0 kc/sec.

The equipment supplied with a magnetometer includes the sensing element, magnetometer console, interconnecting cable, and their associated power supplies. The sensing element is a toroidal coil surrounding a hydrocarbon fluid with selected characteristics. This is mounted in a container suitable for the proposed application, i.e., a "bird" or a "fish" for airborne or seaborne work. The hydrocarbon used in this case was kerosene. By energising the coil surrounding the hydrocarbon, the protons were aligned in the direction of the applied field. After allowing a few seconds for the alignment of the protons to reach equilibrium, the polarizing field is suddenly removed. The aligned protons then precess round the Earth's field, causing an alternating voltage, initially of the order of 1 μV, to be induced in the coil. This voltage, which

decays as precessional coherence is lost, is applied to a frequency-measuring circuit through a tuned high gain amplifier. The minimum operating cycle for reliable results is about .3 sec.

In practice, the coil is arranged co-axially with respect to the head, so that it makes a satisfactory angle with the geomagnetic field everywhere except on headings close to the magnetic meridian near the magnetic equator.

A system employing two mutually perpendicular coils may be used any where.

The general arrangement of a magnetometer using this method of measurement is shown in Fig. 8.

The console operates directly from a source of DC power ranging from 22 volts to 32 volts.

The time sequence is shown in Fig. 9.

One of the portable proton precession magnetometers was used as a base station to record the daily variations. The sensor was set on the top of an 2.4 m foot pole near the base camp. The principle of operation is the same as for the above equipment.

The recorder has a somewhat small scale and in reading the variations the reading errors are about ± 5 gammas. The daily variations at the base camp are shown in Fig. 13.

The second portable magnetometer was used for ground surveys, and is useful for accurate investigations of small areas to look at shallow structures.

The airborne survey was carried out using a Hiller 12E helicopter. The bird was lifted from the ground on the end of its 80.5 m cable by taking off vertically. Landing was done using the reverse procedure. The

19
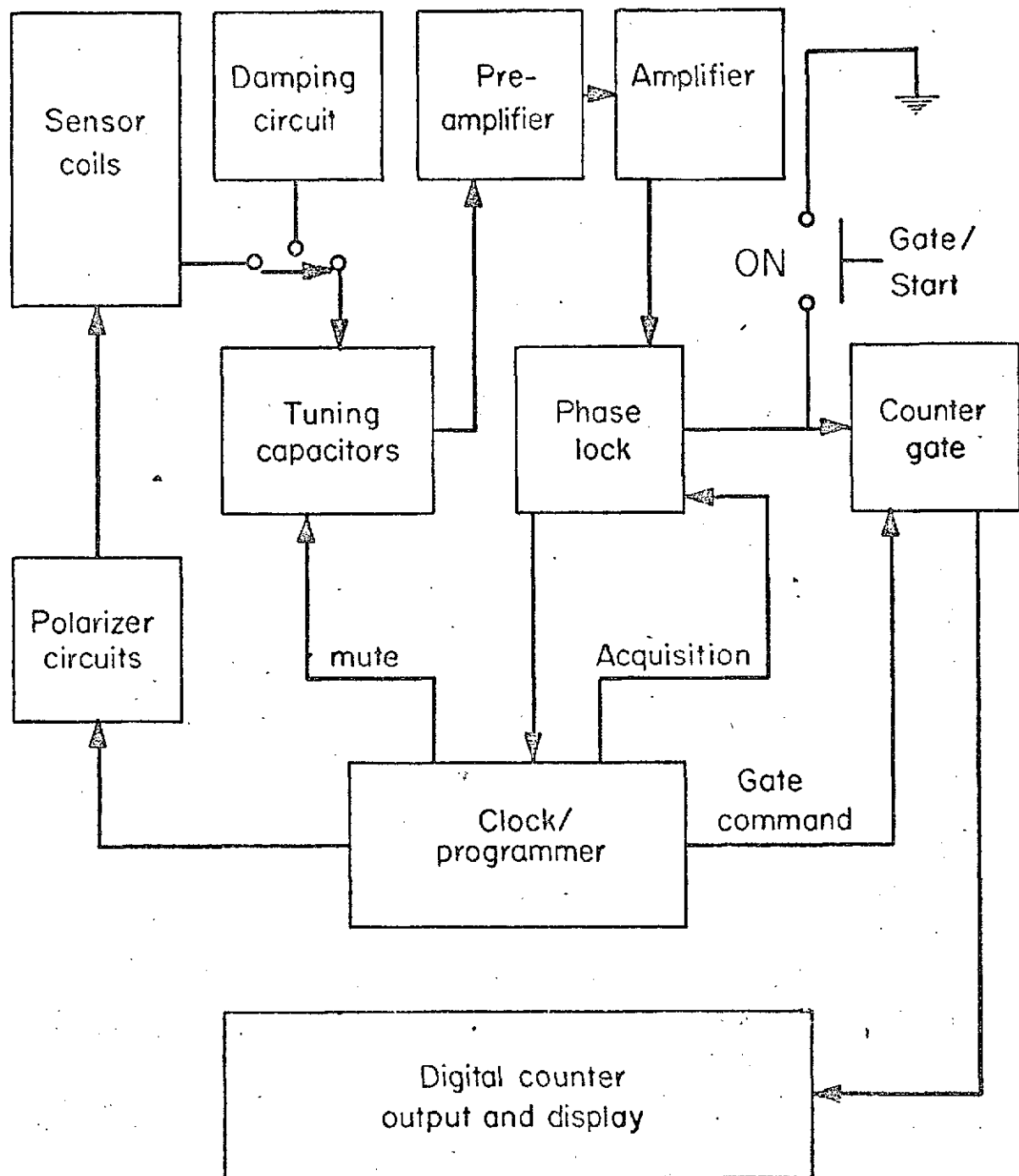
Fig. 8. Signal Flow Block Diagram.

20

POLARIZE
INTERVAL

DISPLAY RESET

READ INTERVAL

XFER. TO MEMORY

THE TRAILING EDGE
MAY BE USED TO
COMMAND EXTERNAL
EQUIPTMENT

Fig. 9. Time Chart.

21
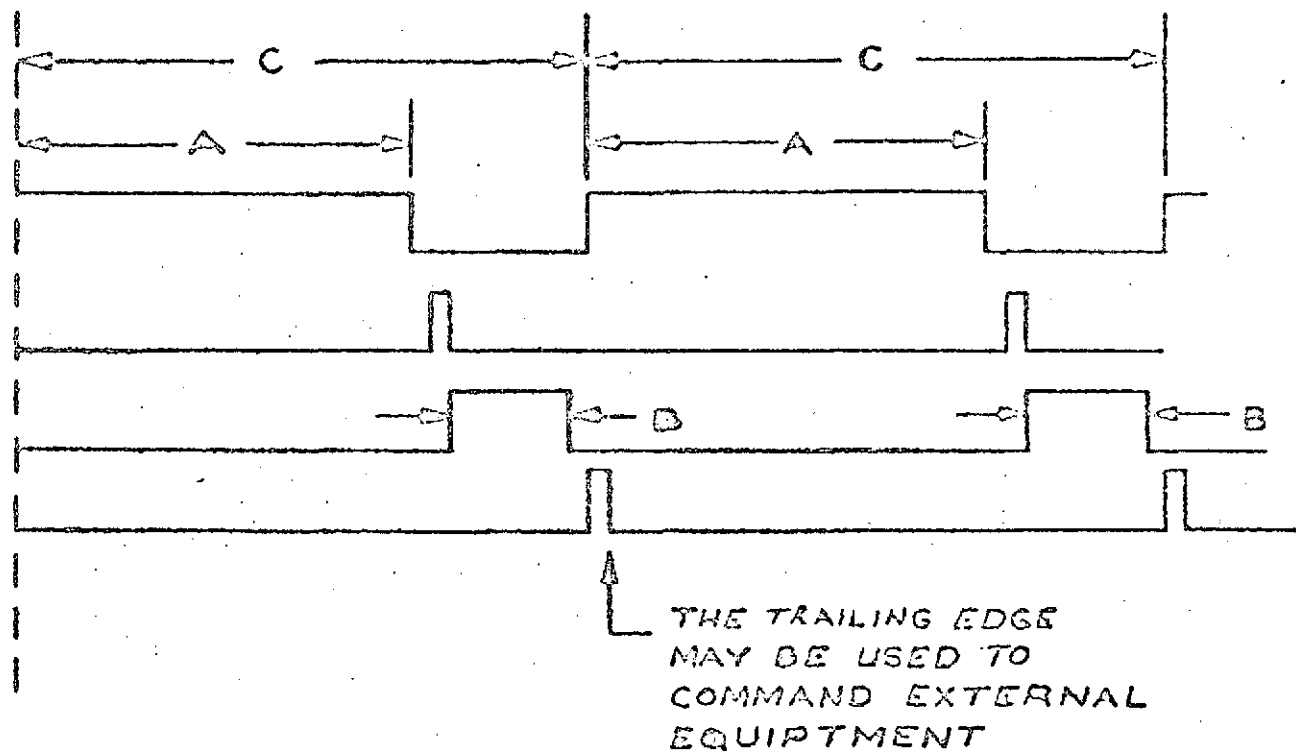
Hiller 12E helicopter is small and only allows two people together with the magnetometer.

Methods of Investigation

Airborne surveys are usually made along a series of parallel traverses oriented as closely as possible to right angles to the trend of the geologic units. The direction may be chosen parallel to some obvious geographic feature to aid navigation. The spacing between traverses is usually one chosen to be approximately equal to or less than the depth of burial of the magnetic source. Perhaps the most difficult problem in an airborne survey is to determine the location of aircraft at any instant in time. The position of a number of distinct points such as mountain tops, cliff edges, and creek or stream junctions were located on maps, and in some cases large red panels were laid out for landmarks.

The landmarks could be clearly seen from the start and end positions of each flight line, a direct course between them being flown by eye. The beginning and end points, and the crossing of intermediate landmarks were also judged by eye, each being marked on the magnetometer recording using a hand controlled event marker. Because it is possible to fly slower, surveys using helicopters are easier than those using fixed wing aircraft, however, altitude, speed and direction are not as stable.

To process the data the magnetometer chart was divided into one-tenth mile sections by extrapolation of the known distances between navigation points on the map, and the length of record between successive marks representing these landmarks. The precision of this method is not high, and differences can be seen in the same line flown twice at different altitudes, however, as each line was flown at least twice in opposite

22

directions (Fig. 16), and the anomalies are generally very large, this is not considered a serious hazard.

Interpretation of the magnetic profiles depends on ground elevation, the flight altitude was recorded manually and the ground elevation read off the map for each of the profiles. The flight directions were often at different azimuths which were also recorded. Many of the flight lines concentrated around the center of Novarupta.

The starting point and end points were either marked with flags on the ground or consisted of conspicuous topographic features, which were located using a geodimeter and a theodolite.

The plotting was done on a 1:21,120 scale map. Because of the errors inherent in the method, the cross points of different lines are not well defined, however, they are very close.

Data Analysis

The total intensity of the magnetic field at any point on the surface of the earth can be obtained mathematically by means of a harmonic analysis of values obtained by direct observation; potential,

$$w = a \sum_{n}^{\infty} \sum_{n}^{n} (g_n^m \cos m\phi + h_n^m \sin m\phi) P_n^m (\cos \phi),$$

where the values of a, g, h are known, and assuming no crustal sources contribute sensibly to the harmonics of degree less than n.

The magnetic field at the Earth's surface (Fig. 10) can be represented approximately by the field of an eccentric dipole. The difference between the observed field and the field generated by a dipole is considered as the anomalous or non-dipole field. The anomalies that are generated in magnetic materials in the Earth's crust are called regional anomalies and are assumed to be due to magnetic minerals. These can only ex-

23
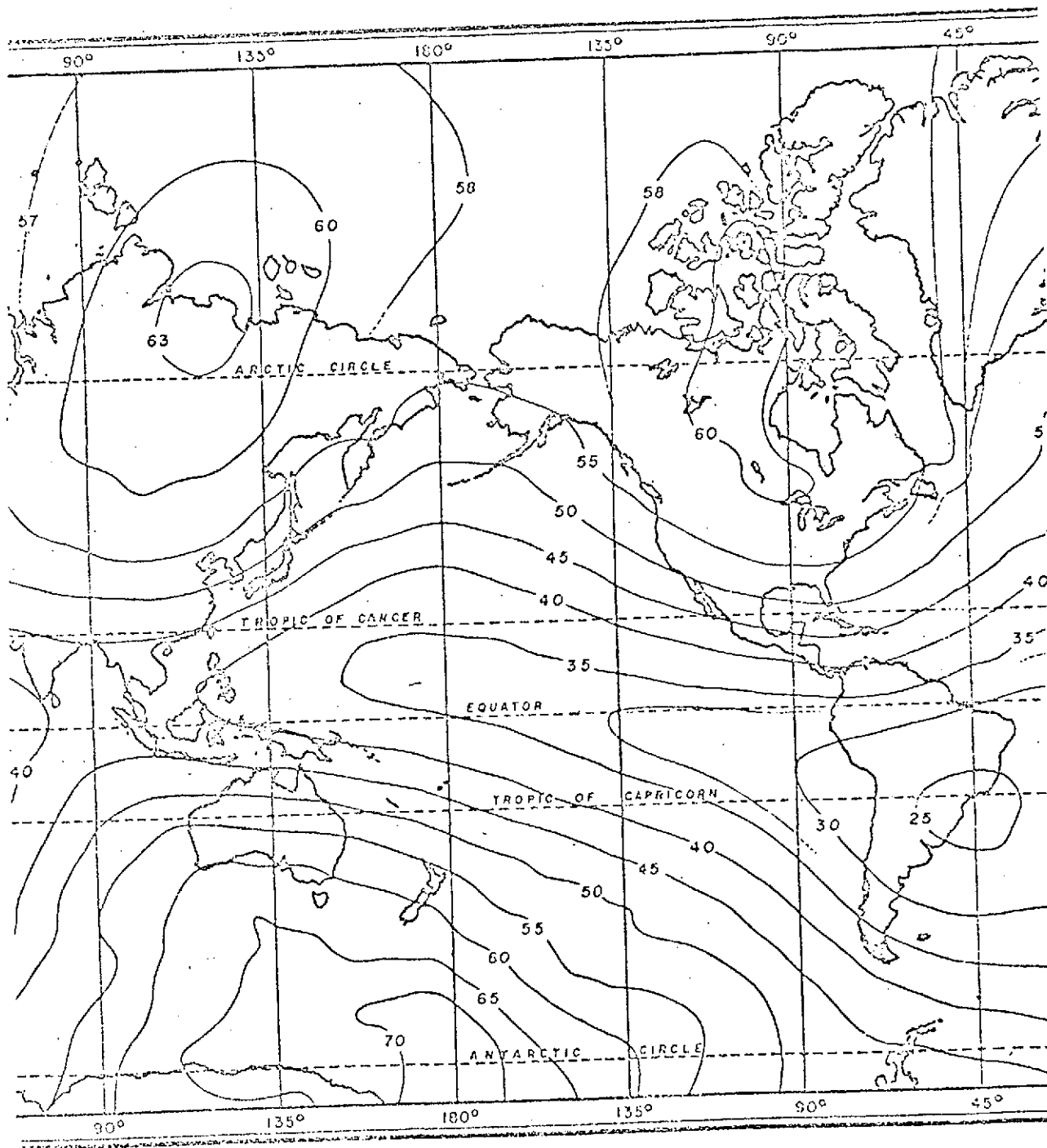
Fig. 10. The total intensity of the earth's magnetic field expressed in kilogammas.

ist up to the Curie temperatures of the minerals causing them, so must be located relatively near the surface of the crust.

Regional intensity anomalies are often related to magnetite deposits or rocks rich in magnetite, and the wave length of the anomaly give an indication of its depth. Long wave anomalies usually indicate that the magnetic body is situated at greater depths.

The earth's magnetic field increases in intensity from south to north at a uniform rate of 4-5 gammas per mile (Brosge and others 1970). The Katmai area has such high local gradients and is so small that it is reasonable to neglect this gradient and use the mean values derived from the average of all the data as the base value (53655 gammas). The true value should be obtained from a spherical function of the earth's magnetic field, but as it is only the relative intensities related to local structures that are of interest, the total magnetic intensities used were obtained from:

$$F_{ob} - F_m = F_{an}$$ where F_{ob} = observed value

F_m = mean value

F_{an} = magnetic anomaly

Any anomalies found indicate a source underground, such as high magnetic susceptibility rocks, or non-magnetic materials, the later appearing as a relative decrease in magnetic intensity. If we know the regional field, it is possible to calculate the magnetic dipole moment of a source capable of producing the observed anomaly. In the case of an aeromagnetic survey, that calculation is not important, because the magnetic intensity is inversely proportional to the cube of the distance from the magnetic body The surveys flown at a high altitude in Katmai give intensities that are almost the same as the Earth's magnetic dipole field, except in the

25

vicinity of Novarupta.

The instrument drift was checked, and daily variation eliminated by
means of measurements made at the base station. The aeromagnetic data
were corrected for daily variations, when magnetic disturbances exceeded
the base value of 53700 ± 5 gammas.

In the auroral zone magnetic disturbances show large variations with-
in short distances, though the distances are still large compared with the
scale of the Valley, so any important variation would have been seen
at the base station.

The reduced total intensity anomaly maps shown below were compiled
from this data using an IBM 360 computer and the program given in Appen-
dix II.

Interpretation of Model Studies

It is possible to estimate the volume and depth of a magnetic body
from the anomalous field produced at the surface. This will be due to the
total intensity of the Earth's magnetic field plus that due to the buried
magnetic material. The intensity of a given magnetic body can be calcula-
ted as follows (Fig. 11):

let F = total intensity observed

   H = total intensity of the regional field

   B = field due to the buried mass

Using a coordinate system with its origin at the dipole representing the
buried mass, and letting

   θ = the angle to the observer relative to the dipole axis

   m = the effective dipole moment

   r = the distance from the dipole center to the observer

26
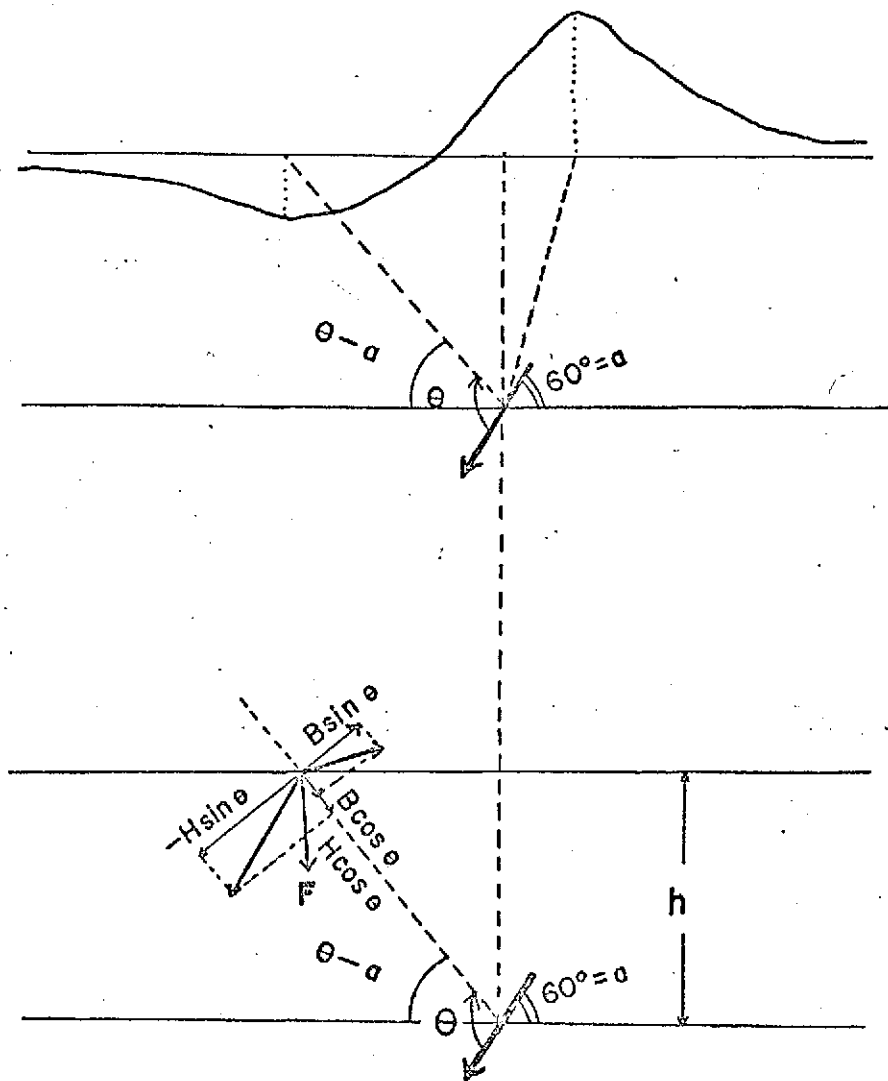
Fig. 11. Idealized model profile and vector composition (see Model Studies p.   ).

then

$$\vec{H} = H_\theta \vec{1}_\theta + H_r \vec{1}_r$$

$$\vec{B} = B_\theta \vec{1}_\theta + H_r \vec{1}_r$$

where

$$B_0 = \frac{m}{r^3} \sin\theta, \qquad\qquad B_r = \frac{2m}{r^3} \cos\theta$$

$$H_\theta = -H\sin(\pi-\theta) \qquad\qquad H_r = H\cos(\pi-\theta)$$

$$\vec{F} = \left(\frac{2m}{r^3}\cos\theta + H\cos\theta\right)\vec{1}_r + \left(\frac{m}{r^3}\sin\theta - H\sin\theta\right)\vec{1}_\theta$$

then the total intensity

$$F = \sqrt{(F_r^2 + F_\theta^2)} = \sqrt{\left\{\cos^2\theta\left(\frac{2m}{r^3} + H\right)^2 + \sin^2\theta\left(\frac{m}{r^3} - H\right)^2\right\}}$$

where

$$h = r\sin(\theta-a)$$

therefore

$$F = \sqrt{\left\{\cos^2\theta\left(\frac{2m}{h^3}\sin^3(\theta - a) + H\right)^2 + \sin^2\theta\left(\frac{m}{h^3}\sin^3(\theta-a) - H\right)^2\right\}}$$

We can get the model profiles from above equation for any given volume, magnetic moment and distance.

Measurements

A series of flight lines was proposed on the basis of the ground survey made in 1969 by M. Trible (1971). In practice the lines flown depended on the weather, and it was not possible to make a systematic survey. The aeromagnetic survey was carried out between July 8 and July 28. As a result, the flight altitude direction and helicopter speed were variable. The flight lines were concentrated in the vicinity of Novarupta, but a number of Valley crossings were also made.

2.4 M (8 feet)

620	655	651	677	645	688	704	702	706	707
600	622	618	621	648	666	721	715	654	707

5.0 m

4 feet

53750—

8 feet

53650—

1.2 M (4 feet)

750	764	744	772	735	778	796	779	775	751

Basic Station

715	738	706	726	672	671	730	822	782	703

53750—

4 feet

53650—

8 feet
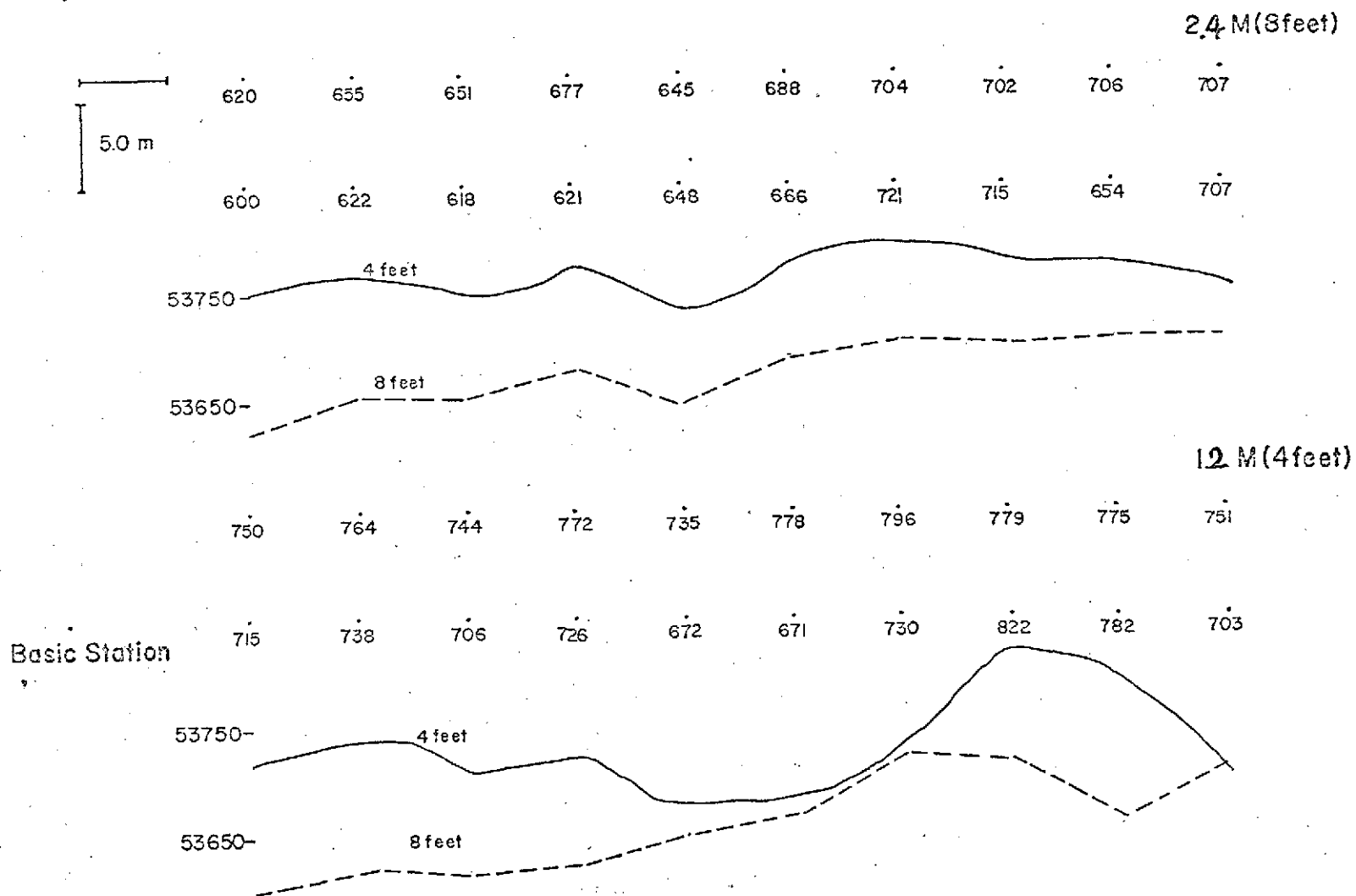
Fig. 12. Total magnetic intensity profiles near Base Camp (BMC).

08.00 09.00 10.00 11.00 12.00 13.00 14.00 15.00 16.00 17.00 18.00 19.00 20.00

JULY 13

JULY 15

JULY 16

53700 JULY 17

50 gammas

JULY 18

JULY 19

JULY 25

JULY 28

JULY 4,5,1971
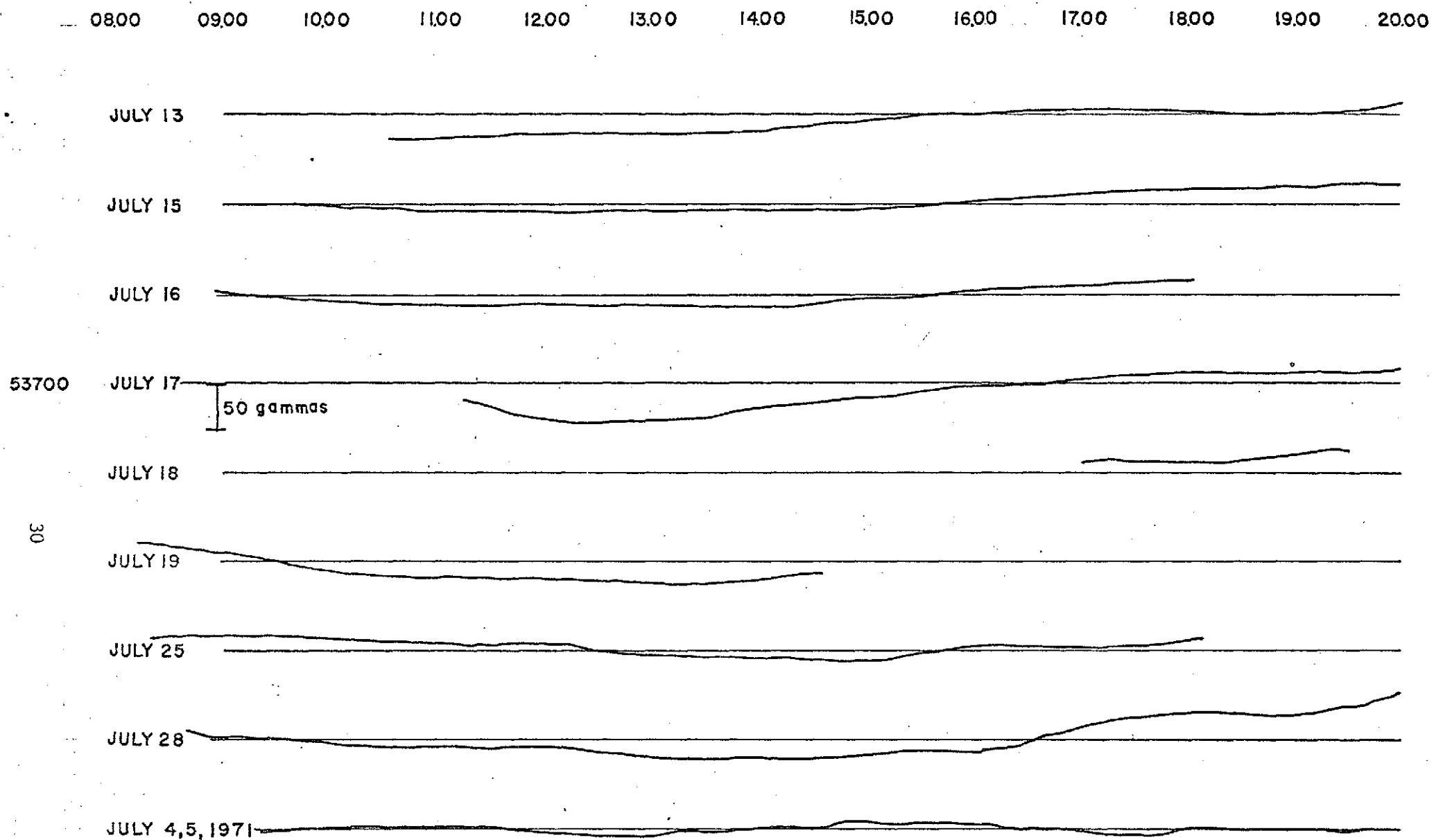
Fig. 13. Daily variation of total magnetic intensity on the Baked mountain camp
(4 feet pole). Base line for each day 53700 gammas.

A base station was established at Baked Mountain camp, the location of which is 58°17.5'N, 155°12.0'W and the elevation is 899.3 m. To obtain a value for the magnetic intensity at the base camp, two lines 66 m long and 0.6 m apart were marked with stakes at 0.6 m intervals. Magnetometer readings were made at each stake, the variation of intensity was 100 gamma over this area. Measurements were made at two probe heights, 2.4 m and 1.2 m from the surface (Fig. 12). The upper values show small differences from the lower ones, the mean values being 53680 and 53700 gammas.

The aeromagnetic mean value of the base field used was calculated from all the available data. Using the average value obtained for each different altitude, the individual mean fields were calculated. Fig. 15 shows the values obtained, and also shows a pronounced difference compared with total field values obtained from spherical harmonic analysis. The mean of the mean values was used as the regional field. The anomaly value ΔF was calculated from: $\Delta F = F$ observed $- F$ mean field $- F$ daily variation. The mean field used to prepare the anomaly maps was 53655 γ. This method is very convenient for looking at anomaly patterns and tectonic structures over small areas such as the Valley of Ten Thousand Smokes. Table 2 presents the direction, altitude, speed, time and course of the individual profiles. The isopach maps of geomagnetic field anomaly for each group of flight lines indicates the regional residual intensity. Six flight levels were used, 550-670m, 730-760m, 915-975m, 1005-1070m, 1160-1190m and 1220m above sea level. The flight altitudes chosen depended on the topography and the weather.

There were 62 aeromagnetic lines flown, of which two-thirds were concentrated in the vicinity of Novarupta. This area is important in

TABLE 2

Flight Course Number	Flight Direction		Elevation m, feet	Time (Date	Time)	Flight Course Number	Flight Direction		Elevation m, feet	Time (Date	Time)
2	SW	193.5	745 m(4000)	July 13		34	NE	37.0	640 m(2100)	July 18	19:50
3	SW	200.5	760 m(2500)			35	SW	227.5	760 m(2500)	July 25	13:30
4	E	66.0	775 m(2550)			36	NE	211.5	760 m(2500)		
5	E	50.5	760 m(2500)			37	SW	27.3	1070 m(3500)		
6	NW	278.0	915 m(3000)			38	NE	194.5	1160 m(3800)		
7	SW	219.0	760 m(2500)			39	W	241.5	1160 m(3800)		
8	E	74.5	610 m(2000)			40	NW	290.0	1160 m(3800)		
9	Sw/E	211.5	915 m(3000)			41	N	136.5	1160 m(3800)		14:30
11	E	50.5	irregular			42	N	139.9	760 m(2500)		10:00
12	W	50.5	975 m(3200)	July 15	12:20	43	N	248.5	760 m(2500)		
13	E	50.5	1080 m(3550)			44	E	40.5	775 m(2550)		
14	N	309.0	1065 m(3500)			45	S	139.9	915 m(3000)		
15	E,W	254.0	610 m(2000)		16:30	46	N		915 m(3000)		
			670 m(2200)			47	E	92.3	915 m(3000)		
16	S	153.5	670 m(2200)			48	W	250.0	975 m(3200)		
17	E	65.1	670 m(2200)			49	E	75.5	975 m(3200)		
18	S	158.5	745 m(2450)			50	S		1005 m(3300)		
19	S	170.0	915 m(3000)			51	S	143.0	1005 m(3300)		
20	NE	23.5	915 m(3000)			52	W	245.5	825 m(2700)		
21	W	227.8	915 m(3000)			53	E	251.0	730 m(2400)		10:50
22	SE	117.5	915 m(3000)			54	N	328.5	790 m(2600)		
23	E	72.2	915 m(3000)			55	S	166.0	1220 m(4000)	July 4	19:30
24	N	345.5	915 m(3000)			56	N	344.7	1220 m(4000)		
25	SW	194.5	1190 m(3900)			57	S	172.0	1220 m(4000)		
26	N	317.0	1190 m(3900)			58	N	353.5	1220 m(4000)		
27	NW	300.0	760 m(2500)	July 17	19:30	59	S	169.5	1220 m(4000)		
31	NE,SW	35.0	550 m(1800)	July 18	19:50	60	E	79.2	1220 m(4000)	July 5	11:30
			670 m(2200)			61	W	281.5	1220 m(4000)		
32	SW	43.5	580 m(1900)			62	N	346.5	1220 m(4000)		
			700 m(2300)								
33	NW	49.0	610 m(2000)								
		219.0	730 m(2400)								
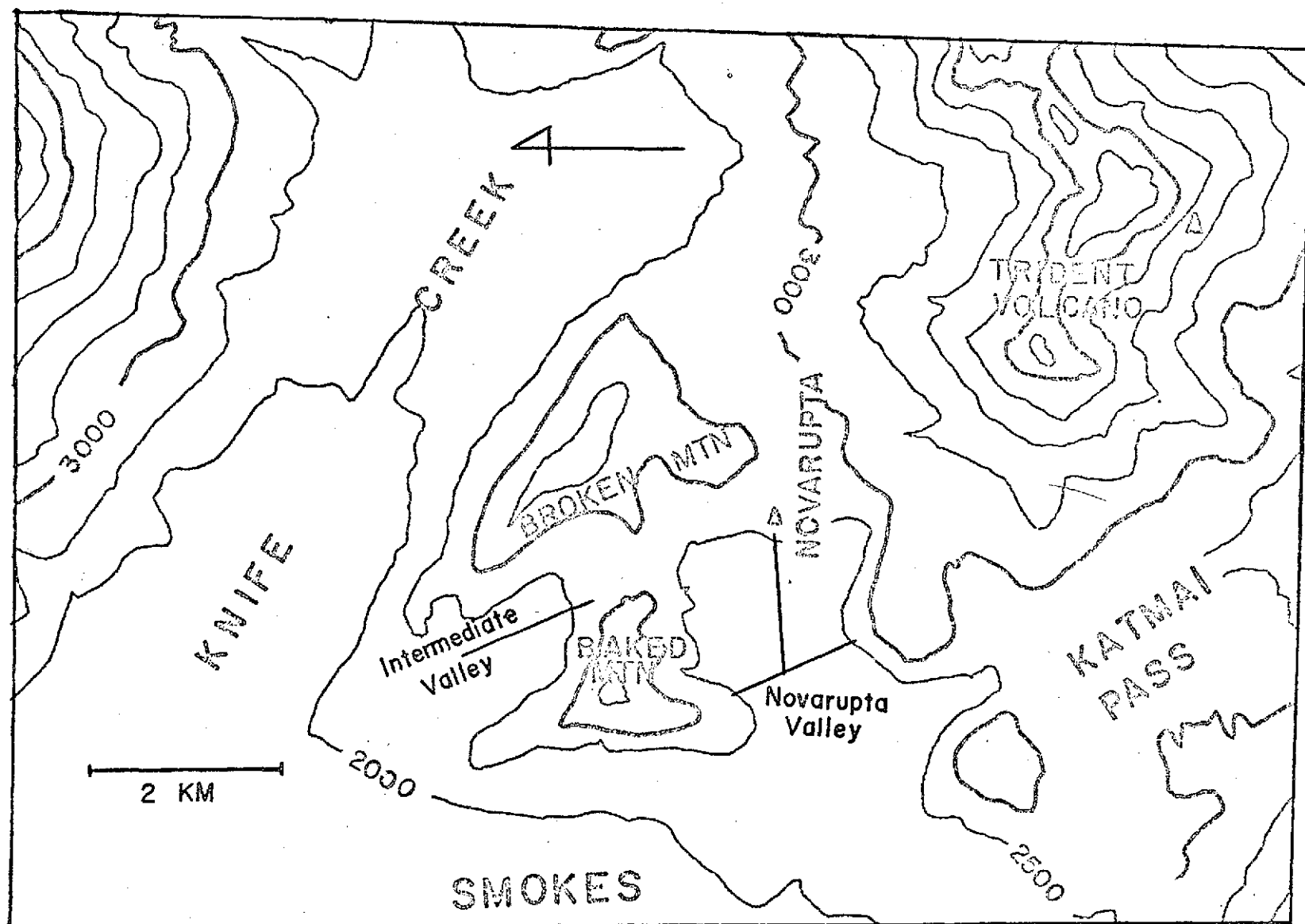
Fig. 14. Index map of ground traverse in Intermediate and Novarupta valleys.

550 580 610 640 670 700 730 760 790 825 655   915   975   1035   1098   1160   1220 M

FLIGHT ALTITUDE

gammas

53900

53800

53700

MEAN AVERAGE 53655 gammas

53600

53500

53400

53300

34

Fig. 15.   Average values of Magnetic total intensity for different flight levels.

terms of investigating the role of Novarupta in the 1912 eruption, however, preliminary and analysis indicates the need for more data in the surrounding areas.

The uneven distribution of flight lines makes computation difficult. Each of the profiles, Nos. 11, 12, 13, 15, 25, 31, 32, 33, 38, 39, 45, 51, were flown at two or more levels in both directions. Generally the reversed profiles correspond very well with the original, however, as the speed was usually uncertain and different in each direction due to wind changes, the extrapolation between known markers on the profiles has an error due to the speed/distance estimates. An example of the general correspondence is seen in profile No. 33 (Fig. 16). The location of the profiles are shown in Figs. 32, 35, 38, 41. The individual profiles are described below:

No. 15 E and W (Figs. 18, 29, 31)

This line traverses the Lethe Valley at 660 m and 726 m. The profiles are generally similar, the higher one gives lower values and a smoother curve. There is a difference of about 80 gammas between the lines, which is comparatively large compared with the other profiles. This may be an indication that this area has a thicker flow unit beneath it than those further down valley.

No. 31 (Figs. 19, 29)

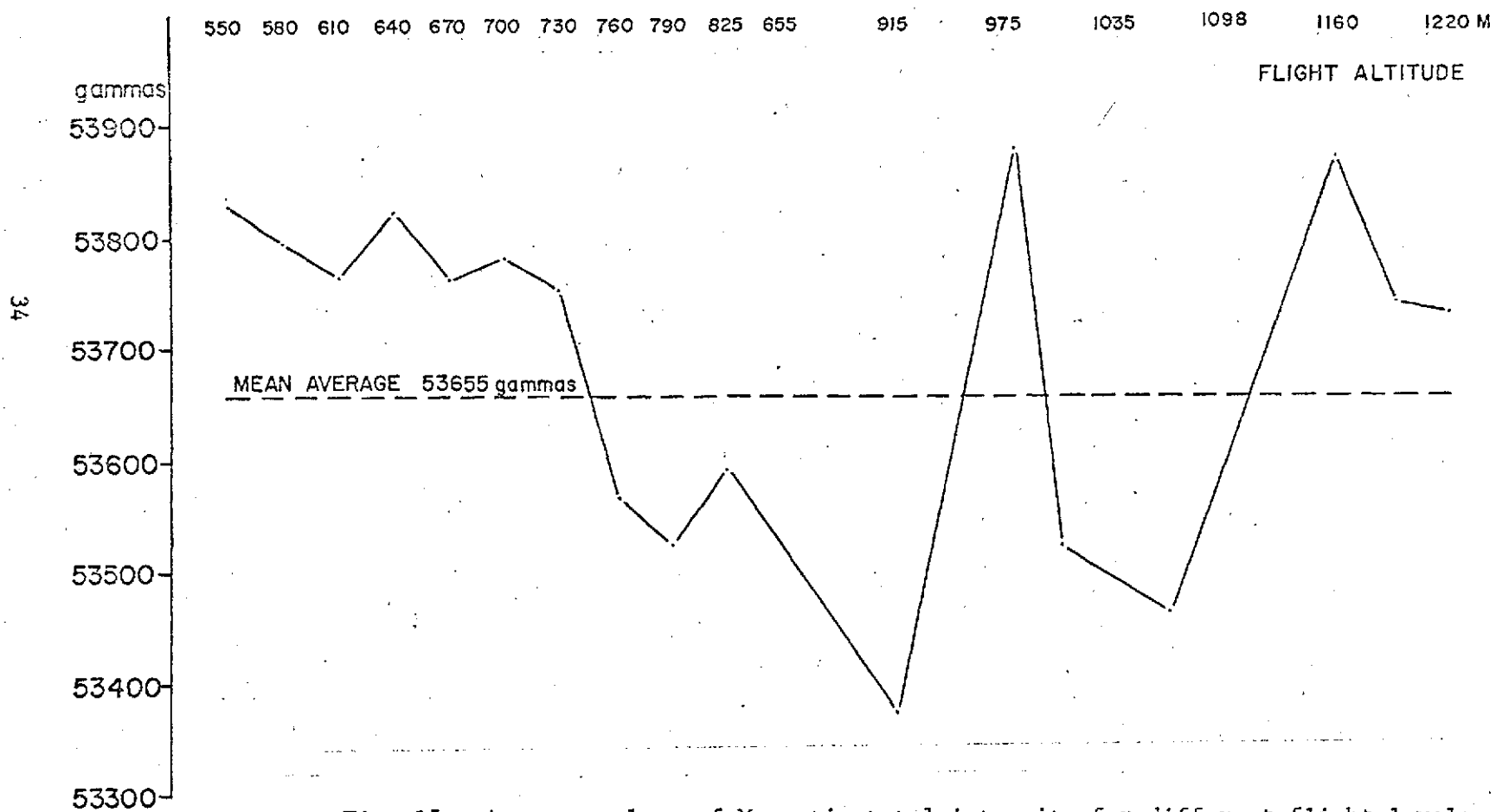Line No. 31 was flown at 594 m and 726 m. The residual differences between the two lines are less than 60 gammas on the west side of the valley, reducing so that the whole east side showed no difference between the two elevations.

No. 32 (Figs. 20a, 29)

This profile has the same pattern as line 33, but shows more fluctuation in the readings obtained.
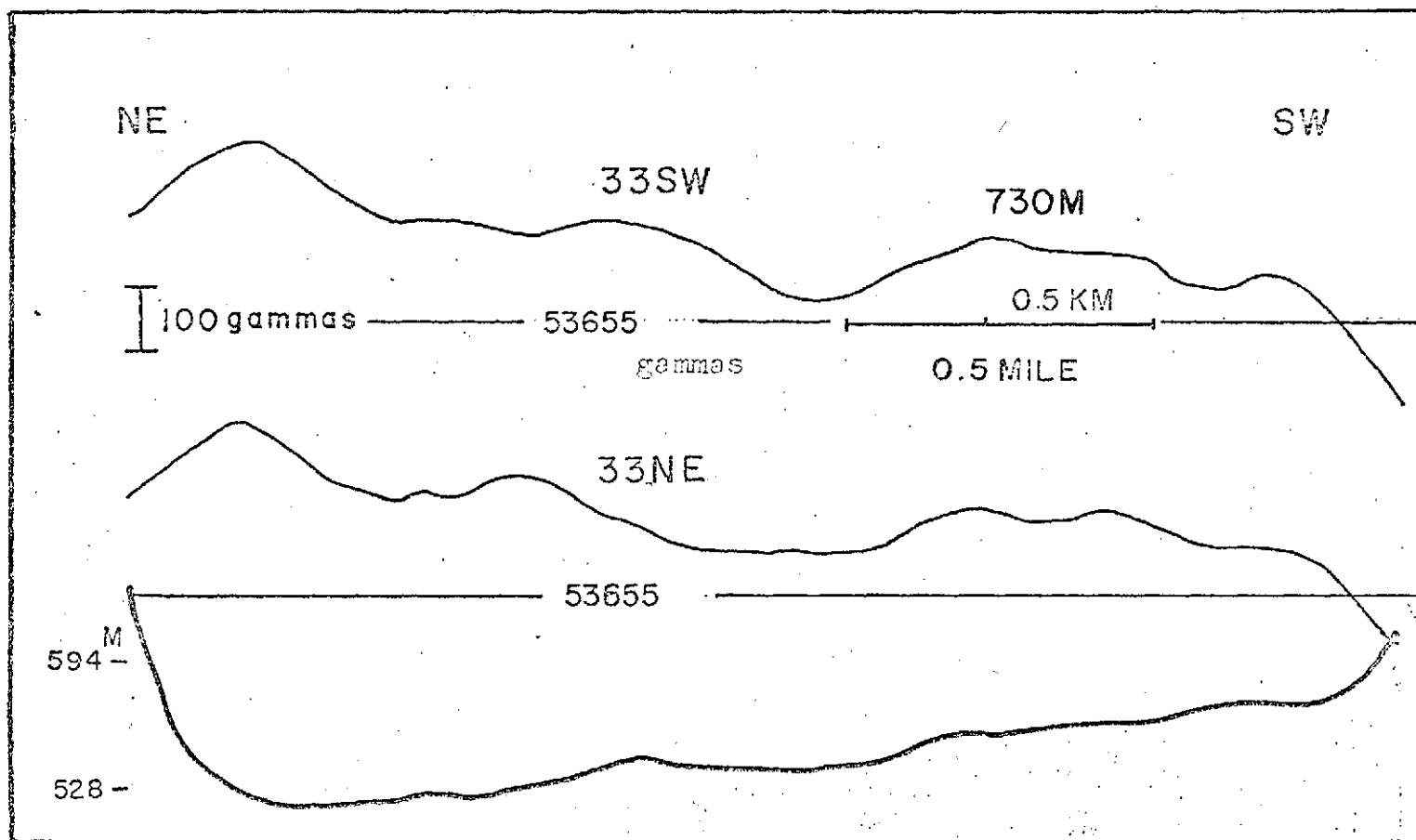
Fig. 16. Total magnetic intensity profiles of lines at elevation flown in
opposite directions (see Fig. 33).

Fig. 17. Total magnetic intensity profiles for different flight levels and a topographic profile over Broken Mountain and Novarupta (Fig. 14, 33, 36, 39).

Fig. 18.   Total magnetic intensity profiles for two flight levels
           in the Lethe Valley (see Fig. 25, 33).
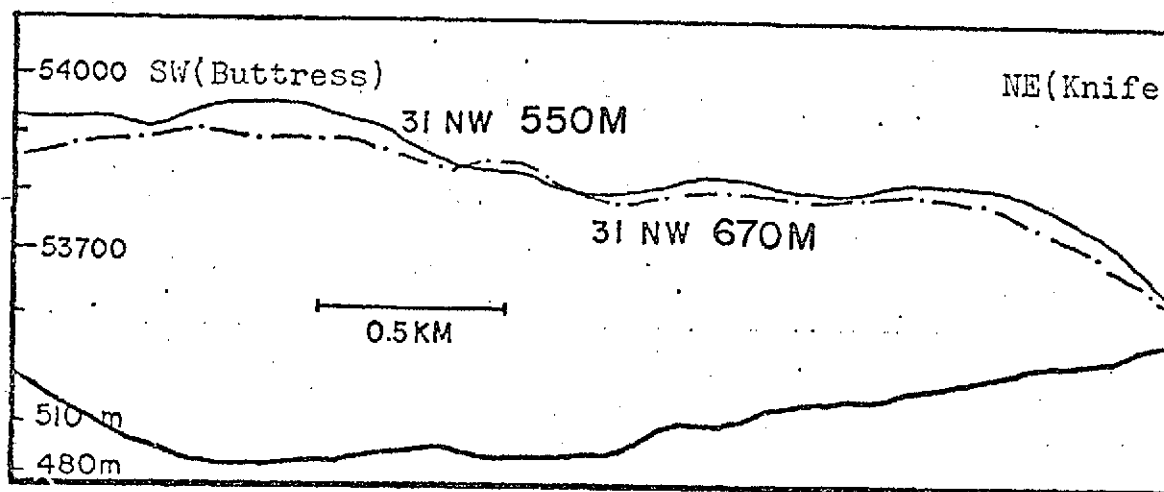
Fig. 19.   Total magnetic intensity profiles for two flight levels in the
           Main Valley (see Fig. 29).

No. 33 (Figs. 20b, 33)

This line was flown at 792 m and 726 m, and had an upper limit of the between-line differences of about 50 gammas, although there was an elevation difference of more than 66 m.

Lines Nos. 12, 13, 39, 11 and Ground Traverse(Fig. 17)

These lines were centered around Novarupta, and the intensity decreased with increasing elevation of the flight lines, the vertical gradients also decreased, being about 1.14 gammas/m between 1160 m and 1065 m 1.33 gammas/m from 975 m to 915 m. The reason for this may be explained by the higher magnetisation of the dacitic rocks forming Novarupta Dome. Thin section studies on these rocks show about 3% magnetite.

The ground survey profile (Fig. 14) in the same area showed many more small scale variations, the highest of which was a 1450 γ anomaly near the summit of Novarupta. All the profiles showed a positive anomaly located around the lava dome, which is presumably due to the remnant magnetization of the rocks composing Novarupta Dome.

Lines Nos. 41, 45, 58, 59 (Figs. 24, 25)

These lines are located on Katmai Pass and on the flanks of Mt. Trident, crossing Novarupta and Trident Basin to Broken Mountain. Parts of these profiles shown an inverse relationship between relative land elevation and magnetic intensity, which implies that the lower flanks of Trident and Broken Mountain are composed of low susceptibility Naknek sediments. The magnetic difference is clearly seen in the profiles. The vertical gradient is + .3 ∿ .8 gammas/m.

Line Nos. 25 and 38 (Fig. 21, 39)

These profiles traverse Novarupta from south to north at 1155 m and 1187 m. They show symmetrical magnetic features all positive with respect
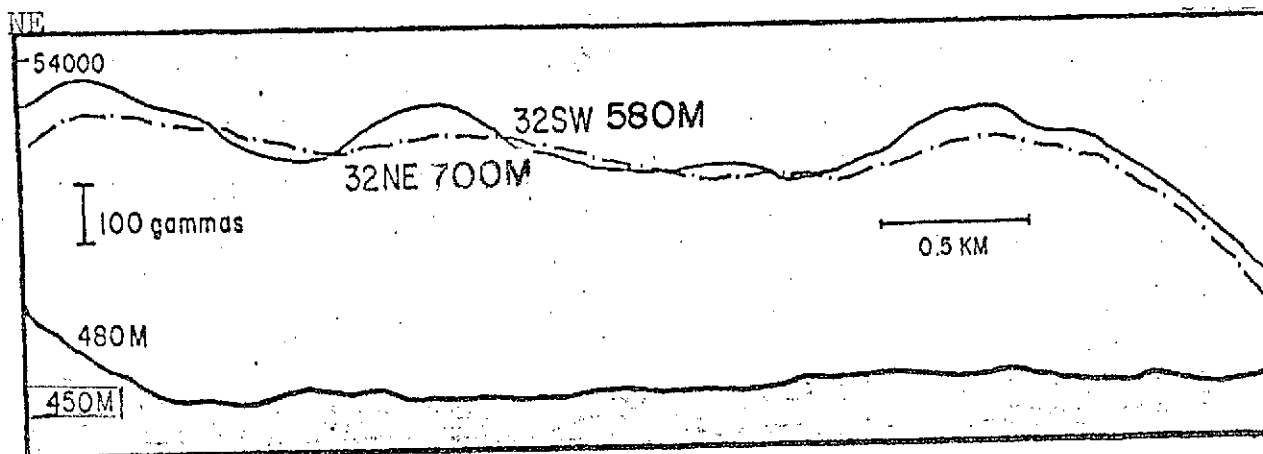
Fig. 20 a.
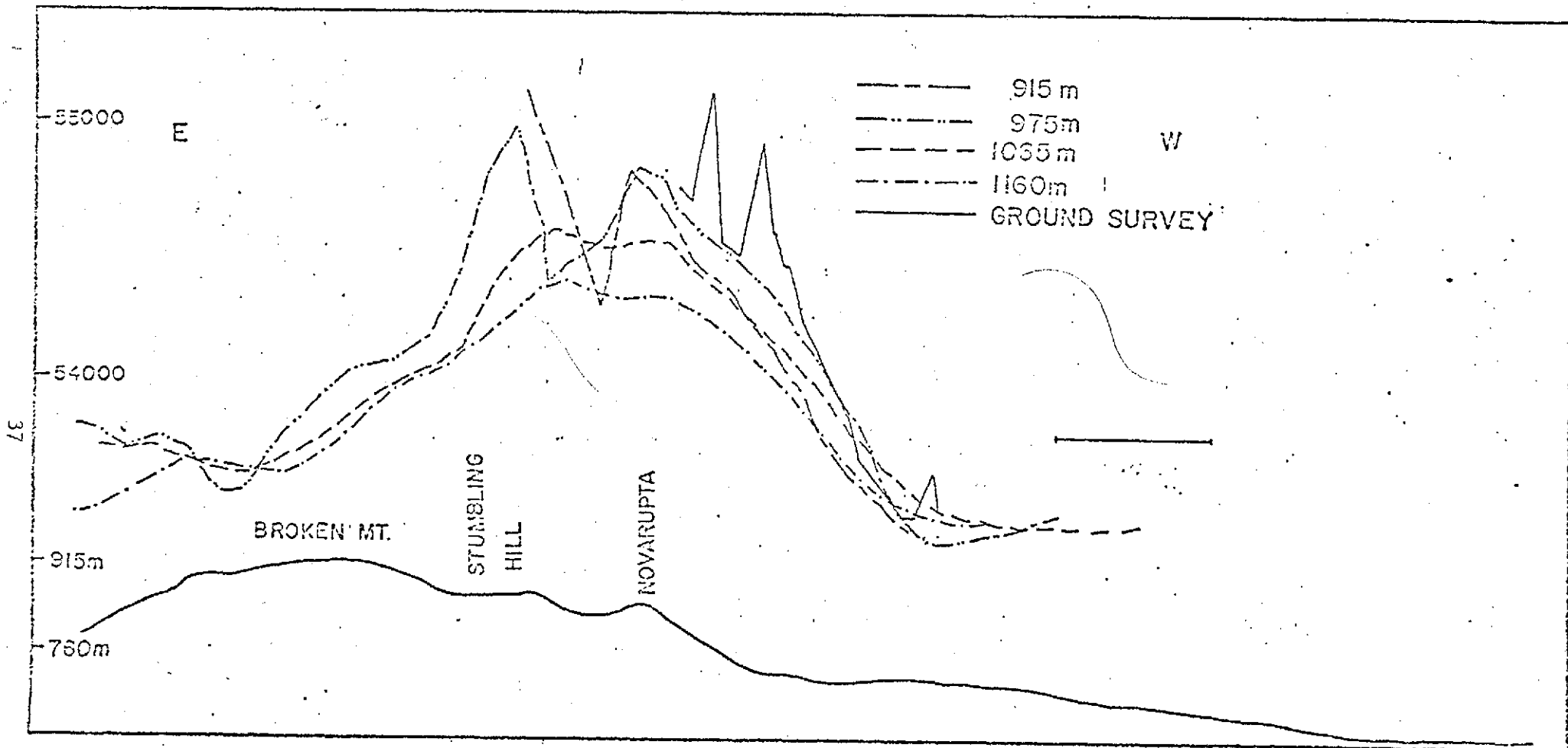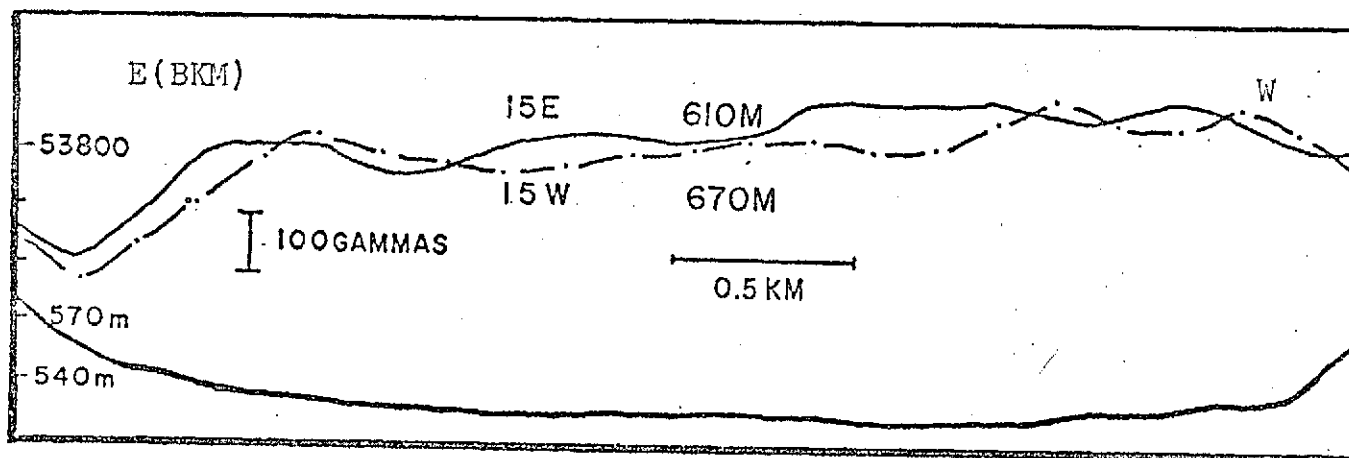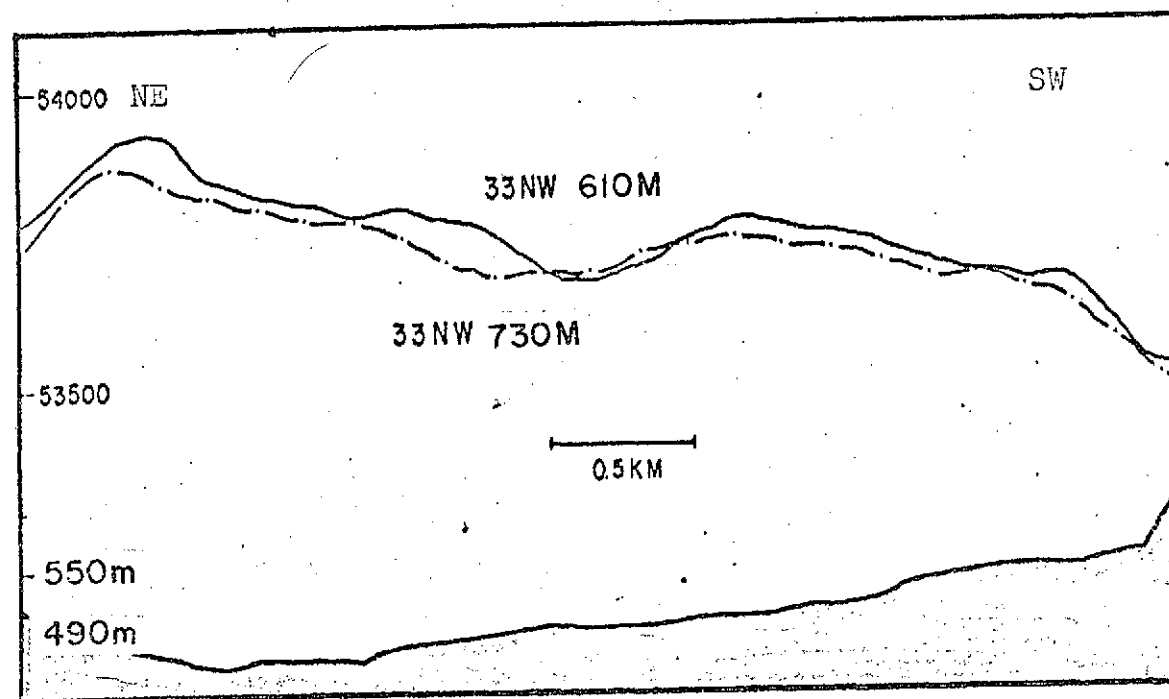

Fig. 20 b. Total magnetic intensity profiles at two flight levels across the
Main Valley (see Fig. 29, 30).
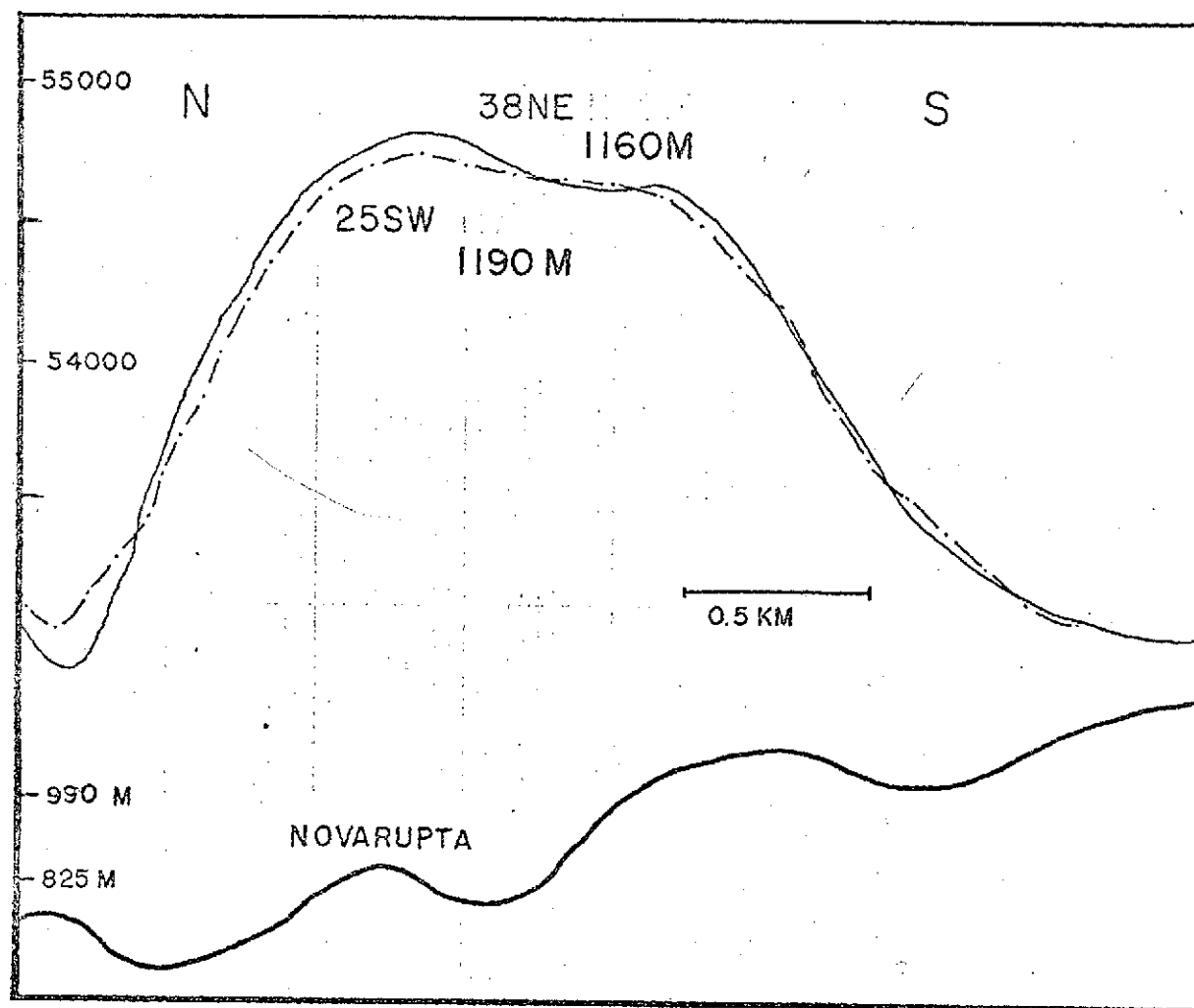
Fig. 21. Total magnetic intensity profiles in gammas and, topographic
profile in meters over Novarupta (see Fig. 39).

to the base line of 53655 γ.

The anomaly pattern is about three times as wide as the visible part of Novarupta lava dome.

No. 56 N (Figs. 22, 42)

56 N (1220 m) crossed from Falling Mountain via Novarupta basin to Baked Mountain. The part of the profile across Falling Mountain is typical of an andesitic volcanic feature. The maximum intensity is 56920 gammas. The steepness of the gradient at the base of Baked Mountain indicates a fault structure between the Naknek sediments of Baken Mountain showing low intensities, and presumed volcanics in the Novarupta Valley.

No. 57 S (1220 m)(Figs. 23, 42)

This profile crossed Broken Mountain via Novarupta to Katmai Pass at 1220 m. It is typical for a body magnetized in the direction of the present field. The depth of an equivalent magnetic dipole has been calculated . Stumbling Hill is of smaller intensity but similar to Novarupta. The relation of Stumbling Hill to the sediments of Broken Mountain is not clear from the profiles.

No. 61 W (1220 m) (Fig. 42)

This section crossed Trident basin via Novarupta, Novarupta basin, and the Lethe Valley. Compared with the lower altitude flights, the section over Novarupta gave magnetic intensities of low frequency and low amplitude.

The section crossing the main valley looks almost flat indicating that this pyroclastic flow has a low effective magnetic intensity.

No. 62 N (Fig. 42)

This flight line, from the base of Mt. Mageik along the west flank of Baked Mountain and across the Knife Creek branch at 1320 m gives an
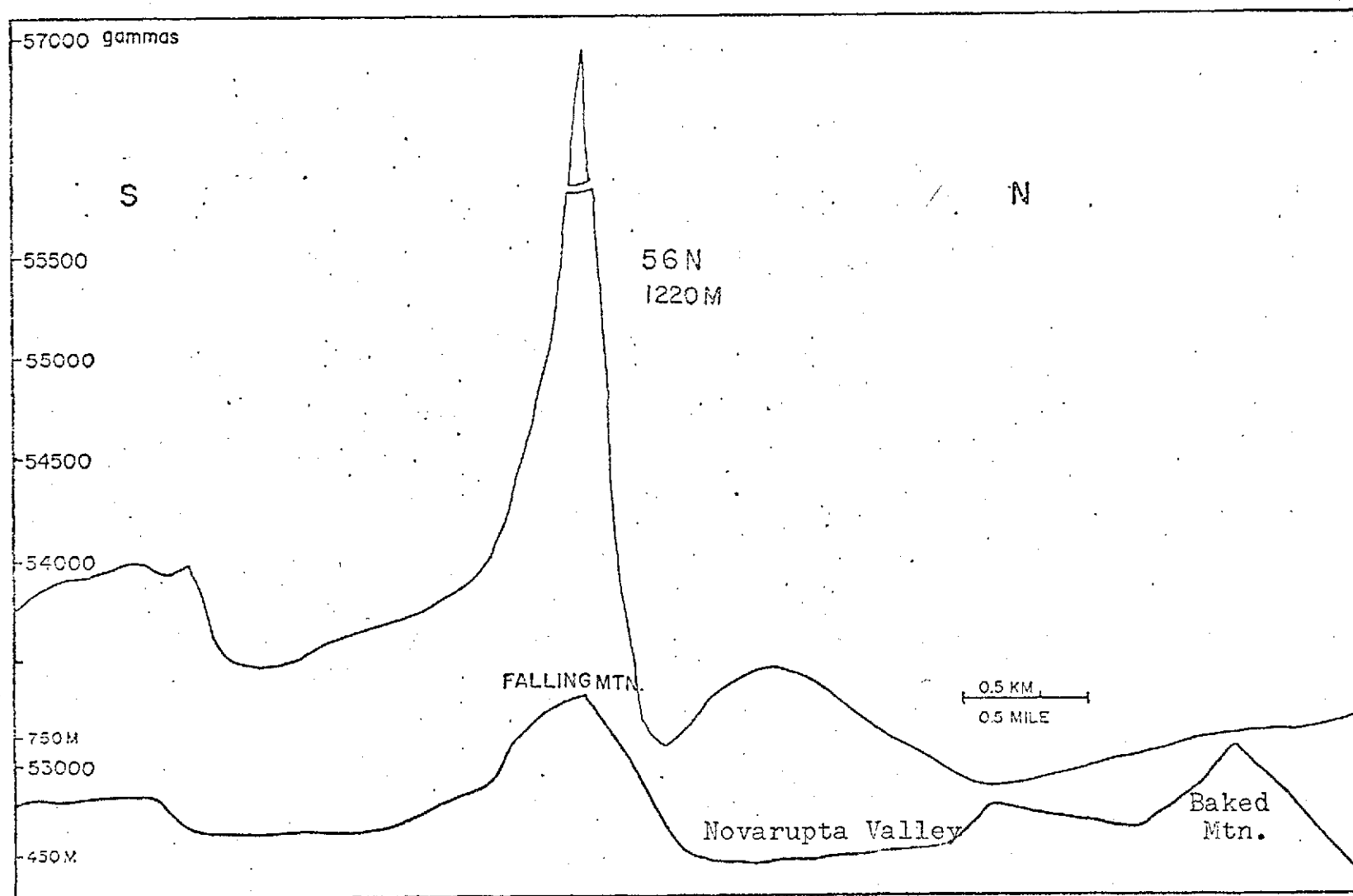
Fig. 22. Total aero-magnetic profile across the Falling Mountain and Novarupta
Valley, flight level 1220 m (Fig. 42).
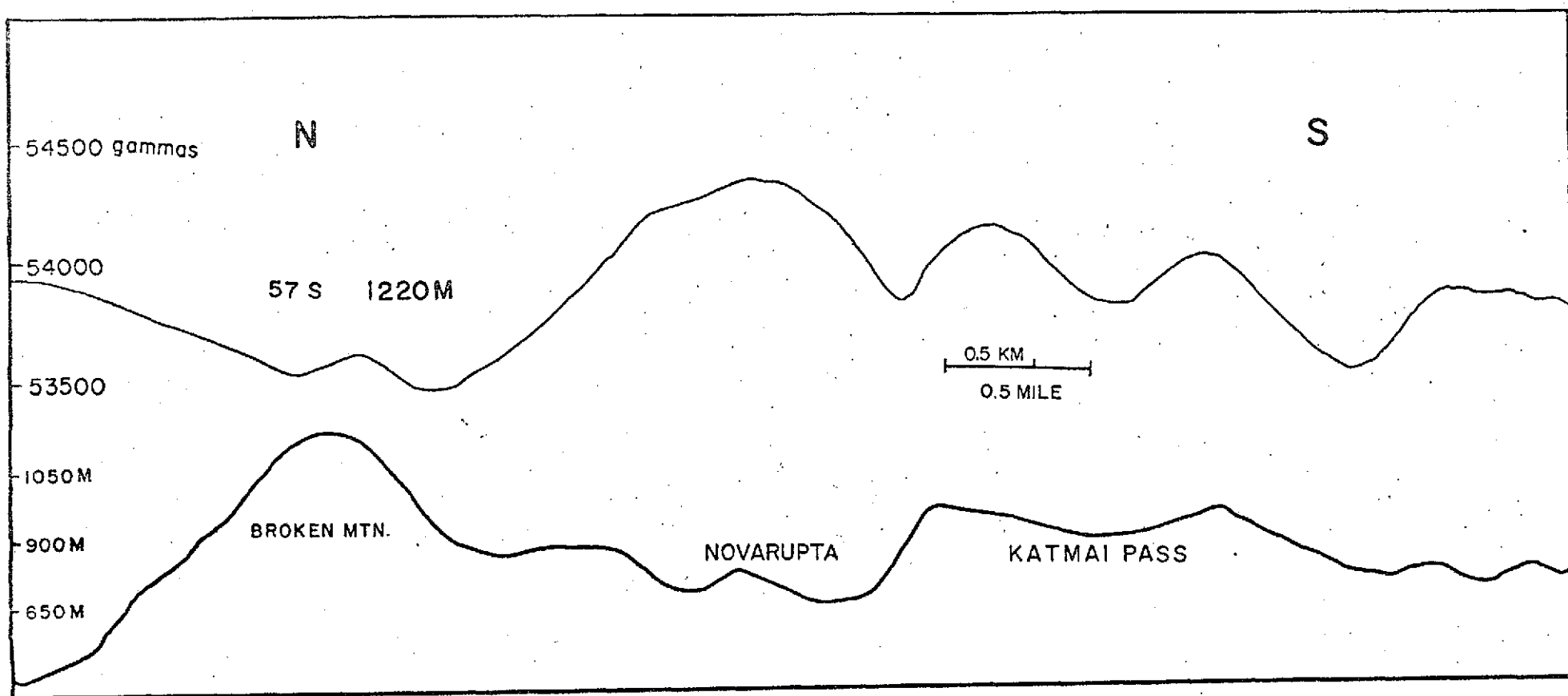
Fig. 23. Total intensity aero-magnetic profile over Novarupta.
Flight level 1220 m (see Fig. 42).
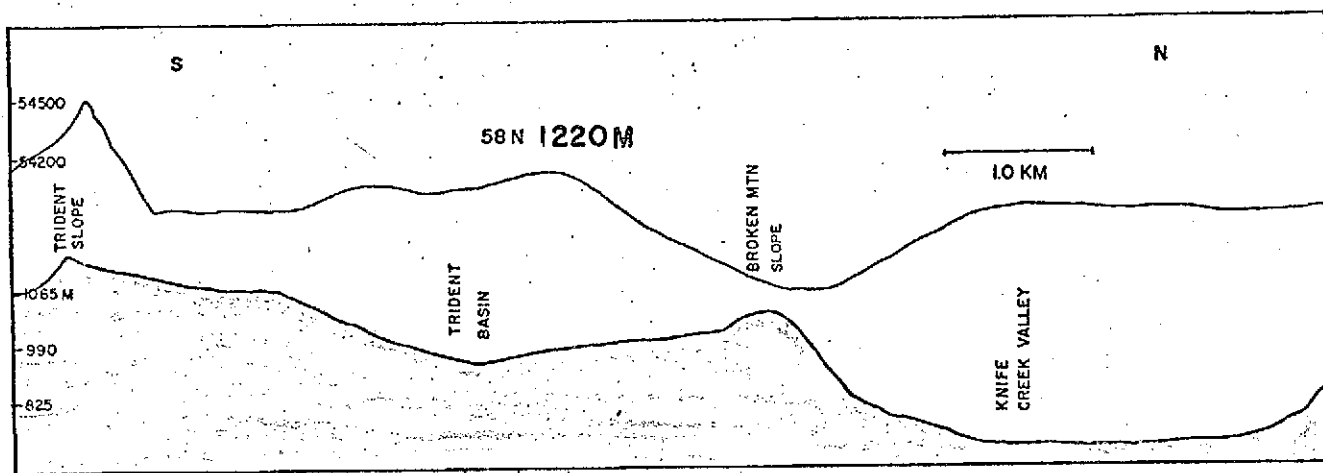
Fig. 24. Magnetic profile across Knife Creek Valley and east of the Novarupta Dome (see Fig. 42).
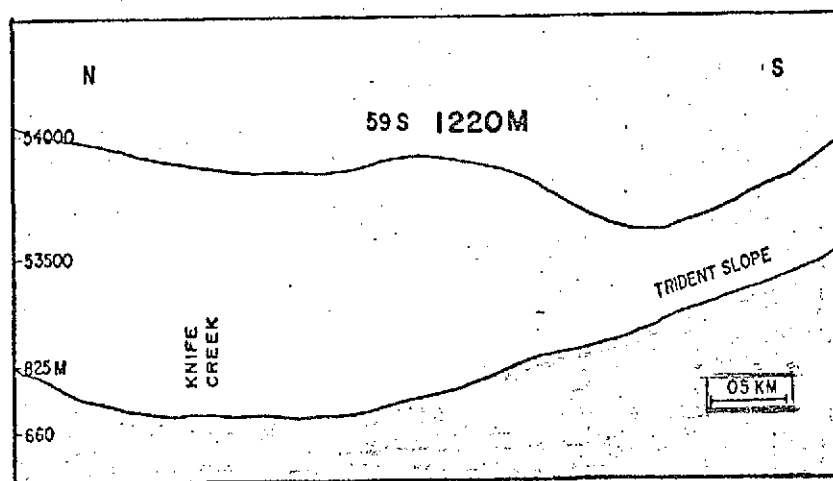
Fig. 25. Magnetic profile across Knife Creek Valley (see Fig. 42).

almost flat magnetic profile and shows no indication of underground

structures or magnetic bodies.

Ground Traverses (Fig. 14)

Although the aeromagnetic anomalies do not give any indication that

the near surface material is irregularly magnetized, a very detailed

magnetometer survey of the outcrops revealed a highly irregular small

scale anomaly pattern. This indicates that the magnetization is not uni-

form over distances of more than a few meters.

The ground magnetic survey covered the head of the Valley of Ten

Thousand Smokes (Figs. 26, 27, 28). Two of the survey lines corresponded

exactly with seismic profiles, these being along a median line down the

Intermediate Valley, between Baked and Broken Mountains (Fig. 27), and a

median line between Falling and Baked Mountains in Novarupta Valley

(Fig. 26). A ground traverse was also made across Novarupta Valley on a

line through the peaks of Falling and Baked Mountains (Fig. 17). The lo-

cation of the magnetometer stations was obtained using a tape measure;

these data are corrected for level changes, i.e., corrected to the hori-

zontal distances between stations. The elevation of each position was

measured using a barometric altimeter. As the magnetometer used for these

surveys normally served as the base station, no record of the daily varia-

tion was available. The readings at the base station before and after the

surveys were noted, and the change over the few hours involved, was assum-

ed to be linear. The data were plotted on 1:21120 scale maps. The length

of sensor support pole was 8 ft. for all these surveys and care was taken

to have no magnetic material around the probe.

The most significant features are associated with fumaroles, this

was particularly true for the line along the axis of Novarupta Valley, where a line of fumarolic holes are located near the foot of Novarupta. The fumaroles are not currently active. The relationship between the fumaroles and the high magnetic anomalies is not clear, but is probably associated with the deposition of magnetite. Near the foot of Novarupta a depression about 20 or 30 m across contains many volcanic bombs and volcanic breccia. It is possible that this ejecta might also be related to the observed magnetic intensity. These profiles showed generally high amplitude and short wavelength anomalies (see also Figs. 17,26).

MAGNETIC PROFILE OF
NOVARUPTA BASIN

Aero-magnetic
profile number
26N 1190M

Ground traverse
(probe height 1.2 m)

Falling Mtn.

Baked
Mtn.

Fumaroles

Fumarolic
discoloration
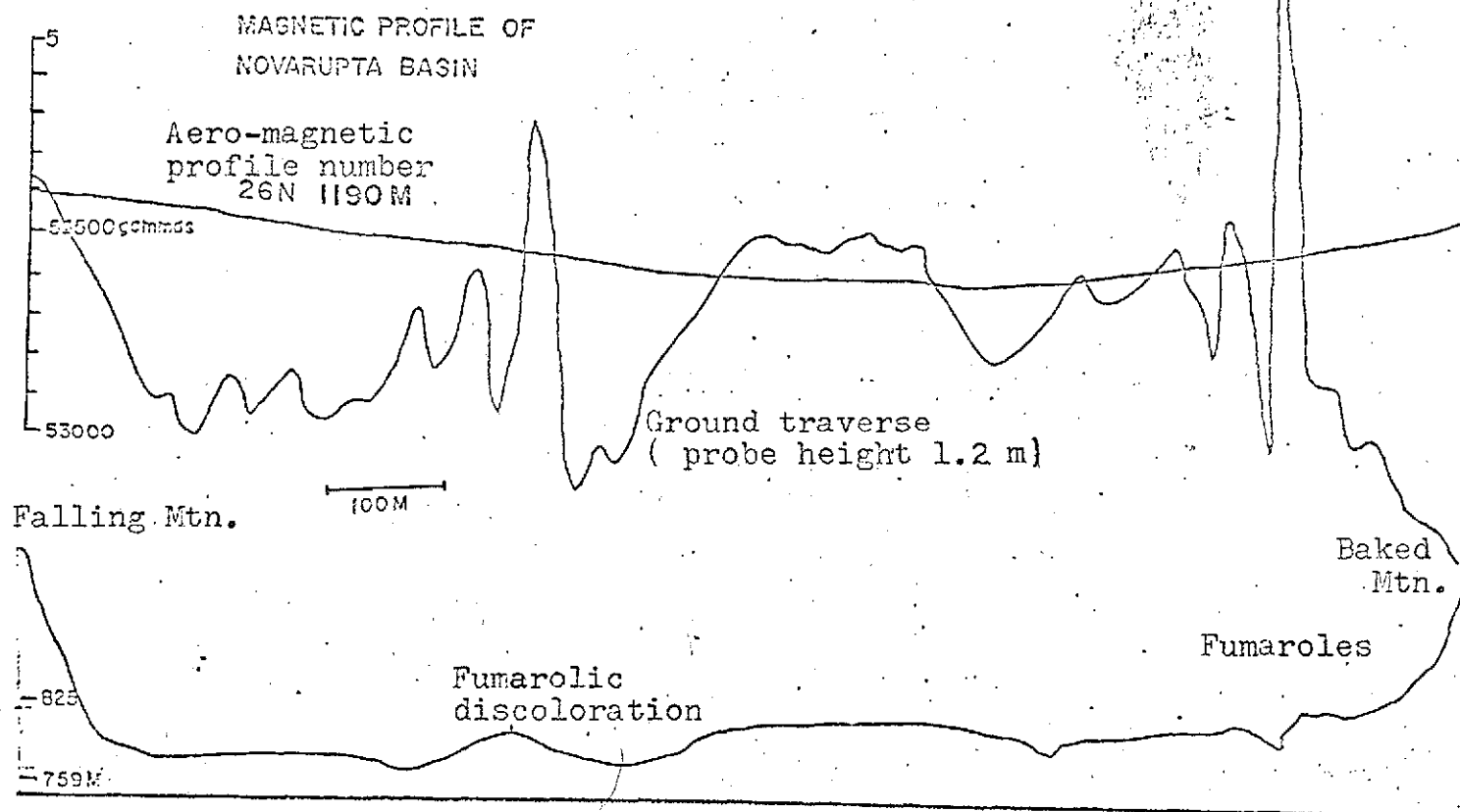
Fig. 26 Aeromagnetic and ground traversed magnetic profiles across Novarupta
Valley on the Baked Mtn. - Falling Mtn, line (see Fig. 14, 39).

MAGNETIC
GROUND SURVEY PROFILE
OF INTERMEDIATE VALLEY

NW

SE

−54000

−53900

−53800

100 M

−53700

⋅—⋅—⋅— 8 feet(2.4 m)
———— 4 feet(1.2 m)

Greasy
Pass

−825M

−759
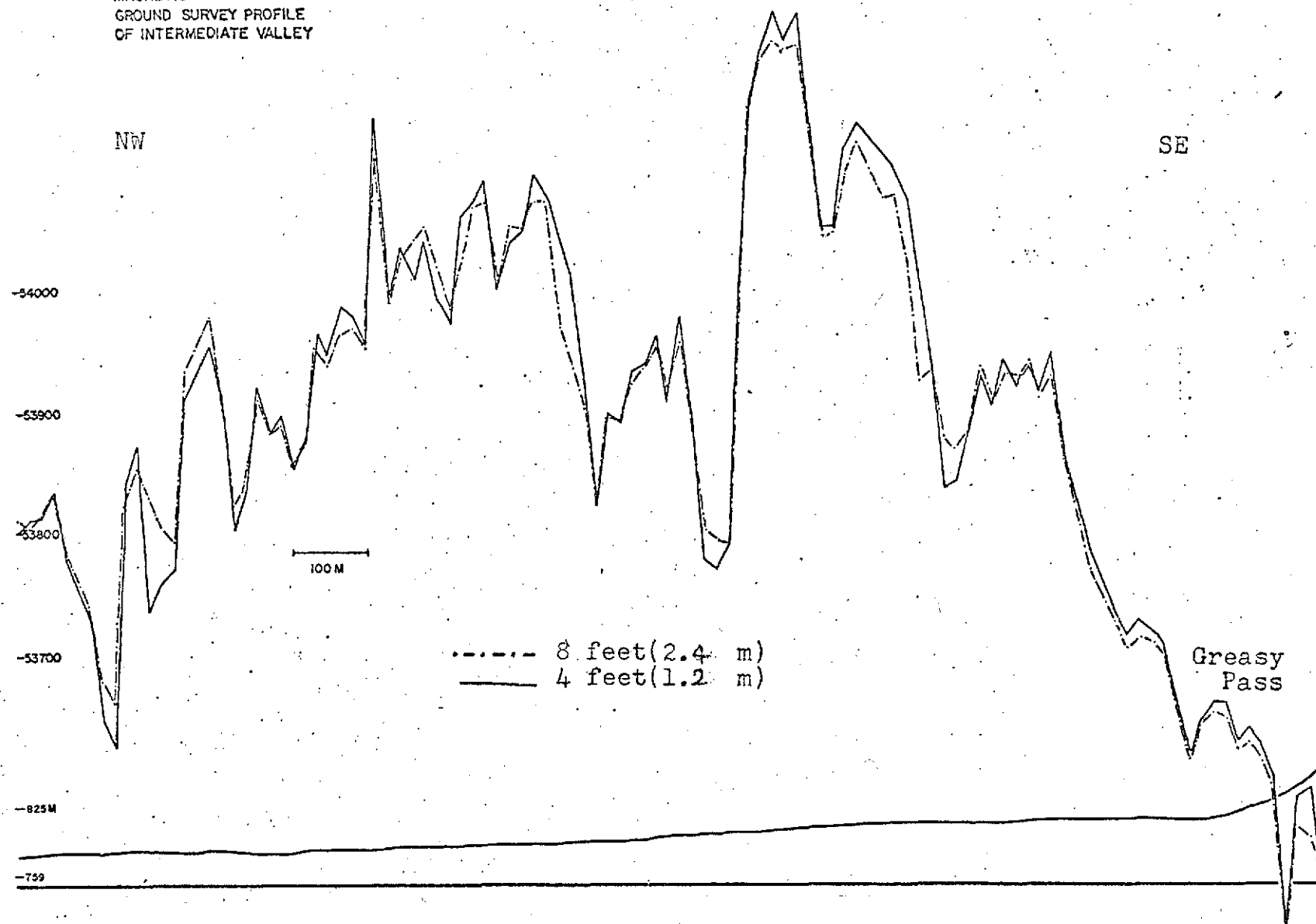
Fig. 27.   Ground based magnetic profile along center line of the
Intermediate Valley at two probe heights (see Fig. 14).

NW

SE

54000
gammas

GROUND SURVEY LINE

50

53500

4IN 1160M

891 M

100 M

825 M

MAGNETIC INTENSITY PROFILE
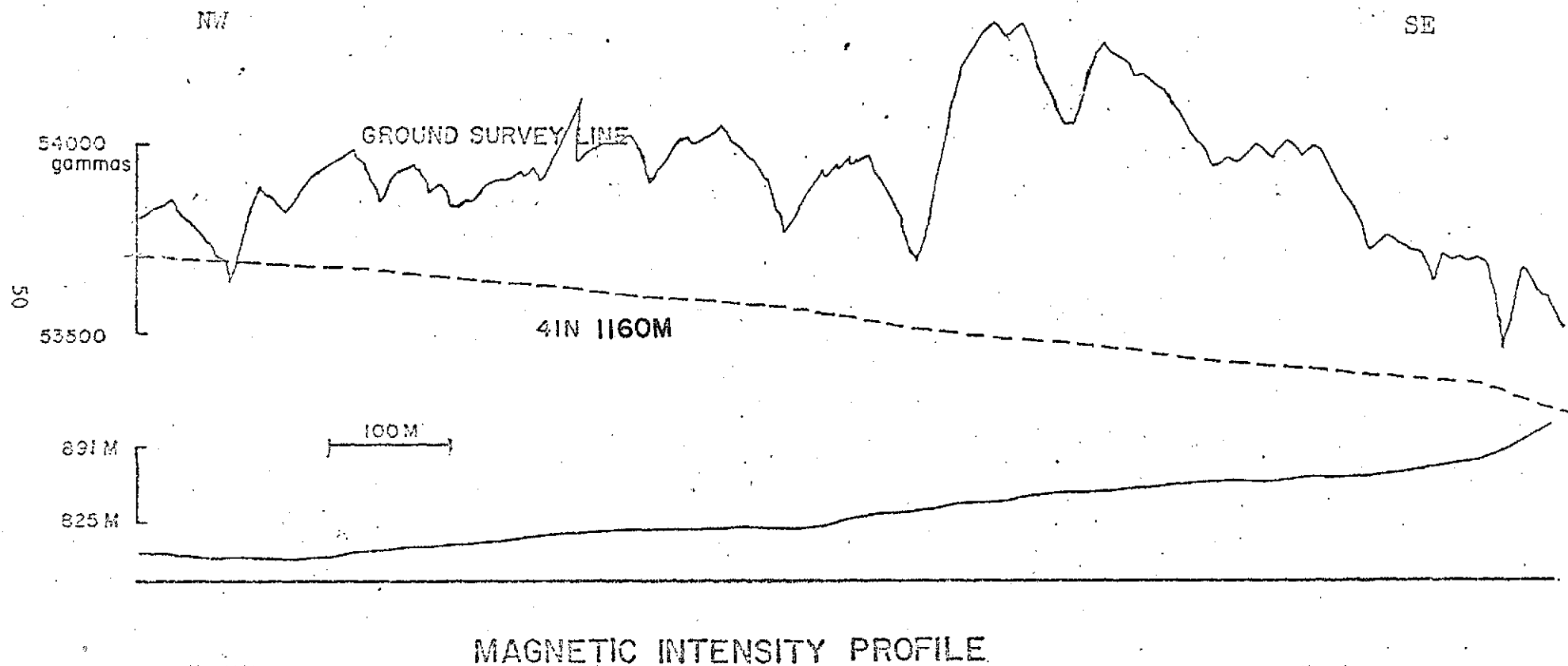
Fig. 28. Comparison between ground survey and aero-magnetic survey of Intermediate
Valley (see Fig. 39).

CHAPTER III

MAGNETIC DATA

The contour maps used in the following sections were produced using the IBM 360 computer. The aeromagnetic data from each range of flight levels has been computed separately, and is presented in three maps, an index map, a total intensity map and an anomaly map using 53655 gammas as a base line.

In general, the two maps have been plotted with different contour intervals, so show features with different scales. It should perhaps be noted here that the computer tends to "create anomalies" for areas in which there is no data, so great caution must be used in interpreting these maps.

Since the base line from which the anomaly maps are drawn is the mean value of the field within the area of the Valley of Ten Thousand Smokes, the anomaly maps are particularly useful in looking for variations within the ash flow.

Novarupta Area

The rim of the Novarupta structures appear as an oval feature elongated east-west with the dome of Novarupta towards the western end.

If Novarupta was the sole source of pyroclastics, then the vent of Novarupta must have been higher during the eruption to account for the present pyroclastic distribution. In this way one eruptive center could account for the whole pyroclastic flow.

The distribution of magnetic anomalies obtained from the 915 m and 975 m flight altitudes (Figs. 36, 37, 38) showed an oval anomaly pattern

51

in the vicinity of Novarupta and Stumbling Hill, which perhaps indicates a simple structure.

The oval magnetic anomaly around Novarupta is not characteristic of crater faulting, because the horizontal magnetic gradient is too shallow (Fig. 44). A negative magnetic anomaly is associated with the crater rim which is probably due to underlying Naknek sediments. In contrast, Falling Mountain has NE-SW fault evidenced by the 100-150 m high north face. The magnetic profiles over these faults show very steep gradients, and Falling Mountain has a very high anomalous field indicating that this mountain is of different material, and has a different susceptibility from that surrounding it.

The postulated collapse of ancestral Novarupta probably took place shortly after the main eruption, and the position and shape of the elongate crater was controlled by the overall faulting in the volcanic area.

The changes in intensity with increasing altitude over Novarupta dome indicates that the magnetic source is relatively shallow.

The magnetic map at the 915 m - 975 m flight altitude over the top of Novarupta shows a conspicious double peak (profiles 5, 9, 12, 13) (Fig. 17) while those flown at 1160 ∿ 1190 m show a smaller difference of magnetic intensity (Fig. 21). The magnetic contour map gives a pattern similar to that expected if the magnetization were in the same direction as the present field. Profile number 11 (Fig. 17) crossing Novarupta and Stumbling Hill seems similar to that predicted by Rikitake and Hagiwara (1965) for a double cone mode (see appendix). They show an anomaly over closely spaced cones, from which it is suggested that the two positive peaks were probably made by adjacent intruded or extruded material. In

52

profile 11, the second peak is associated with the many collapse features of Stumbling Hill, and may thus point to some kind of double volcano. The magnetic map based on 1220 m profiles shows only one peak, the double peak having disappeared. This indicates that the surface of the magnetic body may be roughly concave between Novarupta and Stumbling Hill. In this way lower altitude flights would see a double cone similar to those of Rikitake's model (see appendix II), however in high altitude flight maps the two peaks in the magnetic distribution can be neglected. The center of the second magnetic peak is displaced towards the northeast from the center of Novarupta dome (Fig. 40).

The concealed magnetic body causing the main anomaly may be the same material as the plug of Novarupta, and may be still moving beneath Stumbling Hill as evidenced by very fresh looking fault scarps. There is also the possibility that Stumbling Hill may be a dome similar to Novarupta. Curtis (1968) demonstrated subsidence structures which took place after the eruption of Novarupta, and estimated an elevation change of approximately 150 m. This subsidence alone would not be enough, but the possibility of removal of part of ancestral Novarupta by explosive activity exists.

The Novarupta phenomena seems to be similar in character to Usu Dake in Japan. Nuee ardente type eruptions took place on Usu Dake in 1822, and again in 1910, when the Usu appeared as a crypto-dome (volcano) (rising dacite magma?), and in 1944-45 it made a lava dome as pseudo-belonite.

These rocks were dacites and had a high viscosity of the order of 10^{11} poise, and a temperature of 980°C (Minato et al. 1965).

The only large-scale variations of total intensity seen in the aeromagnetic surveys were those associated with Novarupta dome, Falling Moun-

tain and Cerberus. The investigation has proved useful for looking at the magnetic effects of the central vent, but surprisingly shows nothing that can be clearly interpreted as magnetic peaks away from, but still directly associated with, the dome. For comparison, one can consider the case of Hakone caldera in Japan, where good agreement is found between the magnetic effects and the position of both the cone and the caldera rim. This difference may be due to the number of eruptions of the volcano. Hakone has a more complex history and represents the accumulation of many eruptions. The triple volcano of Hakone is 10 km in diameter and later activities have been controlled by the first eruption which produced local faulting.

The dominant magnetic trend in the Katmai area does not parallel the lines of the Earth's main field, but seems to be affected only by the overall geologic structures and hence only indirectly by previous volcanic activity.

The peak of the anomaly pattern seems to be a little to the east of the topographic high. In the aeromagnetic profiles, Novarupta shows a remarkable positive pattern of about 800 gammas over the dome, furthermore, negative anomalies of about −250 gammas appear in a symmetrical pattern about a ENE-WSW axis, which is parallel to the tectonic trend. These negative anomalies are assumed to be due to sedimentary rocks of low magnetic content (Naknek). Comparing this map with the 1160 ∿ 1190 m flight altitude map (Fig. 41), it seems that the positive anomalies have decreased and are smoother at higher elevations (Fig. 44). The almost circular negative anomaly around Novarupta dome derived from the 915 ∿ 975 m lines (Fig. 38), shows a distribution which also agrees with the surface geology. The main positive anomaly reflects the exposed lava dome.

The total intensity map derived from profiles flown at 1220 m (Fig. 42, 43, 44) show features characteristic of the main tectonic structures in a northeast to southwest direction. These are offset in a small area along an east-west axis making an en echelon structure. Two steep anomalies are associated with Falling and Cerberus mountains (1165 m, 1080 m).

Model Profiles

From the equation used for the model studies (see Model studies),

$$F = \sqrt{\{\cos^2\theta(\frac{2m}{h^3}\sin^3(\theta-a) + H)^2 + \sin^2\theta(\frac{m}{h^3}\sin^3(\theta-a) - H)^2\}}$$

Then, the dipole moment can be represented by:

$m = M_o V$, where M_o is the magnetic moment per unit volume and V is the volume of the body.

h = the distance from the dipole center to the flight line.

a = the inclination of the ambient field.

Assuming this model, the field expected for an ellipsoidal tube was calculated. The values chosen were

$x = 720m$, $y = 650m$ and $M_o = 2 \times 10^{-3}$ emu/cc

where x and y are the semi-major and semi-minor axes of the ellipse. These dimensions are based on the observed size of Novarupta and Stumbling Hill (Fig. 21).

In order to obtain profiles using the above relations, it is necessary to choose values for the three variables V, m and h. This has been done using the "best guess" values based on observations.

From the top of the magnetic body to the flight level was 300m, so that

$h = 300m + L/2$, where L = the length of the tube.

$$V = \pi xy(300 + L/2)$$

$$m = \pi xy(300 + L/2)M_o$$

For any given value of h, it is possible to draw a profile corresponding to the angle θ. The result of these calculations are shown as profile in Fig. 32 . The assumptions used are very rough, however, comparing the observed and calculated data it is possible to recognize similar features in both.

If the dimensions of the system chosen are approximately correct, then the dipole center appears to be located about 1 km below the 1.22 km flight line, or about .9 km below the surface.

Using the simple model described above it is not possible to make both the values of maxima and minima coincide, and at the same time have similar values for the horizontal distance between them when comparing observed and calculated profiles. A better fit could be obtained by using a more complicated shape for the body, and/or increasing the inclination of the magnetization. However, the general fit of the two profiles is sufficiently good to indicate a relatively shallow source at about 900m below the surface for the Novarupta-Stumbling Hill anomalies.

The exposed lava dome is about 300 m in diameter, so if the assumptions are correct, then there is more magnetic material on the northeast side of the present lava dome.

A similar calculation using the technique of Vacquier et al (1951) gives a value for the long axis of the magnetic body beneath Novarupta as about two-thirds of a mile and about half a mile for the short axis.

Profiles 57S and 61E taken in north-south and west-east direction respectively (Figs. 17,23) crossing Novarupta Dome show very elliptical magnetic body features. They show large positive anomalies that coincide
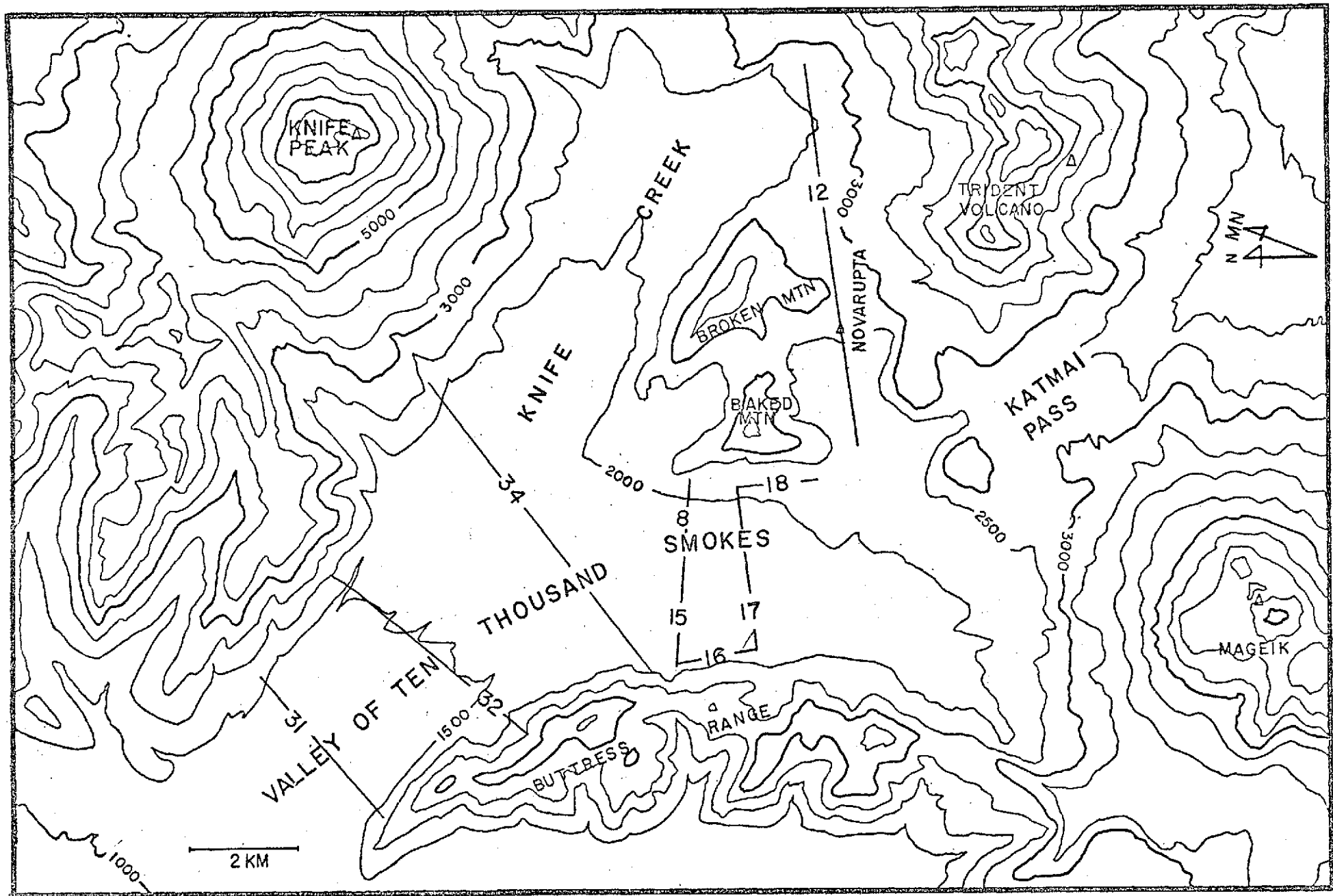
56

Fig. 29. Flight lines of elevation 550 – 670 m above sea level.
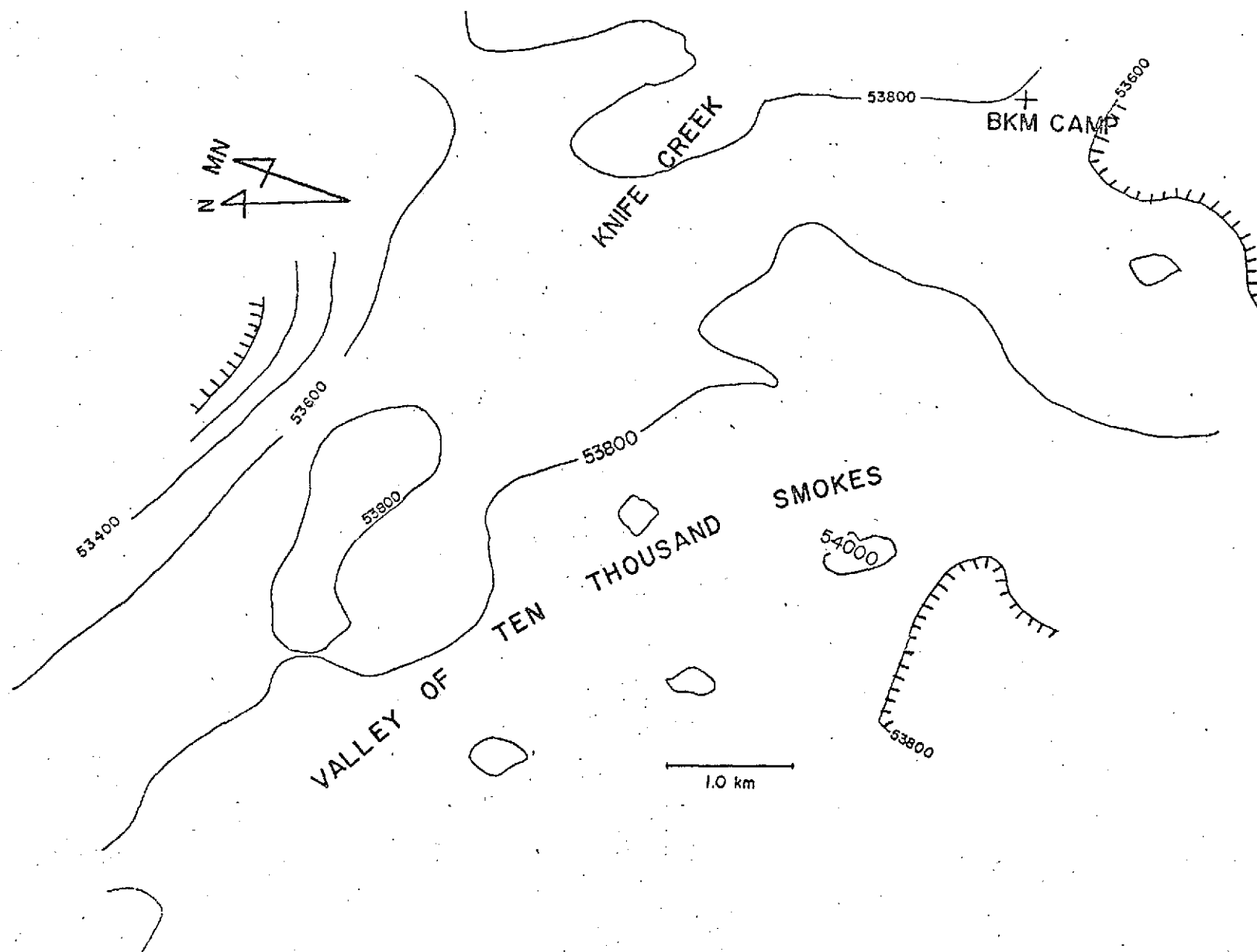
Fig. 30. Total magnetic intensity map of the Valley of Ten Thousand Smokes,
flight height at 550 - 670 m.
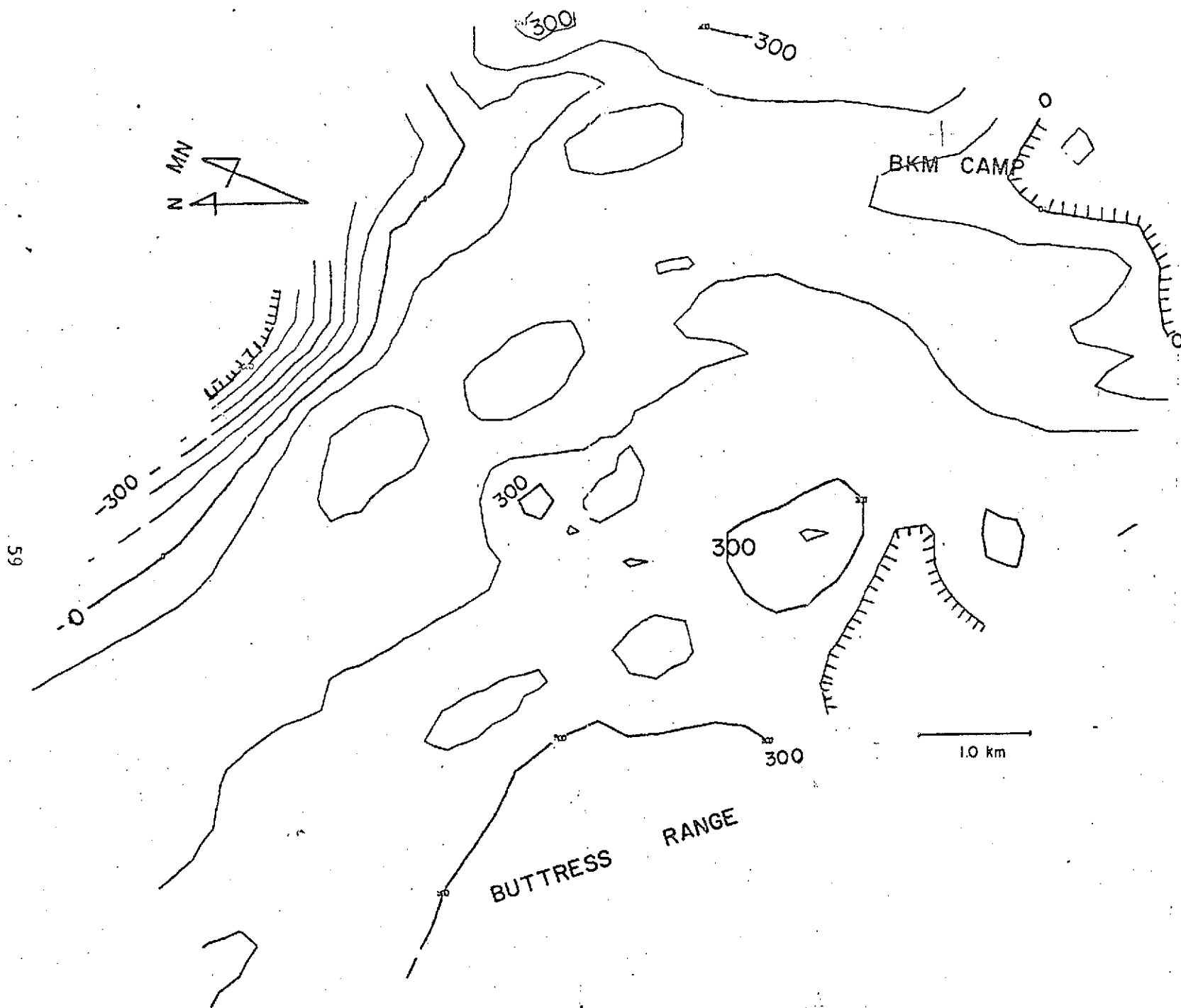
Fig. 31.   Total intensity anomaly map in gammas, flight height at 550 – 670 m.
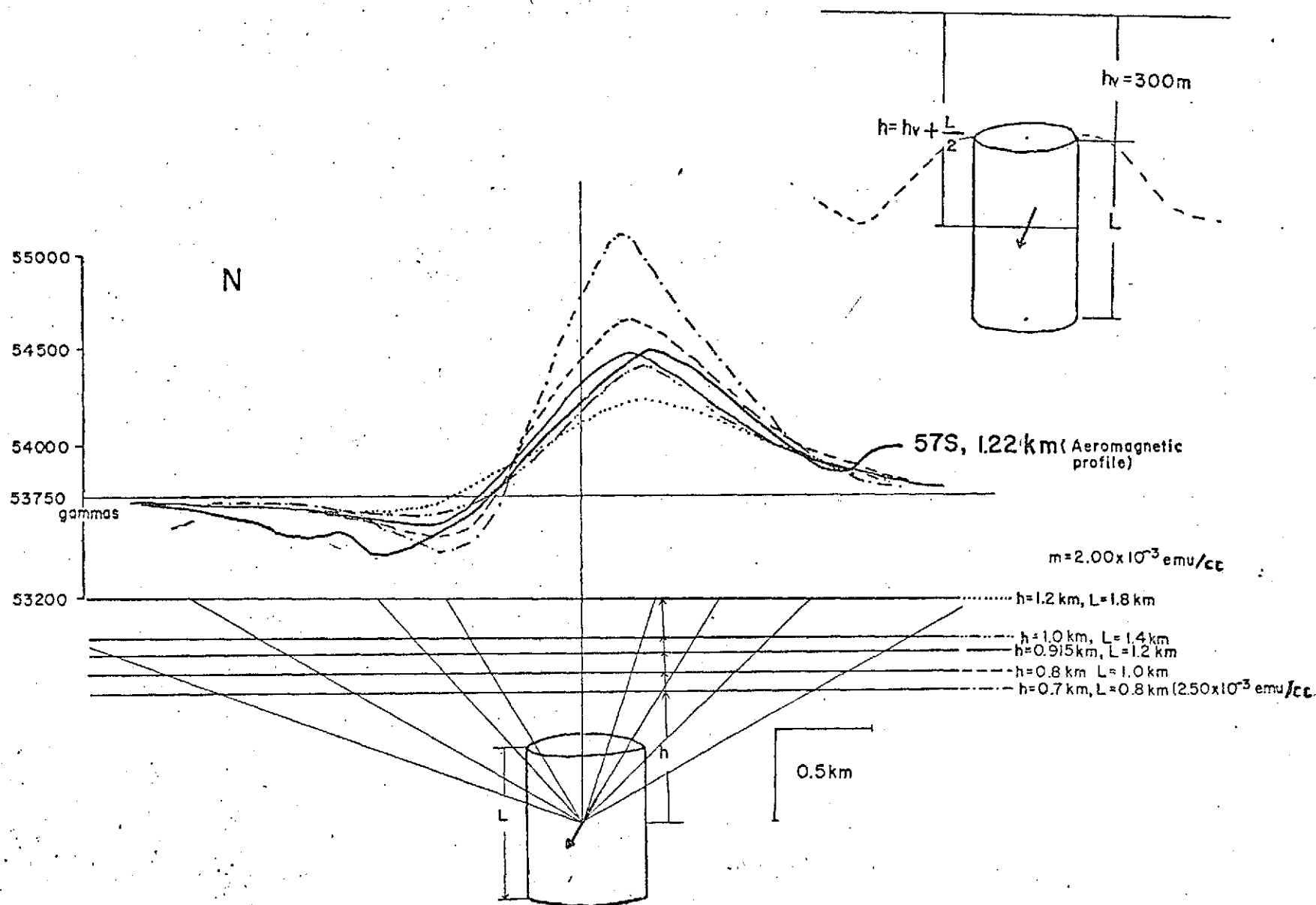
Fig. 32. A comparison of various calculated magnetic profiles with the observed profile over Novarupta.

with the rhyodacite lava dome. The dome is composed of highly magnetic material but must have a wider distribution than is indicated by the exposed dome itself. The maximum anomaly on Falling Mountain is 2500 gammas, it has a very steep gradient and shows a circular cone-like feature. Using similar calculations to those used for Novarupta, the magnetic source has a diameter of about 700 m and the dipole center is located at 1000 ∿ 1050 m below the flight line. These high gradients for the magnetic intensity and the shallow dipole source, support the idea that the volcanoes of the Katmai area are younger than Tertiary. This is because the data precludes a thick sequence of volcanics, unless the temperatures beneath the volcanoes are higher than the Curie Point, also the magnetic distribution would be more complex.

Intermediate Valley and Fumaroles

Magnetic anomalies of fumarolic origin were not generally seen in the aeromagnetic maps except for those in the southern valley located on the supposed fault line and along the flank of Baked Mountain (Fig. 35). This area of fumarolic activity appears to be relatively large and involve a large volume of magnetic material. It is possible that the acidic gases and heat might be supplied by some kind of intrusive source or magma chamber. In general, there appear to be two kinds of fumaroles: a) those that originate in the pyroclastic flow (nuee ardente), and b) those of deeper origin from at least underneath the Naknek sediments which are fault controlled (Gedney 1969).

Ground magnetic profiles along the center line of the Novarupta Valley (Fig. 17) show magnetic anomalies that correspond exactly with aeromagnetic profiles, except for a few sharp, and presumably very local, anomalies. The narrow magnetic anomalies of high frequency and high amplitude

61

in the vicinity of fumaroles are able to be directly related to the
surface expression of fumarole activity (Trible 1971). The high ano-
malies also indicate a source which is both shallow and narrow.

The ground magnetic profile which traversed the Novarupta Valley
from Falling Mountain to Baked Mountain also showed fumarole associated
anomalies (Fig. 25).

Intermediate Valley

The Intermediate Valley has a thin pyroclastic flow in comparison
with the other branches of the Valley (Kienle 1967, Fenner 1922). A de-
tailed survey over a fumarole area (Trible 1970) again gave high frequen-
cy and high amplitude anomalies.

A profile along the median line of the Intermediate Valley was ob-
served at two heights, 2.4 m and 1.2 m (Fig. 27). If the data from these
two elevations are plotted, it can be seen that the sharp high amplitude
anomalies also have high vertical gradients of total intensity of about
16.7 ~ 2.5 gammas/m again indicating a shallow origin. The higher intensity
anomaly areas are all normally magnetized, but the magnetization of the
other smaller anomalies are uncertain.

The margin of Intermediate Valley shows one of the highest anomalies
(250-300 gammas) recognized in the 730-760 m aeromagnetic survey. This
magnetic high correlates with the fumarole grid of Trible (1970) and in-
dicates a considerable mass of magnetic material. According to Trible
(1971), even where large fumaroles existed, the magnetic minerals concen-
trated by the fumarole would leach and weather out very quickly after acti-
vity stopped. Trible also suggests that it is possible for the magnetic

62

minerals to concentrate in the mouth of the fumaroles and to occasionally be preserved. Where the magnetic minerals are preserved, a magnetic anomaly exists, but the absence of magnetic expression does not preclude an old hot fumarole. Therefore, it is suggested that the fumaroles along the margin of the Intermediate Valley were active until comparatively recent time, and the magnetic minerals were formed hydrothermally in the mouth of the fumarole vents, and were also concentrated at depth and presumably preserved in some way.

Knife Creek, Lethe River and Main Valley Profiles

Seven flight lines in the Main Valley and Lethe Valley were flown at 550-670 m and the results contoured (Fig. 29, 30, 31). The total field measurements showed flat profile when compared with those from the head of the valley, but with both sides of the main valley and the northside of Baked Mountain showing lower intensities. In other words, the low values appear to correspond with the sedimentary rocks (Naknek formation) which contain only a small amount of magnetic material.

The anomalies were mostly less than 250 gammas with respect to the average value. This small value could be caused by a source within the pyroclastic rocks.

The contour map of the 730-760 m flight line data (Fig. 33, 34, 35) shows four positive and three negative anomalies in the upper part of the valley. The down valley portion showing the same situation as the 550-670 maps, but with the values decreasing in accordance with a vertical gradient of .2 gammas. The anomalies over the valley floor are not larger and are probably due to the irregular topography of the U-shape valley

left by the last glacial retreat. Significant anomaly patterns seen by

contouring the data are negative and largely associated with areas of

Naknek sediments. A positive anomaly extends over a comparatively large

area in the Knife Creek Valley, a portion of Broken Mountain and the

lower end of the Intermediate Valley, however, in the center of the posi-

tive area is a negative anomaly. This negative anomaly may be a function

of the line spacing, but the overall positive anomaly appears real. The

steepness of the horizontal gradients point to a fault structure, and may

well be connected with the higher fumerolic activity of the area mentioned

before.

With regard to the Main Valley, the total intensity decreased as

expected with higher elevation, i.e., the gradient of the magnetic

field probably represents a normally magnetised feature. The smoothing

of the curve shows that the sources of the irregular field are shallow,

and these profiles show nothing of the deeper structures (Fig. 31, 35).

Profiles in the Intermediate Valley at 1160 and 1190 m, (Fig. 39, 40,

41) suggests a complicated pattern in the distribution of thickness of

volcanics, and by implication a complicated paleotopography.

Negative anomalies correlate with the head of the Intermediate Valley,

and the Novarupta and Trident basins, however, these anomalies show com-

paratively lower amplitudes for higher flight levels as might be expected

for a relatively shallow source. At the 1190 m flight level the negative

anomaly associated with the Naknek sediments of Baked and Broken Mountains

is reduced. This is presumably because the magnetic bodies causing the

positive-negative contrast are shallow and thin. At the higher altitudes

the magnetic profiles do not show any marked effect directly attributable
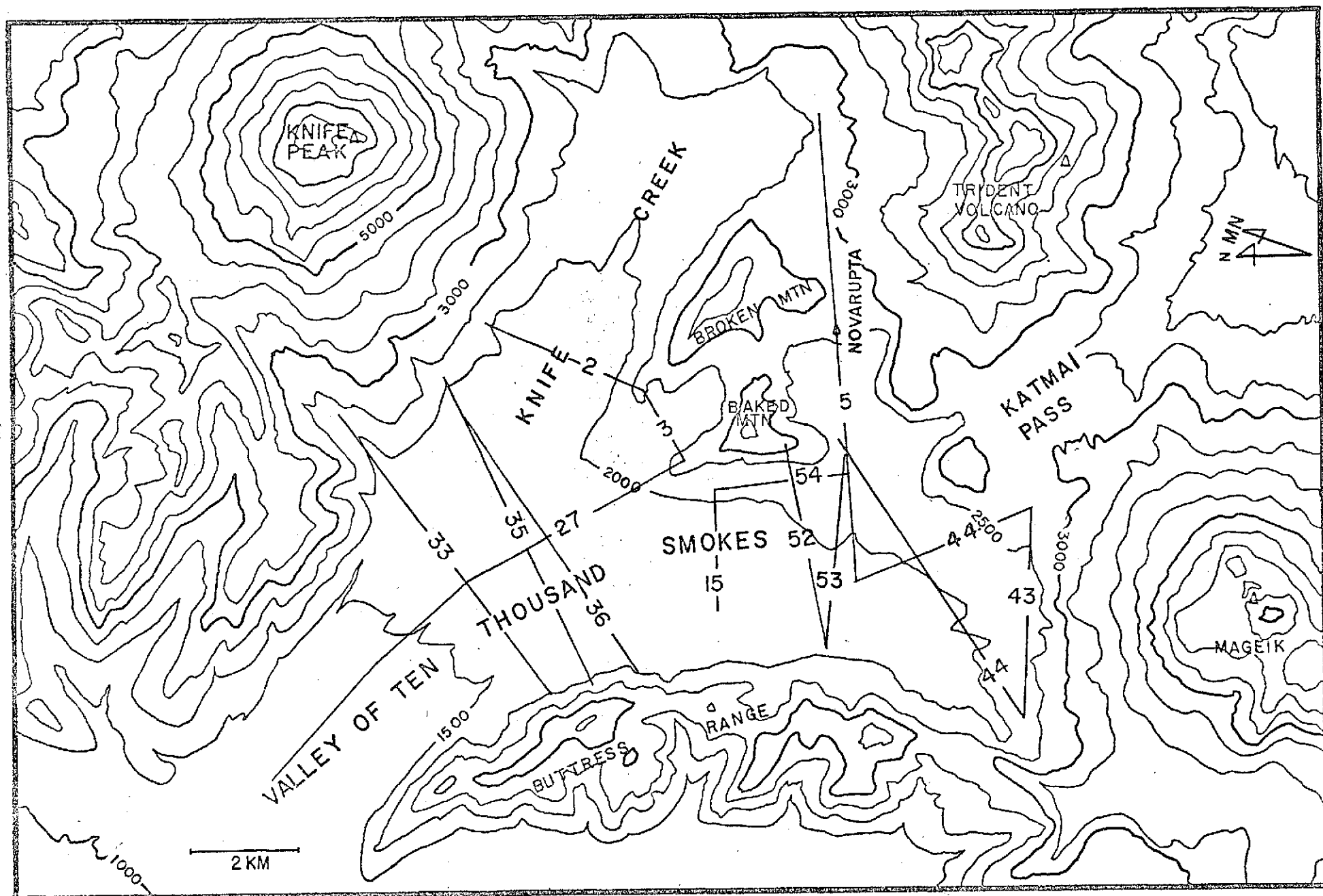
Fig. 33. Flight lines of elevation 730 - 760 m above sea level.
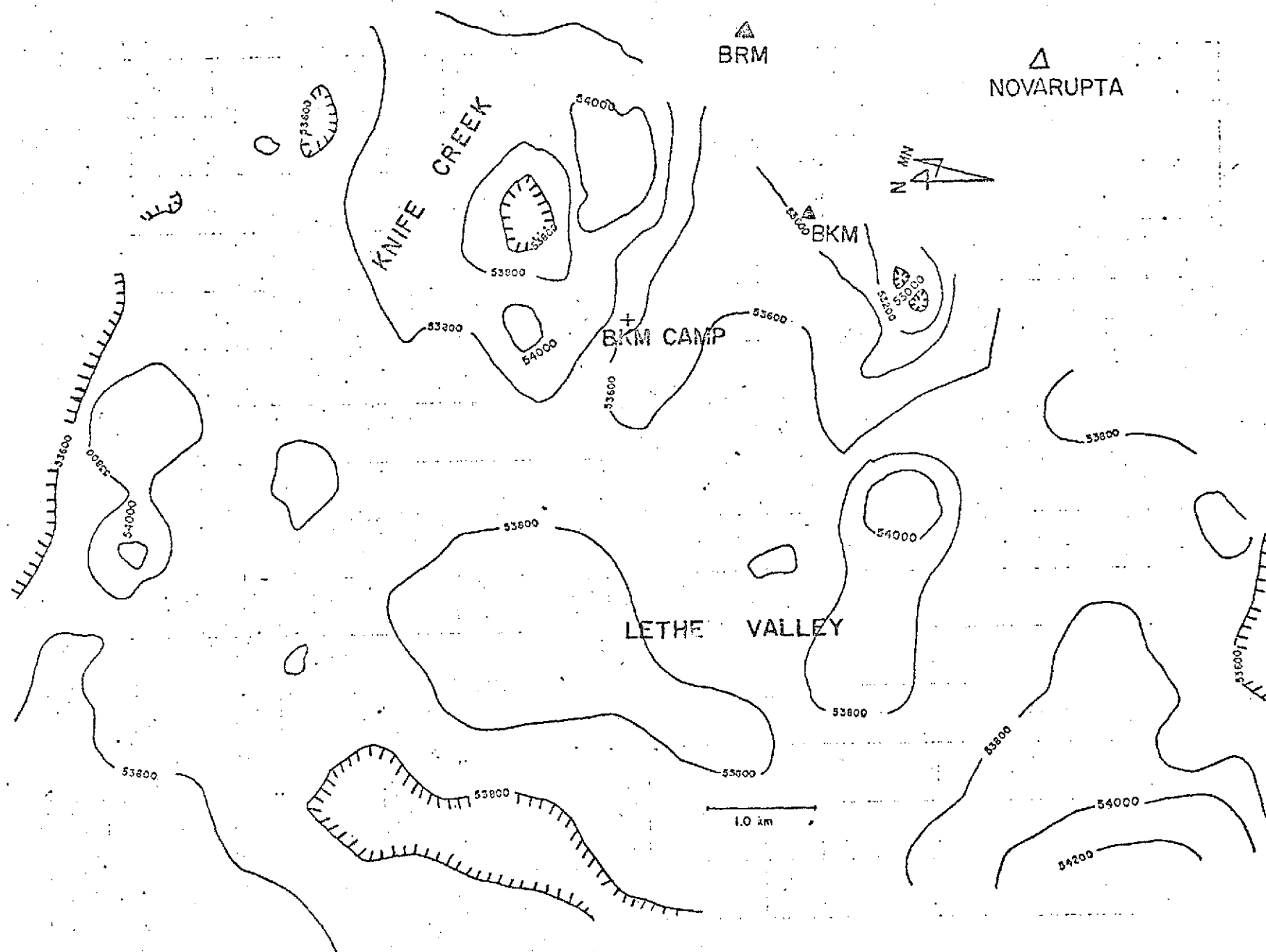
Fig. 34. Total aero-magnetic intensity map of Ten Thousand Smokes, flight height
at 730 – 760 m. BRM: Broken Mt., BKM: Baked Mt.

Fig. 35. Total aeir-magnetic anomaly map in gammas, flight height at 730 - 760 m.
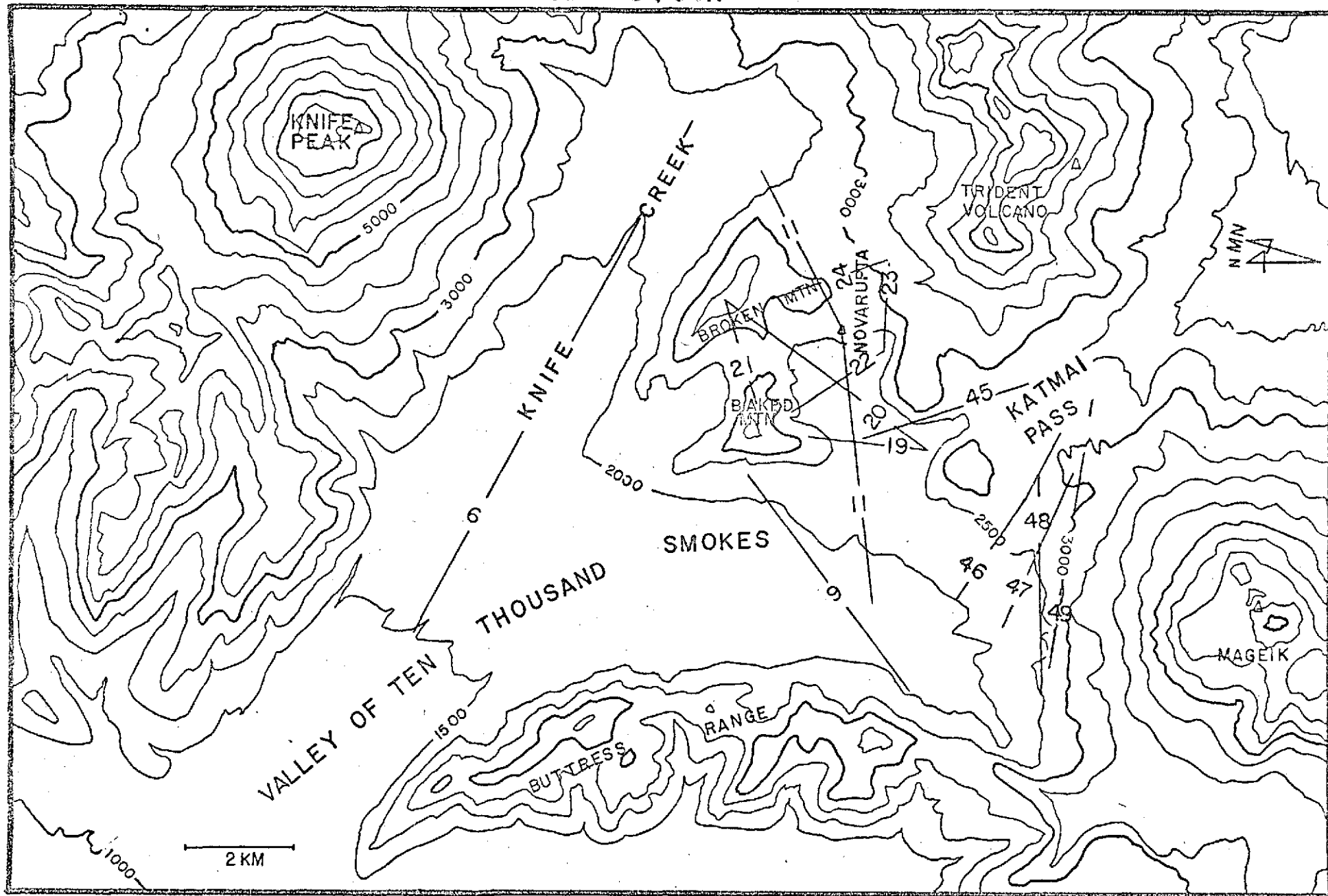
Fig. 36. Flight lines of elevation 915 – 975 m above sea level.
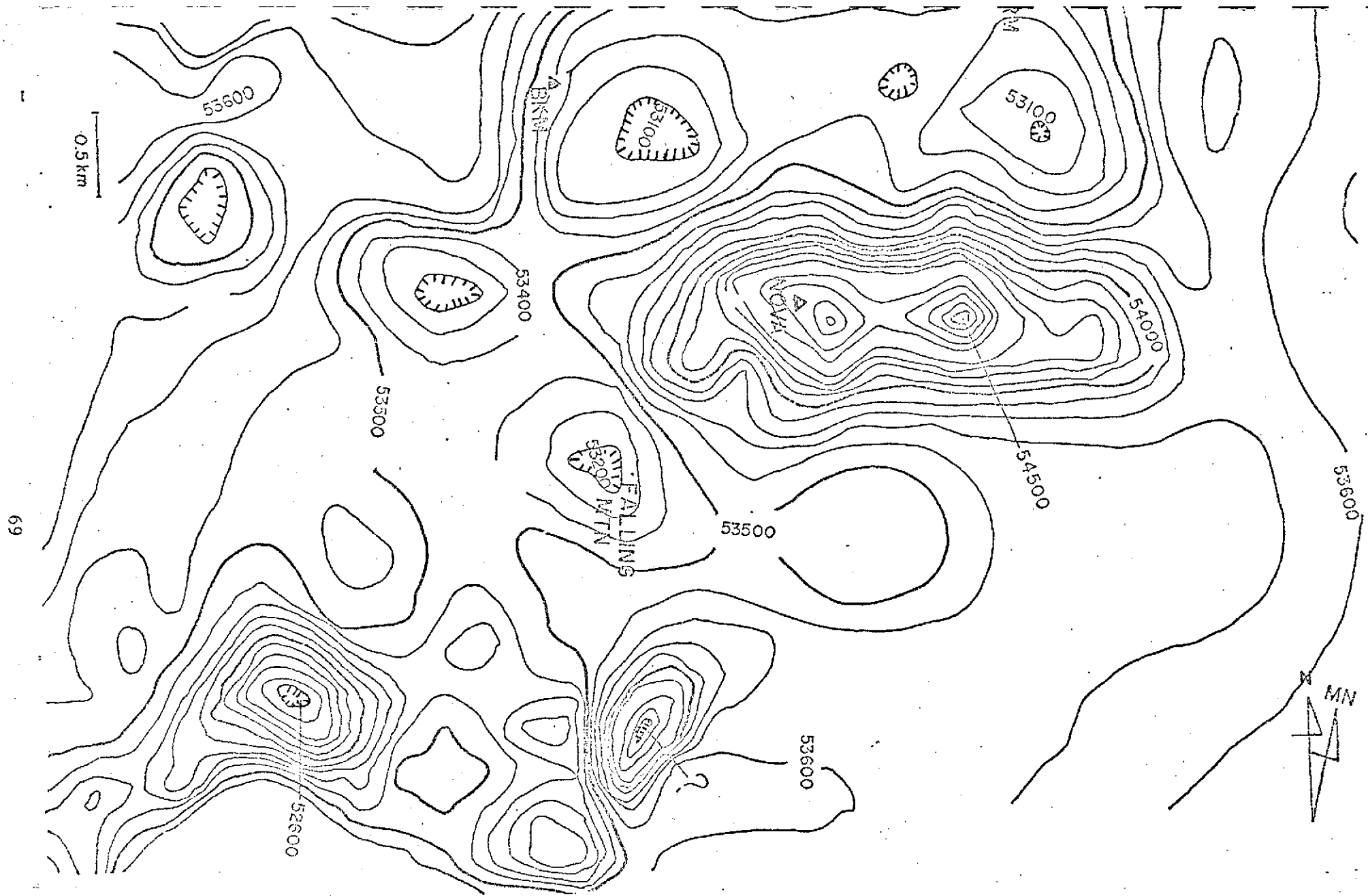
Fig. 37. Total aero-magnetic intensity map over Novarupta, flight height at 915 – 975 m.
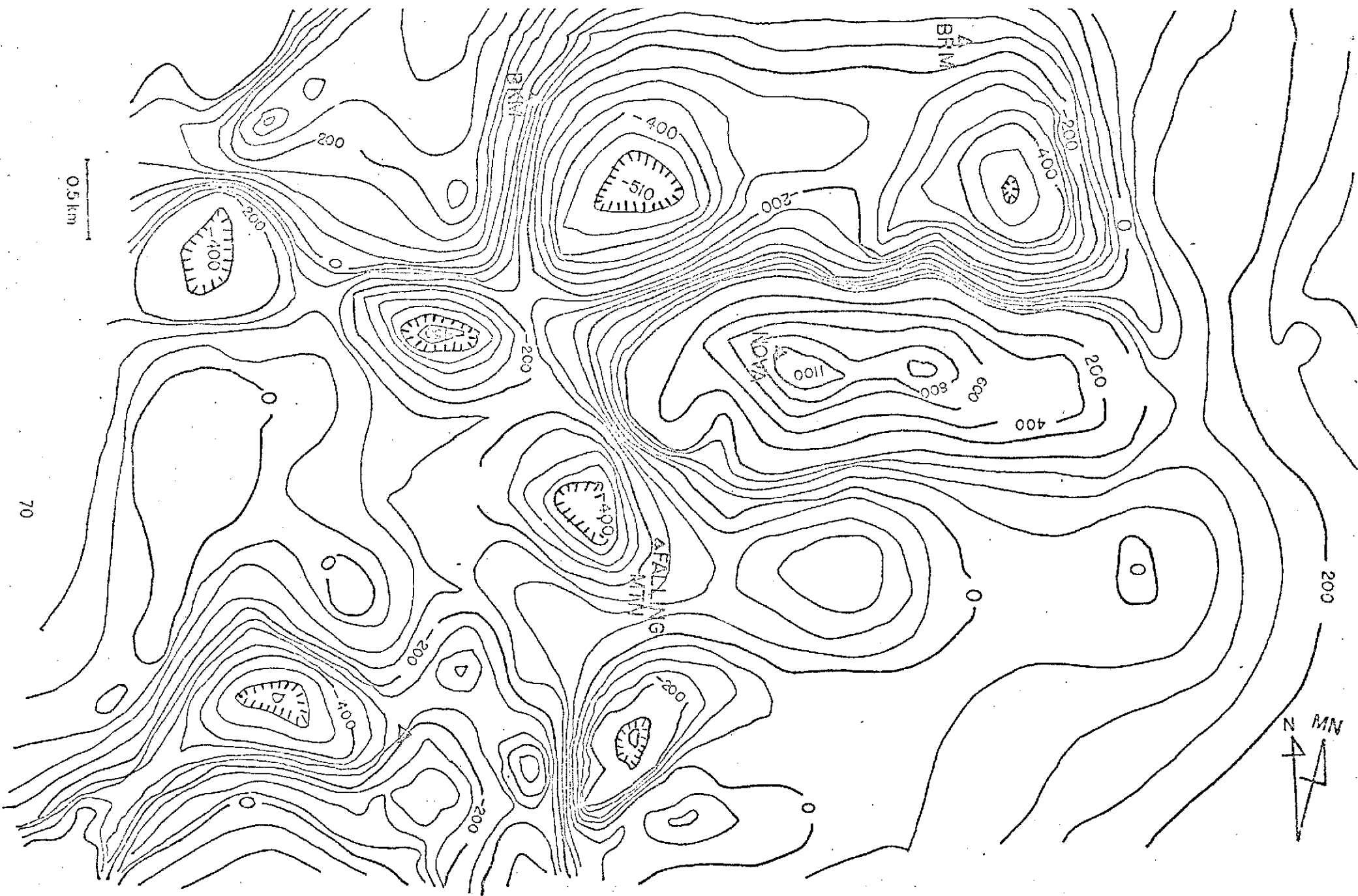
Fig. 38. Total intensity anomaly map over Novarupta.
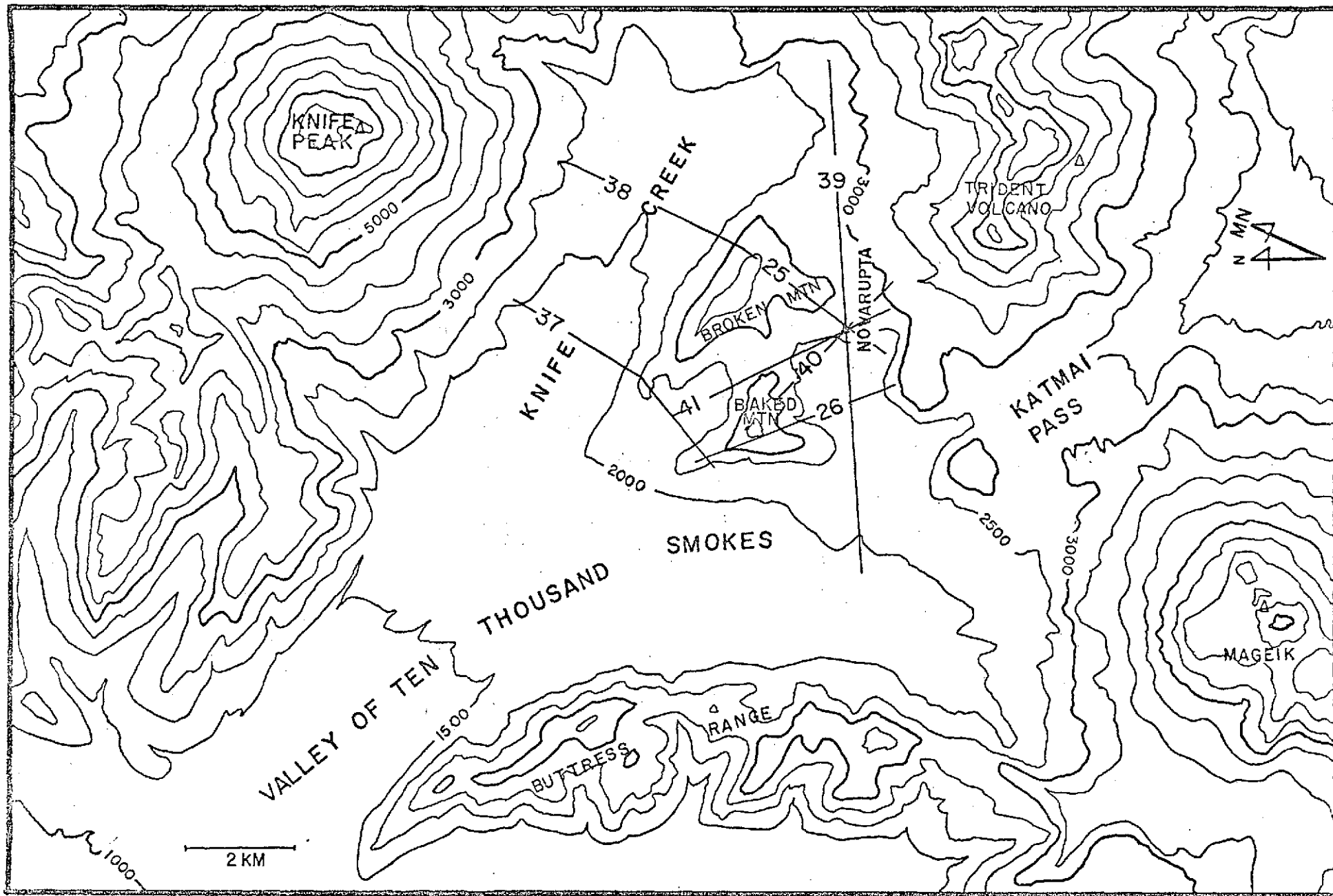
Fig. 39. Flight lines of elevation 1160 – 1190 m above sea level.
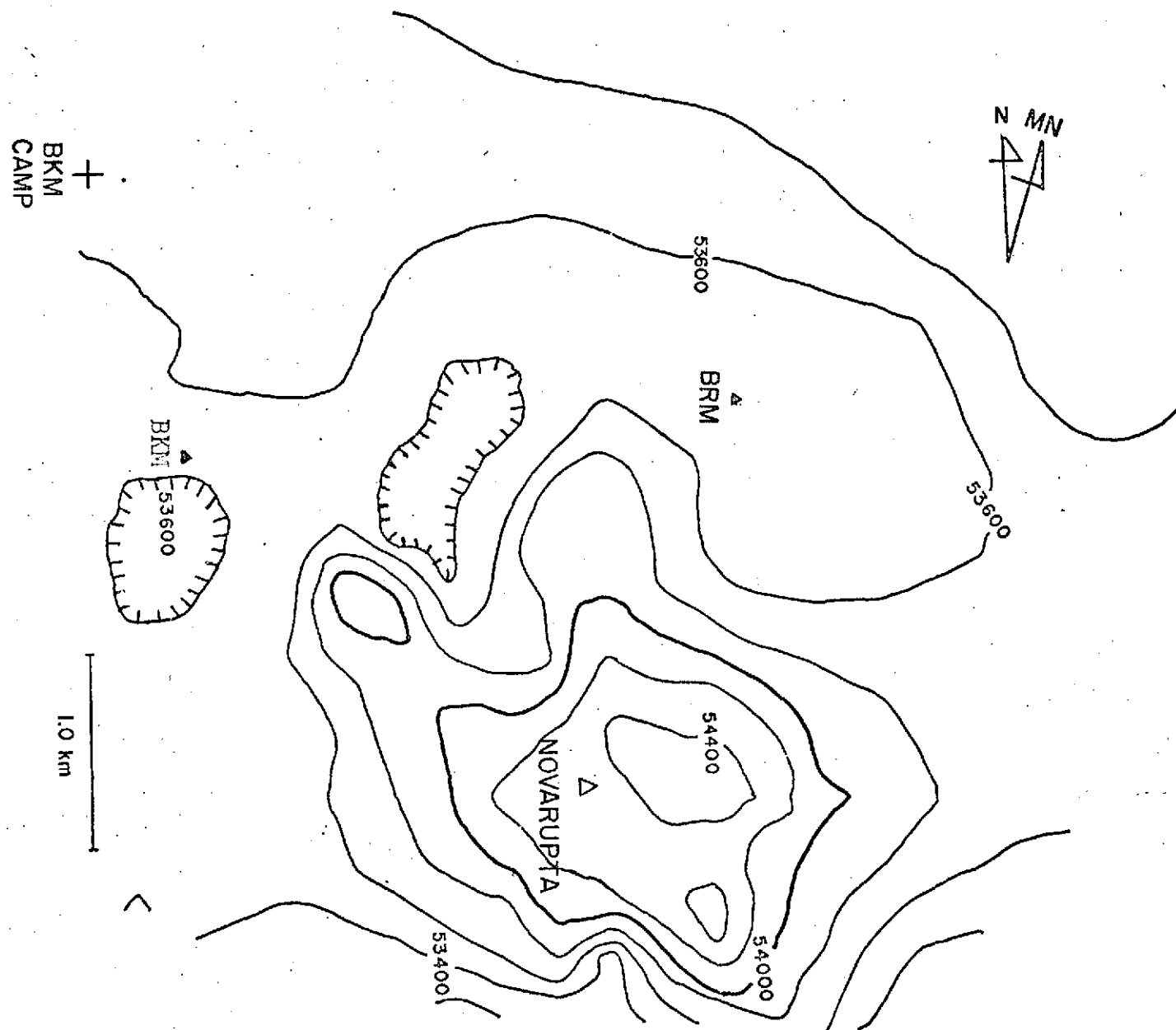
Fig. 40.   Total intensity aero-magnetic map over Novarupta, flight height at 1160 – 1190 m.   BRM: Broken Mt., BKM: Baked Mt.

Fig. 41. Total aero-magnetic anomaly map, over Novarupta, flight height at 1160 – 1190 m. BKM: Baked Mt., BRM: Broken Mt.
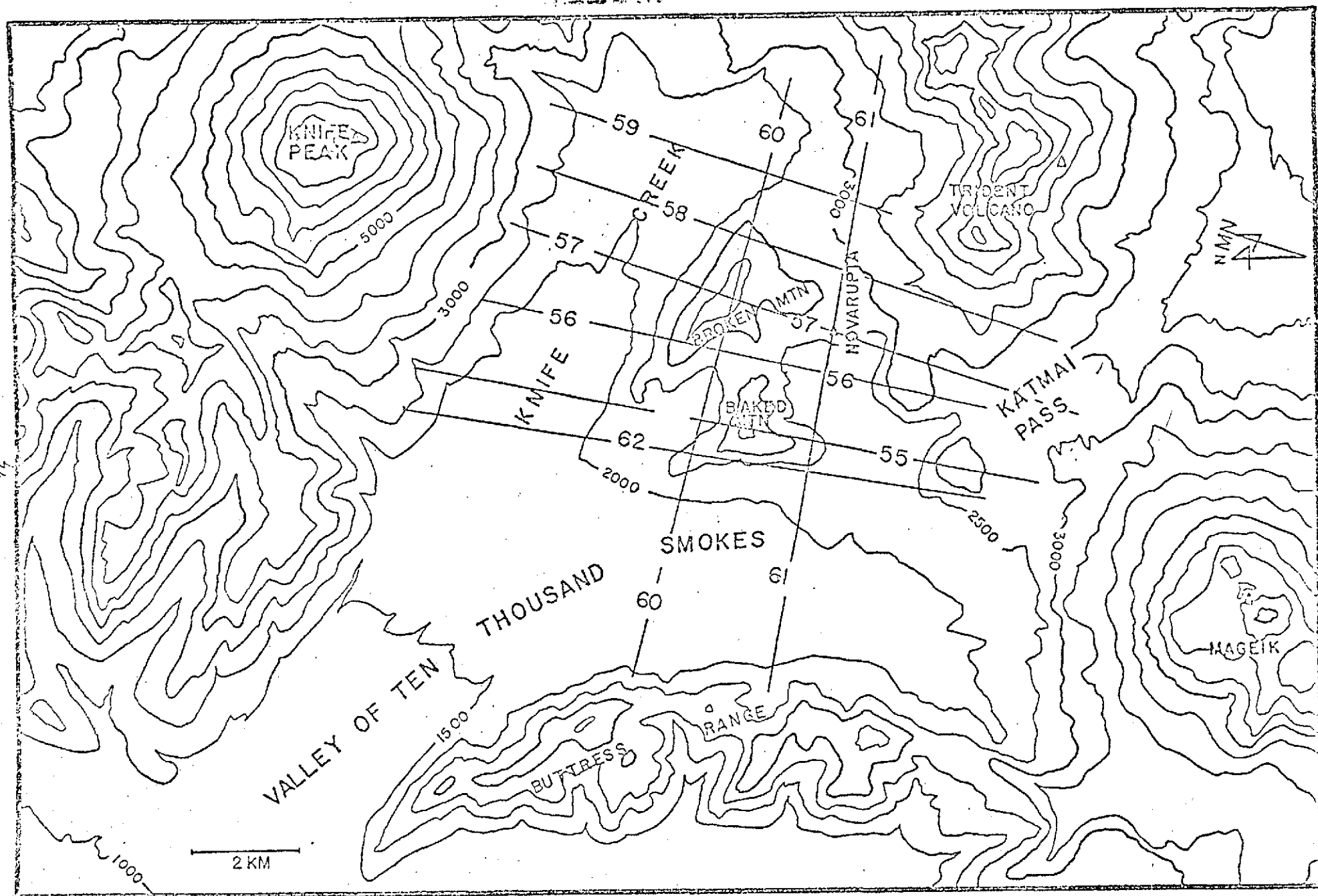
Fig. 42. Flight lines of elevation 1220 m above sea level.

TOTAL AERO-MAGNETIC INTENSITY
MAP OVER NOVARUPTA,
FLIGHT HEIGHT AT 1220 M

BRM

D
54400

NOVA

FALLING
MTN

BKM   53400

BKN CAMP

53800

53600

54000

54400

54000

54000

54000

53600

1.0 km
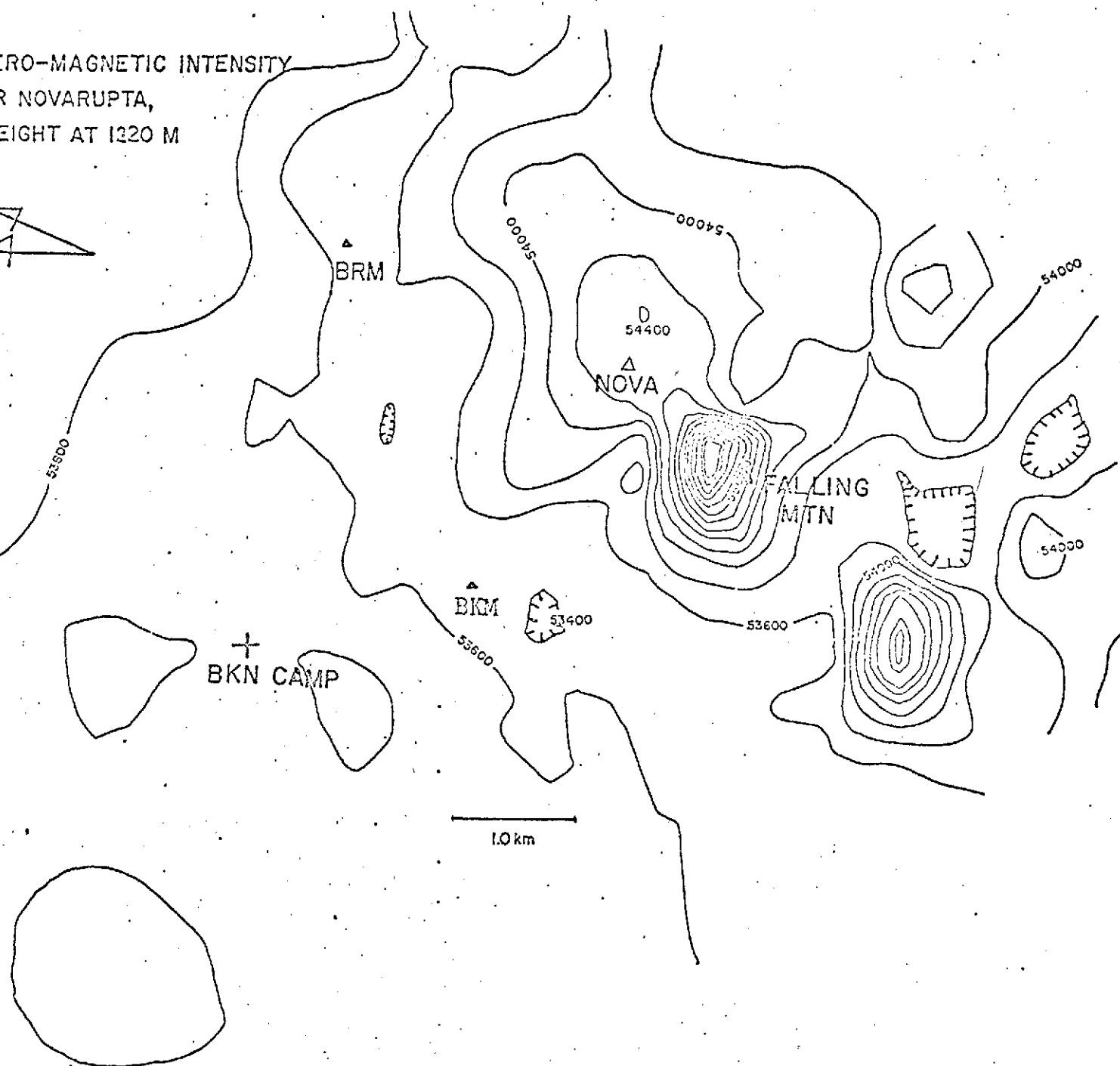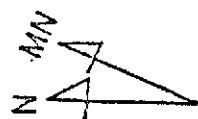
Fig. 43.   BRM: Broken Mt., BKM: Baked Mt.

Fig. 44. Total intensity anomaly map over Novarupta, flight height at 1220 m.
BRM: Broken Mt., BKM: Baked Mt.

to the pyroclastic valley fill. This fact suggests that the pyroclastic flow is not very thick.

Pyroclastic Temperatures

The minimum welding temperature of acidic volcanic glass is about 600°C (Boyd 1961). It is also possible to obtain an idea of the temperature regime from the magnetic properties of the rocks. The presence of a finely dispersed uniformly magnetized magnetite must have been formed under relatively high temperature condition (above the Curie Point for magnetite (560°C)).

The welding and deformation of glass particles can take place at a very low pressure, but the temperature, necessary for a complete welding, should be at least 800°C (Smith and others 1958). Lovering extrapolated back the measured temperature of fumarole No. 1 measured by Zies at 600°C, and found it to be between 800°C and 900°C. The fact that the pyroclastic flows were found to be uniformly magnetized (Trible 1971) along the direction of the present magnetic dipole field, and were magnetically stable, demonstrated that the temperature was higher than the Curie Point of the minerals involved (Packer, personal communication). The pyroclastic flows sampled were not all welded, which indicates lower temperatures prevailed for some areas for some of the time, or alternatively that some areas were heated more than others after deposition.

As shown above, the pyroclastic flows, as opposed to the interbedded airfall deposits, must have been laid down at temperatures between 560° and 800°C.

The average susceptibility of the pyroclastics from the Lethe indurated ash is 1.33 x 10^{-3} emu/cc (Trible 1970), with a maximum value of

1.76 x 10^{-3} emu/cc. Trible (1971) also noted that - "examination of the character of the tuff comprising the individual discs disclosed the correlation of colored streaks with measured susceptibility: white and brown streaks are prominent in discs of lower susceptibility, black bands are associated with the higher values". The Knife Creek pyroclastic flow units have a mean value of 1.8 x 10^{-3} emu/cc and other susceptibility measurements on the tuff unit from various locations in the Valley give comparable values.

Proven pre-1912 pyroclastic flows have not been observed and the similarity of the susceptibility of the different tuff units would indicate that if they exist, they had a similar origin to the 1912 flow units. Thus, pre-1912 units would not be distinguishable magnetically.

Samples of the Novarupta banded lava gave a bimodal distribution of magnetic susceptibility values. The gray glass gave a susceptibility of 0.3 x 10^{-3} emu/cc in contrast with an average for the prominent dark streaks of 1.4 x 10^{-3} emu/cc (see Table 3).

Trible concluded that both the Naknek sediments and the fumarolic altered ash can be represented by 0.5 x 10^{-4} emu/cc. The susceptibilities of the airfall pumice, the water-laid tuff, the indurated ash and the higher mode Novarupta lava gave 1.2 x 10^{-3} emu/cc. Hydrothermally altered sediments and pyroclastic rocks often gave high susceptibility, presumably due to deposition of magnetic minerals. In many cases, as the fumarolic activity becomes weaker, the hydrothermal activity changes in character, and resolution of the magnetic minerals takes place. Unless protected by an impervious layer, the high intensity magnetic minerals disappear.

The altered air fall tuff sediments have a high susceptibility in some fumarolic areas, as indicated by the magnetic ground surveys, though

the volume of effective magnetic minerals is limited. When the elevation of the survey lines was higher than the magnetic mass diameters, their effect was very small.

TABLE III

Mt. Novarupta	Dacite	Dark band	1.4×10^{-3} emu
		Gray Glass	0.3×10^{-3}
Naknek Formation			$1.0 \sim 6.5 \times 10^{-4}$
Indurated Tuff			$1.2 \sim 1.3 \times 10^{-3}$

CHAPTER IV

CONCLUSION

The most outstanding feature of the magnetic anomaly pattern is the magnetic high found in the vicinity of Novarupta. This suggests that the rocks underlying this area are more strongly magnetized than others in the surrounding area. The magnetization of the rocks composing the exposed dome of Novarupta are generally not very strong compared with other volcanics, having susceptibilities around 1×10^{-3} emu/cc.

The magnetic anomaly pattern of Novarupta as seen from lower elevations showed high frequency and high amplitude patterns such as would be generated by double volcanic cones with shallow structures. However, these small scale anomalies disappeared at higher elevations and indicate a single lava dome.

The crater rim features and moat visible around Novarupta are reflected in the magnetic anomaly maps by low amplitude and low frequency magnetic patterns, these are typical of those observed over thick Naknek deposits. The obvious interpretation is in terms of the surrounding material being low susceptibility sediments, through which the plug or dome of Novarupta has been pushed.

The oval anomaly patterns around Novarupta are elongate in an ENE-WSW direction, and include Stumbling Hill. Although no outcrops were found on Stumbling Hill, there is good reason to think that this hill is formed by intruded or domed-up material similar to that of Novarupta.

The magnetic anomaly pattern changes suddenly at the edge of Falling Mountain, Mt. Mageik and Mt. Trident. This is presumably due to the mass of magnetic material forming these mountains.

A pair of negative and positive magnetic anomalies is associated with each of Novarupta, Falling Mountain and Mt. Cerberus, and is similar to that expected if each of these is considered as a dipole magnetized in the direction of the present geomagnetic field. It is of interest to note that the elongation of the Novarupta magnetic anomaly and the volcanoes of the area are all roughly aligned parallel to the structural trend of the Alaska Peninsula.

The most acceptable model based solely on magnetic data suggests that Novarupta and Stumbling Hill are pipes of magnetic igneous material intruded through the essentially non-magnetic Naknek formation. This then makes it difficult to visualize a much larger ancestral Novarupta, high enough to be the source of the pyroclastic fill for all parts of the Valley of Ten Thousand Smokes at once. This would require that either the material of ancestral Novarupta was largely low susceptibility and thus similar to the Naknek, and the destruction of the original peak was by collapse, or, that it was a composite cone similar to the volcanoes seen in the area today, and the material was removed explosively. This would presumably require that the whole composite cone down to Naknek bedrock be removed. Neither of these possibilities fit well with the field evidence.

Subsidence by some form of block faulting is also a possibility, but these will only be seen magnetically where there is a sufficiently large susceptibility contrast. High horizontal magnetic gradients indicative of faulting are seen along the base of Falling Mountain, and also associated with the northern part of Broken Mountain. The gradients in these two areas may well have been enhanced by fumarolic action along the proposed fracture zones.

Over the flat portion of the Valley, no large marked anomalies are found, though a number of small scattered local magnetic highs are usually associated with fumarolic features. At the foot of Broken Mountain and across the lower end of the Intermediate Valley, negative anomalies of the order of a few hundred gammas are found around the recently active geothermal areas.

A number of weak magnetic highs seem to be associated with sharper peaks over apparently thicker pyroclastic flows. As these anomalies amount to only a hundred gammas or so, and are local in extent, they probably represent minor variation in the thickness of flow units or perhaps an accumulation of magnetite from fumaroles.

Trible (1971) discussed the possibility that the glacial drift has a high susceptibility and could account for some of the magnetic highs, and it is also possible that some material interpreted as high susceptibility glacial drift may in fact be pre-1912 flow units.

REFERENCES

Aramaki, S. 1969 Some problems of the theory of caldera formation, Bull. Volcanol., Ser. 2, Vol. 14, No. 2, pp. 55-76.

Barazangi, M. and J. Dorman 1969. World seismicity maps compiled from ESSA, Coast and Geodetic Survey, Epicenter data, 1961-1967, Bull. Seism. Soc. Am., Vol. 59, No. 1, pp. 369-380.

Beloussov, V. I. and B. V. Ivanov. 1967. Pumice formations in the area Uzon Depression Geysernaia River Valley in Kamchatka, Bull. Volcanol. Tome XXX, pp. 75-80.

Berg, E., S. Kubota and J. Kienle. 1967. Preliminary determination of crustal structure in the Katmai National Monument, Alaska, Bull. Seism. Soc. Am., Vol. 57, No. 6, pp. 1367-1392.

Bowen, N. L. 1928. The evolution of the igenous rocks, Princeton Univ. Press, pp. 54-62.

Boyd, B. 1961. Welded tuffs and flows in the rhyolite plateau of Yellowstone Park, Wyoming, Bull. Geol. Soc. Am., Vol. 72, No. 3.

Brosge, W., E. E. Brabb and E. R. King. 1970. Geologic interpretation of reconnaissance aeromagnetic survey of Northeastern Alaska, U. S. Geological Survey Bull. 1271-F.

Burk, C. A. 1965. Geology of Alaska Peninsula-Island Arc and Continental Margin, Geol. Soc. of Am., Memoir No. 99, Part 1 - 3.

Curtis, G. H. 1968. The stratigraphy of the ejecta from 1912 eruption of Mount Katmai and Novarupta, Alaska, in: Studies in Volcanology - a memoir in honor of Howell Williams, Geol. Soc. Amer. Mem. 116, pp. 153-210.

Decker, R. W. 1963. Proposed volcano observatory of Katmai National Monument, Alaska, A preliminary study, Dartmouth College.

Fenner, C. N. 1920. The Katmai region, Alaska and the great eruption of 1912, J. of Geol., Vol. 28, No. 7, pp. 569-606.

_____ 1922. Evidences of assimilation during the Katmai eruption of 1912 (abs.), Geol. Soc. Am. Bull., Vol. 33, No. 1, p. 129.

_____ 1925. Earth movements accompanying the Katmai eruption, J. Geol., Vol. 33, No. 2, pp. 116-139, No. 3, pp. 193-233.

Fenner, C. N. 1926. The Katmai magmatic province, J. Geol., Vol. 34, No. 7, pp. 673-772.

_____ 1950. The chemical kinetics of the Katmai eruption, Part 1, Am. J. Sci., Vol. 248, pp. 593-627.

Forbes, R. B., D. K. Ray, T. Katsura, H. Matsumoto, H. Haramura, and M. J. Furst. 1969. The comparative chemical composition of continental island vs. arc andesites in Alaska, Proceedings of the Andesite Conference, International Upper Mantle Committee, pp. 111-120.

Gedney, L., C. Matteson and R. B. Forbes. 1970. Seismic Refraction Profiles of the Ash Flow in the Valley of Ten Thousand Smokes, Katmai National Monument, Alaska, J.G.R., Vol. 75, No. 14, pp. 2619-2624.

Gorshkov, G. S. 1958. On some theoretical problems of volcanology, Bull. Volcanology II, Vol. 19, pp. 103-113.

Grant, F. S. and G. F. West. 1965. Interpretation theory in applied geophysics, (Part II), geomagnetic field, McGraw-Hill Book Company.

Griggs, R. G. 1922. The Valley of Ten Thousand Smokes, Am. Geograph. Soc., p. 340.

Grim, P. J. and B. H. Erickson. 1969. Fracture zones and magnetic anomalies south of the Aleutian trench, J. Geophys. Res., Vol. 74, pp. 1488-1494.

Grow, J. A. and T. Tanya. 1970. Mid-Tertiary tectonic transition in the Aleutian arc, Geol. Soc. Am. Bull., Vol. 81, No. 12, pp. 3715-3722.

Hagiwara, Y. 1965. Analysis of the results of the aeromagnetic surveys over volcanoes in Japan (1), Bull. Earthquake Res. Inst., Vol. 43, pp. 529-547.

Kagami, H. and R. Tsuchi. 1968. Miocene marine fossils on the Japan trench, Records of Oceanography, Works in Japan, Vol. 1, p. 1.

Kanamori, H. 1970. Mechanism of earthquakes, Shizen (Nature) 25, No. 10, pp. 92-99.

Keller, S. A. and H. N. Reiser. 1959. Geology of the Mount Katmai area, Alaska, U. S. Geological Survey, Bull. 1058-G, pp. 261-298.

Kienle, J. 1969. Gravity survey in the general area of the Katmai National Monument, Alaska, Univ. of Alaska, Ph. D. Thesis.

Kienle, J. 1970. Gravity Traverses in the Valley of Ten Thousand Smokes, Katmai National Monument, Alaska, J.G.R., Vol. 75, No. 30, pp. 6641-6649.

Kienle, J., D. Bingham and R. Forbes. 1970. Seismic and geological evidence of pre-1912 tuff deposits in the Valley of Ten Thousand Smokes, Katmai National Monument, Alaska (abstract), EOS Trans. AGU. 51, p. 829.

Kubota, S. and E. Berg. 1967. Evidence for magma in the Katmai volcanic range, Bull. Volcanol., Tome XXXI, pp. 175-214.

Kuno, H. 1956. Volcano and volcanic rocks, Iwanami Public Co.

Kuno, H. 1968. Origin of andesite and its bearing on the island arc structure, Bull. Volcanol., Tome XXX, pp. 142-176.

Luntey, R. S. and others. 1954. Katmai National Monument, U. S. National Park Service Interim Report.

Matsumoto, T. 1971. Seismic bodywaves observed in the vicinity of Mt. Katmai, Alaska, and evidence for the existence of molten chamber, Geol. Soc. Am. Bull., Vol. 82, pp. 2905-2920.

Matsuzaki, T. and T. Utashiro. 1966. On the aeromagnetic surveys in the Kagoshima Bay and its vicinity, Rep. of Hydrographic Res., No. 1, pp. 23-25.

Minakami, T. T. Ishikawa and K. Yagi. 1951. The 1944 eruption of volcano Usu in Hokkaido, Japan – History and mechanism of formation of the new dome "Showa-Shinzan", Bull. Volcanol., Series II, Tome XI, pp. 45-157.

Minato, M., M. Funahashi and M. Gorai. 1965. The geologic development of the Japanese Islands, Tsukiji Shokan, Chapter 5.

Nayudu, R. Y. 1964. Volcanic ash deposits in the Gulf of Alaska and problems of correlation of deep-sea ash deposits, Marine Geol., Vol. 1, No. 3, pp. 194-212.

Peter, G., D. J. Elvers and M. Yellin. 1965. Geologic structure of the Aleutian Trench, Southwest of Kodiak Island, J. Geophys. Res., Vol. 70, No. 2, pp. 353-366.

Ray, Dipak, K. 1967. Geochemistry and petrology of the Mount Trident adnesites, Katmai National Monument, Alaska, Univ. of Alaska, unpublished doctoral dissertation.

Rikitake, T. H. Tajima, S. Izutuya, Y. Hagiwara, K. Kawada and Y. Sasai. 1965. Gravimetric and geomagnetic studies of Onikobe area, Bull. Earthquake Res. Inst., Vol. 43, pp. 241-267.

Rikitake, T. and Y. Hagiwara. 1965. Magnetic anomaly over a magnetized circular cone, Bull. Earthquake Res. Inst., Vol. 43, pp. 509-527.

Runcorn, S. K., et al. (eds.). 1967. International Dictionary of Geophysics (2 vols.) Oxford: Pergamon.

Smith, R. L. and others. 1958. Welded tuffs, Experimental I (abstract), Am. Geophys. Union Trans., Vol. 39, No. 3, pp. 532-533.

Snyder, G. L. 1954. Eruption of Trident Volcano, Katmai National Monument, U. S. Geol. Sur., Circular 318, p. 7.

Speranskaia, I. M. 1967. Okhotsk inimbrite province, Bull. Volcanol., Tome XXX, pp. 56-61.

Stacey, F. D. 1969. Physics of Earth, Part 6, pp. 157-191, John Wiley and Son.

Sugimura, A., T. Matsuda, K. Chinzei and K. Nakamura. 1963. Quantitative distribution of late Cenozoic volcanic materials in Japan, Bull. Volcanol., Tome XXVI, pp. 125-140.

Sugimura, A. 1967. Chemistry of volcanic rocks and seismicity of the earth's mantle in the island arcs, Bull. Volcanol., Tome XXX, pp. 319-334.

Sumner, L. 1952. Magnificent Katmai - the unfolding story of a great wilderness in tradition - Katmai National Monument, Sierra Club Bull., Vol. 37, No. 10, pp. 29-52.

Tobin, D. G. and L. K. Sykes. 1966. Relationship of hypocenters of earthquakes to the geology of Alaska, J. Geophys. Res., Vol. 71, pp. 1659-1667.

Trible, M. 1967. Thesis

Tsuboi, C. 1961. The history of earth, Part II, pp. 29-58, Iwanami Public Co.

Tsuya, H. and R. Morimoto. 1963. Types of volcanic eruptions in Japan, Bull. Volcanol., Tome XXVI, pp. 209-222.

Uyeda, S. and A. Sugimura. 1968. Island arcs, Iwanami Science series.

Vacquier, V., N. C. Steenland, R. G. Henderson and I. Zeiz. 1951. Interpretation of aeromagnetic maps, Geol. Soc. Am. Memoir 47.

Vacquier, V. and S. Uyeda. 1967. Paleomagnetism of nine seamounts in the western Pacific and of three volcanoes in Japan, Bull. Earthquake Res. Inst., Vol. 45, pp. 815-848.

Von Huene, R. and G. G. Shor, Jr. 1969. The structure and tectonic history of the Eastern Aleutian Trench, Geol. Soc. Amer. Bull., Vol. 80, No. 10, pp. 1889-1902.

Williams, H., G. Curtis and W. Jule. 1954. Preliminary notes on geological works date on Mt. Katmai and in the Valley of 10,000 Smokes, Alaska, U. S. National Park Service, Interim Report.

Yokoyama, I. 1965. Structure of calderas and their origin, Bull. Volcanol. Ser. 2, Vol. 10, pp. 119-127.

Yokoyama, I. 1969. Some remarks on caldera, Bull. Volcanol., Ser. 2, Vol. 14, No. 2, pp. 77-83.

Yukutake, T. and Y. Hagiwara. 1965. Magnetism of volcanoes, Bull. Volcanol. Ser. 2, Vol. 10, pp. 100-109.

Appendix I

Steinberg and Rivosh (1965) concluded that the magnetic anomalies were controlled by the shape of the volcanic pile by using the Rikitake model. This was especially true for dormant volcanoes, where there is a magma reservoir maintaining temperatures over the Curie Point, as it is recognized that the anomalies are dependent on the remnant magnetization of rocks. Figs. I, II, III and IV show the analytically computed total magnetic intensity anomaly at five different elevations above Magnetized Circular Cone (after Rikitake and Hagiwara, 1965).
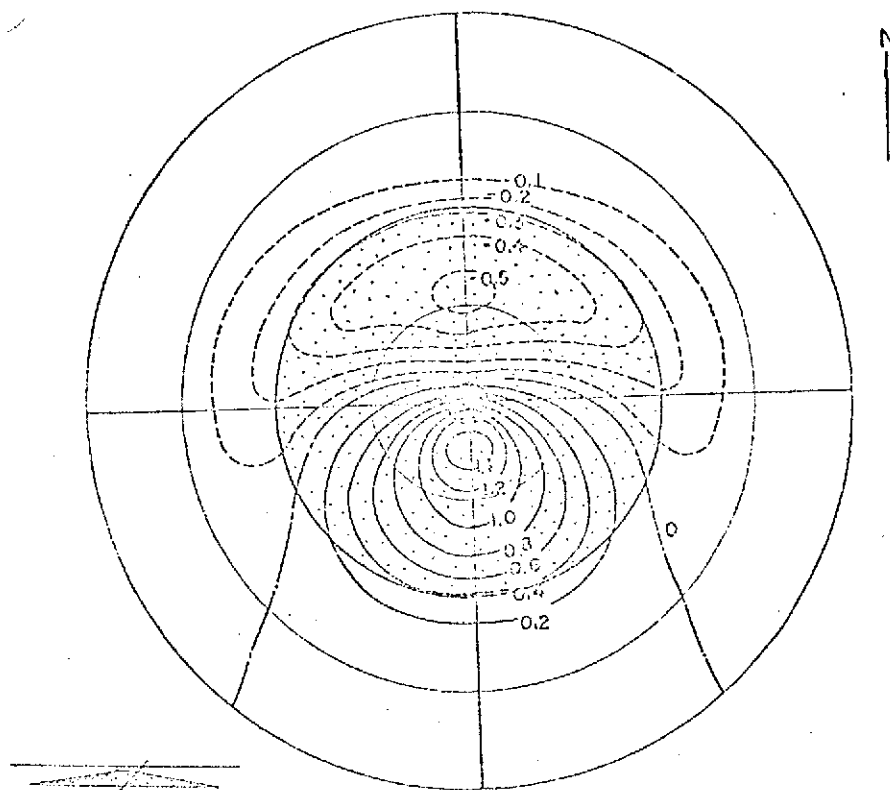
Fig. I. ΔF over a magnetized circular cone, which
is shown by the shaded circle, at a height of 0.2 in
units of the bottom radius. The numerals indicate the
field intensity when the intensity of magnetization
and the bottom radius are taken as unity. It is assumed
that the direction of magnetization lies in the magnetic
meridian plane and that its inclination agrees with the
geomagnetic dip which is taken as 48°. The slope angle
is assumed as 10°.
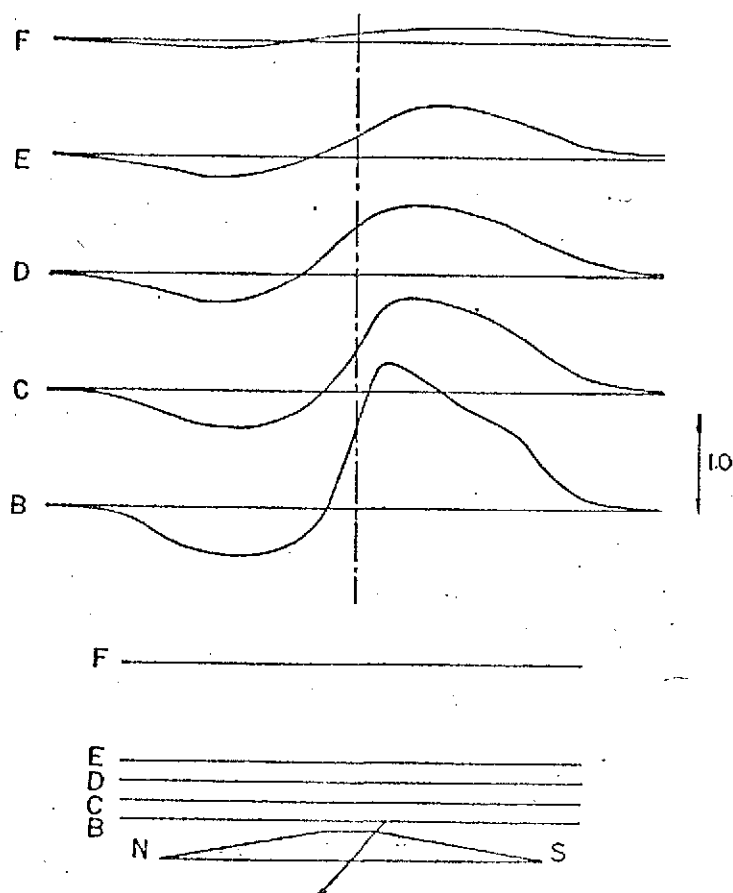
Fig. II. ΔF profiles along the north-south line passing
through the centre of a cone of which the slope angle is
10°. The direction of magnetization and its relation to
the geomagnetic field have been given in the caption of
Fig. I. The intensity of magnetization and the bottom
radius are both taken as unity. The flight heights are
taken as 0.1, 0.2, 0.3, 0.4, 0.5 and 1.0.
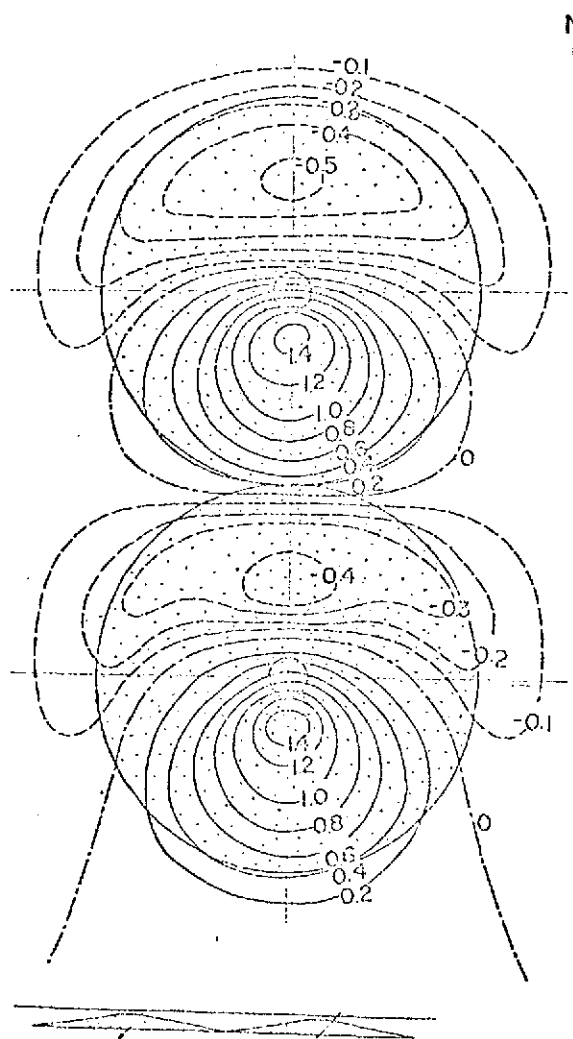
Fig. III. ∆F over two cones closely placed. The line connecting the centres runs in a north-south direction. The parameters of the cones and the relation between the magnetization and the geomagnetic field are the same as those for Fig. I.
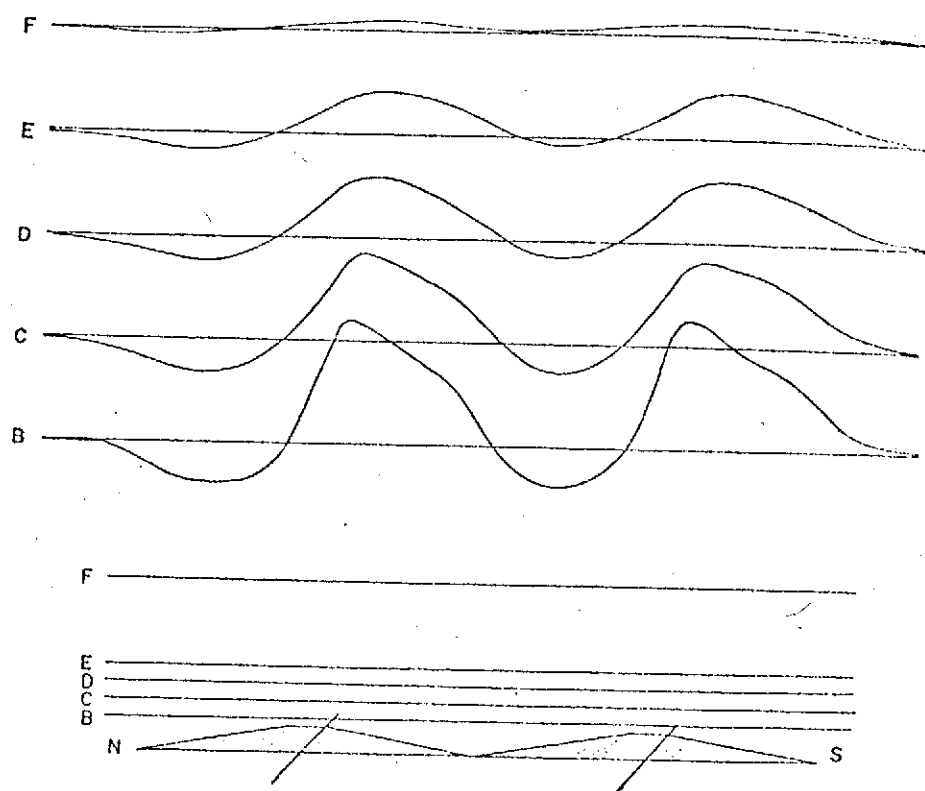
Fig. IV. ΔF profiles for the cones as shown in Fig. III.
The flight heights are 0.2, 0.3, 0.4, 0.5 and 1.0.

```
      C
      C PROGRAM TO DRAW PROFILES FOR MAGNETIC DATA AND ALTITUDES WHEN NEEDED
      C
0001        DIMENSION    ISYM(5),  XP(100),  YP(100),  ZP(100)
0002        REAL         NAME(2)
0003        DATA         ISYM / 0, 12,  5, 2, 4 /
0004        CIN = 2.57
      C
      C INITIALIZE PLOT TAPE
      C
0005        CALL PLOTST
      C
      C READ FIRST CARD OF SERIES - MIN X,Y,  MAX X,Y,  NBR PROFILES,  HEADING
      C AND RANGE OF ALTITUDE IF NALP IS SET
      C XMIN AND YMIN = STARTING POINT AND XMAX YMAX = END POINT XMIN MAY BE
      C ACTUALLY NUMERICALLY LARGER THAN XMAX
      C CURRENT LIMIT IS FIVE PROFILES PER PLOT.  THERE IS 1 FILE PER PROFILE
      C CHANGE PEN COLORS FOR DIFFERENT FLIGHT ALTITUDES IF DESIRED/
      C
0006      5 READ (1,1000, END = 900 ) HEAD, XMIN, YMIN, XMAX, YMAX,
          1       AMIN, AMAX, NPR, NALT
0007   1000 FORMAT ( 7F10.0, 2I2 )
      C
      C IF MORE THAN FIVE (5) PROFILES ARE REQUESTED - TRUNCATE TO FIVE AND
      C SET CODE TO TERMINATE JOB AFTER THOSE FIVE
      C
0008        ITERM = 0
0009        IF ( NBR .LE. 5 ) GO TO 6
0010        NBR = 5
0011        ITERM = 1
      C
      C CALCULATE LENGTH OF AXIS, DRAW & ANNOTATE
      C
0012      6 DX = XMAX - XMIN
0013        DY = YMAX - YMIN
0014        XLEN = SQRT( DX * DX  +  DY * DY )
0015        CALL PLOT ( 1.5, 2.0, 3 )
0016        XL = 1.5 + ( XLEN / CIN )
0017        CALL PLOT ( XL, 2.0, 2 )
0018        DO 10 I = 1,5
0019        FAC = ( I - 1. ) / 4.
0020        XN = XMIN + FAC * DX
0021        YN = YMIN + FAC * DY
0022        X = 1.5 + FAC * ( XLEN / CIN )
0023        Y = 2.0
0024        CALL SYMBOL ( X, Y, .14, 13, 0.0, -1 )
0025        Y = 1.9
0026        CALL NUMBER ( X, Y, .14, XN, 270., 2 )
0027        CALL SYMBOL (-0.0, -0.0, -0.0, ' ', 270., +1 )
0028        CALL NUMBER (-0.0, -0.0, -0.0, YN, 270., 2 )
0029     10 CONTINUE
      C
      C DRAW AND LABEL MAGNETIC AXIS
      C
```

```
0030                CALL PLOT ( 1.5, 10.0, 3 )
0031                CALL PLOT ( 1.5, 2.0, 2 )
0032                YN = 52000.
0033                X = 0.5
0034                X1= 1.5
0035                Y = -.5
0036                DO 15 I = 1,4
0037                YN = YN + 1000.
0038                Y = Y + 2.5
0039                CALL PLOT ( X, Y, 3)
0040                CALL NUMBER ( X, Y, .14, YN, 0.0, -1 )
0041                CALL SYMBOL ( X1, Y, .14, 13,  90., -1 )
0042             15 CONTINUE
           C
           C DRAW AND LABLE ALTITUDE AXIS
           C
0043                IF ( NALT .EQ. 0 ) GO TO 19
0044                DA = AMAX - AMIN
0045                NL = DA / 500. + 1
0046                CALL PLOT ( XL, 9.5, 3 )
0047                CALL PLOT ( XL, 6.0, 2 )
0048                YN = AMIN
0049                X = XL + .2
0050                DO 18 I = 1, NL
0051                F = I - 1
0052                YN = AMIN + F * 500.
0053                Y = ( YN - AMIN ) / DA * 3.5 + 6.0
0054                CALL PLOT ( XL, Y, 3)
0055                CALL SYMBOL ( XL, Y, .14, 13, 90.,-1 )
0056                CALL NUMBER ( X, Y, .14, YN, 0.0, -1)
0057             18 CONTINUE
0058                CALL SYMBOL ( XL, 9.5, .14, 13, 90., -1 )
0059                CALL NUMBER ( X, 9.5, .14, AMAX, 0.0, -1 )
0060             19 IP = 0
           C
           C END FILE ON PLOT TAPE FOR THE JUST PLOTTED FLIGHT RECORD
           C
0061             20 IP = IP + 1
0062                IF ( IP .EQ. 1 ) GO TO 26
0063                IF ( IP .LE. NPR ) GO TO 25
0064                XNEW = AMAX1 ( XNEW, 15.0 )
0065                XNEW = XLEN / CIN + 5.
0066                YNEW = 0.0
0067                CALL PLOT ( XNEW, YNEW, -3)
0068                IF ( ITERM .EQ. 1 ) GO TO 900
0069                GO TO 5
0070             25 CALL PLOT ( 0.0, 0.0, -3 )
           C
           C READ CARD FOR INDIVIDUAL PROFILE
           C
0071             26 READ(1,1001) ALT, NAME
0072           1001 FORMAT ( F10.0, 2A4 )
0073                I = 0
           C
```

93

```
           C READ DATA CARDS
           C
0074          30 READ(1,1002) IX, IY, IZO, IZ1
0075        1002 FORMAT ( 4I10 )
0076              IF ( IZO .EQ. 0 ) GO TO 35
0077              I = I + 1
0078              X = IX / 100.
0079              Y = IY / 100.
0080              DX = X - XMIN
0081              DY = Y - YMIN
0082              XP(I) = 1.5 + ( SQRT( DX * DX + DY * DY ) / CIN )
0083              ZO = IZO - 53000.
0084              YP(I) = (ZO / 1000. ) * 2.5 + 2.0
0085              IF ( YP(I) .GT. 10.0 ) YP(I) = 10.0
0086              Z1 = IZ1
0087              ZP(I) = (Z1 - AMIN ) / DA * 3.5 + 6.0
0088              IF ( ZP(I) .GT. 10.0 ) ZP(I) = 10.0
0089              GO TO 30
0090          35 X = -1.5 + IP * 3.
0091              Y = 0.0
0092              CALL NUMBER ( X, Y, .21, ALT, 0.0, -1 )
0093              CALL SYMBOL (-0.0, -0.0, -0.0, ' FT ', 0.0, 5 )
0094              CALL SYMBOL (-0.0, -0.0, .21, ISYM(IP), 0.0, -1 )
0095              Y = 9.6
0096              X = -1.0 + IP * 3.
0097              CALL SYMBOL( X, Y, .21, NAME, 0.0, 8 )
           C
           C PLOT MAGNETIC PROFILES
           C
0098              CALL PLOT(XP(1), YP(1), 3)
0099              DO 40 J = 1, I
0100              CALL SYMBOL ( XP(J), YP(J), .07, ISYM(IP), 0.0, -2)
0101          40 CONTINUE
0102              IF ( NALT .EQ. 0 ) GO TO 20
           C
           C PLOT PROFILE OF ALTITUDE
           C
0103              CALL PLOT ( XP(1), ZP(1), 3)
0104              DO 50 J = 1, I
0105              CALL SYMBOL(XP(J), ZP(J), .07, ISYM(IP), 0.0, -2 )
0106          50 CONTINUE
0107              GO TO 20
           C
           C AT END OF FILE
           C
0108         900 WRITE (3,3000)
0109        3000 FORMAT ( '      END OF JOB ' )
0110              CALL PLOT ( 0.0, 0.0, 99 )
0111              CALL EXIT
0112              END
```

94

```
      C
      C PROGRAM TO GET MAGNETIC DATA READY FOR STAMPEDE PROGRAM.   X AND Y
      C VALUES GIVEN ONLY AT FIRST AND LAST POINT - VALUES IN BETWEEN NEED TO
      C BE CALCULATED. AVERAGES FOR EACH ALTITUDE AND OVERALL AVERAGES AND
      C ANOMALIES ARE CALCULATED
      C
0001        DIMENSION    FLD(50),  IMF(50)
0002        DIMENSION    X(100),   Y(100),   IZ0(100), IZ1(100), IZ2(100)
0003        REAL*8       NAME,     NAMEC,    BLANK,    DATE,     NAMEX
      C
0004        DATA  BLANK, NAMEX  /'        ', 'EXTRA ' /
      C
0005        EOF = 0.
0006        I=0.
0007        DO 5 J = 1,50
0008        FLD(J) = 0.0
0009        IMF(J) = 0
0010     5 CONTINUE
      C
      C READ LIMITS OF DATA TO ACCEPT IF THERE ARE ANY - JUST FIELD DATA
      C A BLANK CARD WILL MEAN ALL FIELD VALUES WILL BE INCLUDED
      C
0011        READ ( 1, 11 ) MINF, MAXF
0012     11 FORMAT ( 2I5 )
0013        IJK = MAXF - MINF
0014        IF ( MAXF .EQ. 0 ) MAXF = 999999
0015        IF ( IJK .NE. 0 ) WRITE ( 3,33) MINF, MAXF
0016     33 FORMAT ( '   FIELD VALUES LESS THAN ', I6, ' AND GREATER THAN ',
           1        I6, ' WILL NOT BE INCLUDED IN THE AVERAGES ')
      C
      C READ FIRST RECORD - SHOULD HAVE INITIAL X AND Y
      C
0017        READ(1,10,END=90) NAME, DIR, IFE, XI, YI, IZ, IDZ, IGE, DATE, TIME
0018     10 FORMAT ( A6, F5.1, I4, F6.2, F6.2, I5, I3, I4, 20X, A8, A4 )
0019     15 NAMEC = NAME
0020        JFE = IFE
0021        HDZ = IDZ
0022     40 I = I + 1
0023        IF( IFE .NE. 0 ) JFE = IFE
0024        X(I) = XI
0025        Y(I) = YI
0026        IF ( IDZ .EQ. 0 ) IDZ = HDZ
0027        IZ0(I) = IZ + IDZ
0028        IZ1(I) = IGE
      C
      C TEMPORARILY STORE FLIGHT ALTITUDE IN IZ2 SPACE- NEEDED LATER WHEN
      C A CHANGE IN FLIGHT ALTITUDE GIVES RISE TO A DIFFERENT FLIGHT NAME
      C
0029        JA = JFE / 100
0030        IZ2(I) = JA
0031        IF ( IZ0(I) .GT. MAXF ) GO TO 50
0032        IF ( IZ0(I) .LT. MINF ) GO TO 50
      C
      C SUM FIELD FOR AVERAGING
```

```
C
0033            FLD(JA) = FLD(JA) + IZO(I)
0034            IMF(JA) = IMF(JA) + I
C
C READ LATER RECORDS
C
0035         50 READ(1,10,END=90) NAME, DIR, IFE, XI, YI, IZ, IDZ, IGE, DATE, TIME
0036            IF ( NAME .EQ. BLANK ) GO TO 40
0037            IF ( NAME .EQ. NAMEC ) GO TO 40
0038         60 SP = I - 1
0039            DX = X(I) - X(1)
0040            DY = Y(I) - Y(1)
C
C STORE DATA ON TAPE - FIRST ITEM IS THE NUMBER OF POINTS FOR FLIGHT
C
0041            WRITE (8) I
0042            DO 65 J = 1,I
0043            FAC = (J - 1) / SP
0044            X(J) = X(1) + FAC * DX
0045            Y(J) = Y(1) + FAC * DY
0046            K1 = X(J) * 100.
0047            K2 = Y(J) * 100.
C
C STORE DATA - THE ACTUAL FLIGHT DATA
C
0048            WRITE (8) K1, K2, IZO(J), IZ1(J), IZ2(J), NAMEC, J
0049         65 CONTINUE
0050            IF ( EOF .EQ. 1. ) GO TO 99
0051            I = 0
0052            GO TO 15
0053         90 EOF = 1.
0054            GO TO 60
0055         99 ENDFILE 8
0056            REWIND 8
C
C COMPUTE AVERAGES & LIST THEM
C
0057            GFLD = 0.0
0058            INBR = 0
0059            WRITE (3,3001)
0060       3001 FORMAT('1',/// 10X,'FLIGHT ALT   AVG FIELD   NBR POINTS', // )
0061            DO 105 J = 1,50
0062            IF ( IMF(J) .EQ. 0 ) GO TO 105
0063            GFLD = GFLD + FLD(J)
0064            INBR = INBR + IMF(J)
0065            FLD(J) = FLD(J) / IMF(J)
0066            ALT = J * 100.
0067            WRITE (3,3002) ALT, FLD(J), IMF(J)
0068       3002 FORMAT('0', 12X, F6.0,   6X, F7.0, 7X, I4 )
0069        105 CONTINUE
0070            GFLD = GFLD / INBR
0071            WRITE(3,3022) GFLD, INBR
0072       3022 FORMAT ( '0' //, 12X, '  ALL ', 6X, F7.0, 6X, I5 )
C
```

```
        C REREAD DATA AND CALCULATE ANOMALIES
        C     FIELD IZO = ACTUAL FIELD VALUES
        C     FIELD IZ1 = ACTUAL GROUND ELEVATIONS
        C     FIELD IZ2 = ACTUAL FIELD VALUE - AVERAGE FOR THAT FLIGHT ALTITUDE
        C     FIELD IZ3 = ACTUAL FIELD VALUE - OVERALL AVERAGE
        C
0073        107 READ (8,END=900) NBR
0074            ICNT = 0
0075            DO 150 I = 1,NBR
0076            READ (8) K1, K2, IZO(I), IZ1(I), JA, NAME, J
0077            IF ( I .NE. 1 ) GO TO 110
0078            KA = JA
0079            IXTRA = 0
0080            NAMEC = NAME
0081            WRITE (3,3003) NAMEC
0082       3003 FORMAT ('1',' FLIGHT ',A6,///,'
           1       ZO         Z1            Z2        X * 100       Y * 100
           2   ', /// )                                Z3           ID
0083        110 IF ( KA .EQ. JA ) GO TO 125
0084            KA = JA
0085            IXTRA = IXTRA + 1
0086            ICNT = 0
0087            NAMEC = NAMEX
0088            WRITE (3,3003) NAMEC
0089        125 ICNT = ICNT + 1
0090            IZ2(I) = IZO(I) - FLD(JA)
0091            IZ3 = IZO(I) - OFLD
0092            WRITE (3,3004) K1, K2, IZO(I), IZ1(I), IZ2(I), IZ3, NAME, ICNT
0093       3004 FORMAT (' ', 6 ( 9X, I6 ), 6X, A6, I3 )
0094            IF ( IXTRA .EQ. 0 ) GO TO 140
0095            WRITE (2,2002) K1, K2, IZO(I), IZ1(I), IZ2(I), IZ3, NAME, ICNT
0096       2002 FORMAT( 6I10, 11X, A6,I3 )
0097            GO TO 150
0098        140 WRITE (2,2022) K1, K2, IZO(I), IZ1(I), IZ2(I), IZ3, NAME, ICNT
0099       2022 FORMAT( 6I10, 10X, A6, 1X, I3 )
0100        150 CONTINUE
0101            GO TO 107
0102        900 CALL EXIT
0103            END
```